GEOLOGICA ULTRAIECTINA

Mededeling van de
Faculteit Geowetenschappen
Universiteit Utrecht

No. 309

Aspects of Transverse Dispersion in Porous Media

Mariene Gutierrez Neri

Aspects of Transverse Dispersion in Porous Media

Aspecten van Transversale Dispersie in Poreuze Media

(met een samenvatting in het Nederlands)

PROEFSCHRIFT

ter verkrijging van de graad van doctor aan de Universiteit Utrecht
op gezag van de rector magnificus, prof. dr. J.C. Stoof, ingevolge het
besluit van het college voor promoties in het openbaar te verdedigen
op maandag 29 juni 2009 des middags te 12.45 uur door

Mariene Gutierrez Neri

geboren op 30 May 1978 te Poitiers, Frankrijk.

Promotor: Prof. dr. R. J. Schotting

Dit proefschrift werd (mede) mogelijk gemaakt met financiële steun van
CONACYT, NWO ('Mathematical Analysis of Nonlinear Theories in Flow and
Transport in Porous media') and IF Technology BV.

The ball is an essential part of the game
Johan Cruyff

Dedicated to my family

Samenstelling leescommissie:

Prof. dr. ir. S.M. Hassanizadeh,	University of Utrecht
Prof. dr. ir. A. Leijnse,	University of Wageningen
Prof. dr. D.N. Lerner,	University of Sheffield
Prof. dr. P. Grathwohl,	University of Tuebingen
Dr. Denis Demidov,	Kazan State University

Printed by WPS, Zutphen.

Table of Contents

Chapter 1

Introduction

1.1 Background

Groundwater is the water occurring in underground porous rocks or strata also referred to as *aquifers*. The amount of freshwater found in the aquifers is far more greater than that in surface water bodies such as rivers and lakes, making it a crucial source of drinking water. While most groundwater is of good quality, like any other freshwater resource it is vulnerable to pollution. Pollutants on the ground surface can leak through the soil and rocks into the aquifers. Once a contaminant reaches the aquifer its impact will depend on a number of factors, such as the type of pollutant, the distance between the point of contamination and the point at which groundwater is extracted by e.g., a pumping well, or reaches the surface again. Some contaminants can naturally degrade, others are of persistent nature and have to be separated from the water before it can be used. Groundwater 'plumes' are a manifestation of this type of contamination. Figure 1.1 is a schematics of a drinking water supply reached by a groundwater contaminant plume.

In the last decade, extensive scientific research has been carried out to gain a better understating of the biochemical and hydrological processes that control the evolution of a contaminant plume. A special focus has been placed on studying whether a plume can be remediated or attenuated by naturally-occurring processes. This type of 'in-situ' remediation relies on the combined ability of physical and biochemical processes in the aquifer to degrade the contaminant over a certain period of time. By monitoring the groundwater remediation and predicting its long-term behaviour, natural attenuation has become a (risk-based) remediation strategy in its on right. When this type of remediation strategy involves the injection or emplacement of particular micro-organisms (i.e., bacteria) or chemicals into the aquifer, the term 'enhanced' natural attenuation is often used. However, in order to implement such remediation strategies, the risks involved have to be quan-

tified. A better quantification of this risk (and uncertainty) can only be achieved through a thorough understanding of the fundamental processes governing natural attenuation.

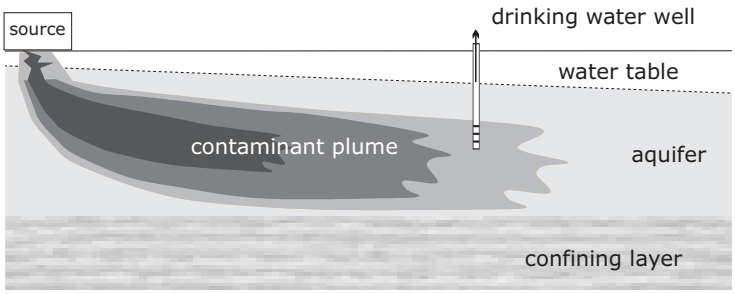

Figure 1.1: Schematics of a contaminant plume reaching a drinking water well.

Another type of groundwater pollution concern comes from the intrusion of saltwater into freshwater aquifers. This environmental issue is usually found in coastal aquifers where there is a natural boundary at which saline and freshwater meet. When freshwater is pumped, this interface moves inwards and saltwater is brought further into the aquifer. This situation can also happen inland when groundwater abstraction by wells causes saltwater to be drawn up from deeper aquifers containing brackish water (salt upconing). A schematics of this scenario is shown in Figure 1.2. If intrusion of saltwater becomes significant, the quality of the water quickly deteriorates making it no longer amenable for drinking purposes. Although seawater intrusion is a common contamination problem in coastal areas, in semi-arid and arid zones where water resources are scarce, its impact can be of larger magnitudes. Especially, if dense population and economical development are coupled with intense exploitation of groundwater. The dynamics of the contact zone between salt and fresh waters plays a crucial role in understanding and tackling practical seawater intrusion problems. An important characteristic is the existence of density differences. While the density of seawater ranges between 1020 and 1030 kg/m^3, brine densities can easily exceed 1200 kg/m^3 when they occur in deep formations. The existence of such high salt concentrations give rise to large concentration gradients within the usually narrow interface. This zone can be considered as a sharp interface (i.e., salt and fresh waters do not mix) or as a dispersive mixing zone.

The assumption of a sharp interface has enabled the derivation of rather simple analytical and numerical solutions to characterise this zone. For instance, the well-known Ghyben−Herzberg relationship, which relates the elevation of the groundwater table to the elevation of the saltwater-freshwater interface assuming a

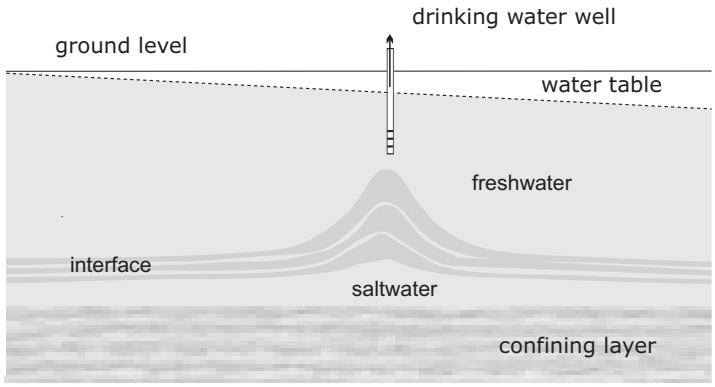

Figure 1.2: Schematics of saltwater upconing beneath a drinking water well.

hydrostatic equilibrium. However, assuming a dispersive mixing zone seems a more realistic attribute especially if a better assessment of the salt concentration distribution in the aquifer is desired. For this assumption, the effects of density differences and density-induced flows have to be taken into account. Density-dependent dynamics are also relevant in other practical applications like thermally-induced flow in deep geothermal energy systems, nuclear waste disposal facilities, and oil recovery processes. Due to this practical importance, density-dependent transport has received increased attention over the last years, aimed at better ways to model flow and transport processes and a better understanding of the controlling mechanisms.

1.1.1 Transverse dispersion

A common factor in the examples of natural attenuation of contaminant plumes and seawater intrusion is the key role that hydrodynamic dispersion processes play. In particular, dispersion occurring perpendicular to the main transport direction, or *transverse dispersion*. Hydrodynamic dispersion is a transport mechanism by which fluid particles entering into the aquifer are spread, occupying an ever-increasing volume as they at transported downgradient. This latter is the result of two fundamental processes: molecular diffusion and mechanical dispersion. Molecular diffusion is driven by the existence of a concentration gradient, i.e., fluid particles move from high-concentration areas to low-concentration areas. The rate at which particles diffuse depends on the physical and chemical properties of the fluid. In contrast, mechanical dispersion is dependent on the structure of the porous medium. Aspects that influence transverse dispersion processes in porous media are the main focus of investigation in this thesis.

1.2 Outline and Objectives of the Thesis

This thesis consists of eight chapters and it is organised as follows: **Chapter 2** gives an introduction to the main governing equations of flow and transport in porous media. The topic of hydrodynamic dispersion is discussed from the conceptual and theoretical point of view. **Chapter 3** consists of an overview to the subject of density-dependent dispersion. Previous experimental and theoretical findings reported in the literature for longitudinal and transverse dispersion are presented. **Chapter 4** presents an experimental study on transverse dispersion processes. For this purpose, a series of horizontal miscible-displacement experiments are carried out in a two-dimensional flow-through tank. The effects of fluid velocity and density differences on the transverse dispersion coefficient are systematically studied. In **Chapter 5** the experimental results are compared with numerical simulations and with theoretical predictions from two different density-dependent mathematical models. The aim is to gain a better understanding of the mechanics of transverse dispersion under high-concentration gradient conditions, typically encountered in seawater intrusion problems.

The second part of this thesis deals with the interaction between transverse dispersion and reactions. These two processes are regarded as competing with each other, i.e, dispersion promoting spreading and dilution, and reaction preventing further dispersion by consuming the fluid. In **Chapter 6** a methodology is presented to model analytically the combined effects of reaction and transport. A numerical validation of this method is carried out. As direct application, the behaviour of groundwater contaminant plumes under naturally attenuating conditions is studied. An explicit expression is derived for the steady state size of the plume. The relevance of transverse dispersion in controlling the plume extent is determined. In **Chapter 7** the same mathematical approach to account for transport and reaction is again employed. However, here the focus is to relate the size of the reactive mixing zone to the transverse dispersion coefficient and hence transverse dispersivity. Highly-resolved vertical concentration profiles are used to estimate the transverse dispersivity and then compared to previously-reported values for the same field-problem. **Chapter 8** summarises the thesis.

Chapter 2

Dispersion in porous media: basic equations and description

In this Chapter the basic equations governing the flow and transport of solutes in porous media are presented. Next, the topic of dispersion in porous media is introduced, with a particular emphasis on transverse dispersion mechanisms. Theoretical models as well as literature data are reviewed.

2.1 Basic Equations

In this thesis, three different transport system in homogeneous porous media are considered: transport of non-reactive tracer, transport of brine, and reactive transport. The systems are 'binary system', i.e., a resident fluid (e.g., fresh water) and an invading fluid that contains a dissolved solute (e.g., salt). Non-reactive tracer transport occurs when the invading fluid contains dissolved matter in small quantities such that the density and viscosity are equal to that of the ambient fluid. Brine transport occurs when the invading fluid is a highly-concentrated salt (e..g, NaCl) solution such that density and viscosity are no longer the same as the resident fluid. When the tracer is no longer passive and is affected by chemical reactions, effects of destruction (or creation) of the tracer have to be imposed on transport. The main equations governing these systems are those of balance of mass and momentum.

2.1.1 Mass balance of the fluid and solute

The mass balance equation of the fluid in a non-deformable porous medium (i.e., constant porosity) reads

$$n\frac{\partial \rho}{\partial t} + \nabla \cdot (\rho \mathbf{q}) = 0, \tag{2.1}$$

where n is the porosity of the medium, ρ is the density of the fluid, and $\mathbf{q}$ is the Darcy velocity vector or specific discharge.
If the fluid is assumed incompressible (i.e., no volume effects), it can be assumed that $(\nabla \rho = 0)$ and $\left(\frac{\partial \rho}{\partial t} = 0\right)$, equation (2.1) reduces to,

$$\nabla \cdot \mathbf{q} = 0. \tag{2.2}$$

Equation (2.2) is also known as the continuity equation. The fluid velocity vector, $\mathbf{v}$, is given by

$$\mathbf{v} = \frac{\mathbf{q}}{n}. \tag{2.3}$$

Next, the mass balance equation of the solute reads

$$n\frac{\partial C}{\partial t} + \nabla \cdot (C\mathbf{q} + \mathbf{J}) = 0, \tag{2.4}$$

where $\mathbf{J}$ denotes the dispersive mass flux vector and C is the solute concentration. The dispersive mass flux $\mathbf{J}$ is typically given by the classical Fick's law of diffusion, which indicates that the dispersive mass flux is linearly proportional to the solute mass fraction gradient,

$$\mathbf{J} = -D \cdot \nabla C, \tag{2.5}$$

where D is the the dispersion tensor. D is typically assumed independent of the solute concentration and its gradient but it is dependent on the fluid velocity (Scheidegger, 1961). The dispersion tensor and its functional form are discussed below when hydrodynamic dispersion models are reviewed.

It is possible to rewrite (2.4) and (2.5) in terms of the mass fraction, ω. Recalling that $\omega = C/\rho$, equations now yield,

$$n\frac{\partial \rho\omega}{\partial t} + \nabla \cdot (\rho\omega\mathbf{q} + \mathbf{J}) = 0, \tag{2.6}$$

and

$$\mathbf{J} = -\rho D \cdot \nabla \omega, \tag{2.7}$$

2.1.2 Darcy's law

The momentum balance equation (also refereed to as Darcy's law) for a non-deformable porous medium reads

$$\mathbf{q} = -K\ \nabla h, \tag{2.8}$$

where K is the hydraulic conductivity and ∇h is the hydraulic gradient. For an isotropic medium K is considered a scalar and is related to the medium's intrinsic permeability and fluid's properties following $K = k\rho g/\mu$. This formulation of Darcy's law is usually employed when density and viscosity are considered invariant (e.g., in tracer transport). An alternative formulation is usually employed when density variations exists (density-dependent transport),

$$\mathbf{q} = -\frac{k}{\mu}\left(\nabla p - \rho\mathbf{g}\right), \tag{2.9}$$

where k denotes the intrinsic permeability, μ is the fluid's viscosity, p is the fluid's pressure, and $\mathbf{g}$ is the gravity acceleration vector. Darcy's law is assumed valid only for fluid flows with Reynolds numbers not higher than 10 (i.e., laminar flow).

2.1.3 Equation of state

The density and viscosity of the fluid are affected by changes in concentration, temperature and to a lesser extent pressure. In this thesis, only concentration-induced changes are considered. Thus, an equation of state is needed that relates the fluid's density to changes in solute mass fraction (or concentration). A common empirical relationship is given by

$$\rho = \rho_f \exp^{\gamma\omega}, \tag{2.10}$$

where ρ_f is the density of the fluid, and ω is a mass fraction coefficient. If freshwater is considered, $\rho_f \approx 1000$ kg/m^3. For salt (NaCl) dissolved in freshwater $\gamma \approx \ln(2)$.

Note that ω can also be seen as a scaled mass fraction $\omega_c = \omega/\omega_s$ where ω_s is the mass fraction of the solution (e.g., freshwater + saltwater). According to Landman (2005), in density-dependent transport the difference between assuming that the scale mass fraction is equivalent to a scaled concentration $C = c/c_s$ is only small. In tracer transport $\omega_c = C$. Hence, (2.10) can also be written in terms of scaled concentration by substituting C in the argument of the exponential,

$$\rho = \rho_f \exp^{\gamma C}, \tag{2.11}$$

Relationship (2.11) is used in Chapter 4 to compute the fluid's density during the experimental runs.

2.1.4 Oberbeck-Boussinesq approximation

In studies of density-dependent flow, it is common to adopt the Oberbeck-Boussinesq (OB) approximation in order to simplify the system of governing equations. The basic premises of this approximation are:

1. Density variations - induced by variations in solute concentration and/or temperature - are neglected in all equations, except for the crucial buoyancy term ρg which is retained in the momentum equation (2.9).

2. All other fluid properties (e.g., viscosity and molecular diffusivity) are assumed constant.

3. Viscous dissipation is assumed negligible.

4. The equation of state is linearized.

The OB approximation is typically assumed valid for systems where density variations are small. However, as density differences tend to zero, the governing equations do not reduce to those used in the OB approximation — in this limit, the gravity (buoyancy) term in the momentum balance equation also vanishes (Landman, 2005). Neglecting the effects of gravity may not be appropriate in many practical scenarios, in particular those where density-dependent flow processes may play an important role, e.g., transport of dense pollutants and seawater intrusion in fresh water aquifers.

The validity of the OB approximation has been studied using numerical approaches, see for instance Johannsen (2003). However, in a recent publication by Landman & Schotting (2007), this limit was revisited using a different approach: the authors derive formal limits for which the governing equations used in the OB can be retained. In particular, explicit limits are derived for changes in fluid volume (neglected in the OB approximation) that render the continuity equation divergence-free, i.e., the fluid is incompressible, and hence $\nabla \cdot \mathbf{q} = 0$.

For isothermal brine transport, the following condition must be fulfilled in order to retain the gravity term and neglect fluid volume changes,

$$NPe = \frac{kg\rho x_0}{\mu D_{mol}} \gg 1 \tag{2.12}$$

where the Peclet number $\left(Pe = \frac{x_0 q}{D_{mol}}\right)$, $\left(N = \frac{kq\rho}{\mu q}\right)$ and x_0 denotes a length scale related to density variations. It is interesting to note that this limit is independent of the density difference itself and the flow velocity (or specific discharge). Although it may be expected that for freshwater-saltwater systems condition $NPE \gg 1$ is easily fulfilled as D_{mol} of salt (NaCl) is very small, the characteristic length scale (x_0) may become an important parameter specially when dealing with small-scales. This limit is recalled in Chapter 5 when examining the experimental data of transverse brine transport.

2.1.5 Density- and viscosity-induced flow

Whenever density differences exist gravitational forces act upon them generating a rotational motion that can be clockwise or counter-clockwise. Rotational flow can also occur as a result of viscosity variations. However in this thesis viscosity variations are mainly disregarded. The phenomenon of rotational flow induced by density and viscosity differences has been studied by a number of authors, see for instance Hellström *et al.* (1988).

The strength of the rotational flow driven by density variations in comparison to viscosity-driven flow was analysed in Landman (2005) for the case of stable vertical flow. The author suggests that the latter effects can be disregarded if

$$q_z << \frac{kg\rho\gamma_p}{\mu\gamma_u} \tag{2.13}$$

where q_z is the specific discharge in the main flow direction. If density and viscosity variations with mass fractions are assumed to vary linearly, the right-hand side in expression (2.13) reduces to the critical velocity (q_c) defined in Hellström *et al.* (1988). Considering only density changes,

$$q_c = \frac{kg\rho\Delta\rho}{\mu_f} \tag{2.14}$$

In this thesis, the effects of rotational flow on dispersion are considered with a particular accent on horizontal and stable flow configuration, i.e, the heavier fluid underlies the lighter fluid.

2.2 Dispersion in Porous Media

Many investigators in the past have studied dispersion in porous media from a theoretical or an experimental view-point. A distinction is commonly made between dispersion occurring in the same direction as the main flow (longitudinal) or perpendicular to it (transverse). As dispersion is not the equal in these two directions, they are usually studied separately. In this thesis, transverse dispersion processes are the main focus of investigation. In the following, dispersion is explained from two well-known situations: i) dispersion in a capillary tube, and ii) hydrodynamic dispersion in porous media. The former is reviewed as the mechanisms occurring in a capillary tube are usually referred to in the description of dispersion in porous media. Moreover, capillary mechanism are relatively well understood for capillaries and give interesting insights into the controlling variables. In addition, the equations describing dispersion in capillary tubes are most of the time of the same form as those for porous media.

2.2.1 Dispersion in a capillary tube

When a fluid flows through a capillary, a velocity profile develops. This velocity profile is not uniform over the cross-section of the capillary. At certain radial positions, the fluid flows faster than at others. Assuming that the flow is laminar the velocity profile that develops has a parabolic shape. The matter present in the fluid moves along with it and is therefore dispersed along the tube axis. Apart from this purely convective dispersion, diffusion can also be of influence. Early experimental evidence by Griffiths (1911) showed that when a tracer is continuously injected into a slowly moving water, it spreads out symmetrically from a point which moves with the average velocity of the fluid in the capillary tube. In Figure 2.1 the development of the tracer front is show schematically.

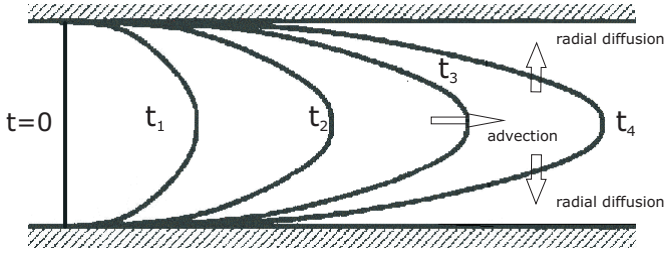

Figure 2.1: Dispersion in a capillary tube (Modified from Bear, 1972).

Suppose that somewhere in the tube we have a small plug of fluid with a composition different from an otherwise similar bulk of fluid. The flow of the fluid causes this plug to disperse, but it also induces radial composition gradients. This leads to diffusive fluxes at the front and back sides of the plug. These fluxes become important if the radial diffusive fluxes are roughly of the same order of magnitude as the convective axial fluxes. This is the case when either the axial velocity is very low, or when the radial distances are very small. When either condition is satisfied, diffusion tends to keep the plug together, in contrast to what one might intuitively expect. So, through the combined action of convection and diffusion, the plug will leave the tube as a broadened, but still more or less compact plug. To achieve this situation, Taylor dispersion experiments are usually carried out in tubes with small diameters, also called capillaries. At sufficiently short times, the shape of the front remains unchanged, i.e., a sharp front. At later times the tracer front elongates at a faster rate due to advection than widens due to radial diffusion. Under this condition, a radial concentration gradient develops and molecular diffusion acts upon it by slowly equalizing the tracer concentration across the capillary section. It must be pointed out that the tracer front does not exhibit the same concentration value everywhere but attains a maximum at half-width. Taylor (1953) shows that the concentration in the capillary tube can be described by

a one-dimensional dispersion equation as follows:

$$\frac{\partial C}{\partial t} = D_{ef}\frac{\partial^2 C}{\partial x^2} \tag{2.15}$$

where C is the tracer concentration at distance x and time t. D_{ef} is an effective dispersion coefficient that reflects the contribution of mechanical (convective) dispersion and molecular diffusion. Equation (2.15) is also known as the Fick's second law of diffusion. It should be noted that this equation is only valid after a sufficiently long time has lapsed from the injection of the tracer. The analytical solution to describe the tracer distribution after at time t after injection is given by

$$\frac{C}{C_0} = \frac{1}{2\sqrt{\pi D_{ef} t}} \exp\left(-\frac{(x-vt)}{4D_{ef}t}\right) \tag{2.16}$$

where C_0 is the initial tracer concentration. If axial molecular diffusion is neglected, Taylor gives the following explicit expression for D_ef

$$D_{ef} = \frac{d^2 v^2}{48 D_{mol}} = \frac{Pe_c^2 D_{mol}}{192} \tag{2.17}$$

where d is the capillary's diameter, D_{mol} is the molecular diffusivity (diffusion in aqueous solution), and Pe_c is the capillary Peclet number. In the later work by Aris (1956) it was shown that if axial molecular diffusion is not left out, the effective dispersion coefficient must contain an additive term as follows:

$$D_{ef} = D_{mol} + \frac{d^2 v^2}{48 D_{mol}} = D_{mol} + \frac{Pe_c^2 D_{mol}}{192}. \tag{2.18}$$

When the injection at the inlet changes from zero to C_0, i.e., a step change. The solution to (2.15) is now:

$$\frac{C}{C_0} = \frac{1}{2}\left(1 \pm \operatorname{erf}\frac{(x-vt)}{2\sqrt{D_{ef}t}}\right) \tag{2.19}$$

where the point $C/C_0 = 0.5$ moves with the velocity v. Neglecting the effects of molecular diffusion, the analytical solution is reduced to:

$$\frac{C}{C_0} = 1 - \frac{x^2}{4v^2 t^2} \tag{2.20}$$

An interesting feature of the breakthrough curves in the definition of a mixing length L_m which is the distance where the tracer changes from 0 to 1 (or from 0.1 to 0.9 of the initial concentration). Based on the latter, the following expression is proposed by Taylor (1953) to calculate D_{ef} in terms of a mixing length

$$D_{ef} = \frac{1}{t}\left(\frac{L_m}{3.625}\right)^2. \tag{2.21}$$

The concept of relating the dispersion coefficient to the value of a mixing length is recalled in Chapter 7 where the size of a reactive mixing zone is used to extract the value of the transverse dispersivity. It should be noted that in the work by Taylor (1953) and Aris (1956) only longitudinal dispersion and axial molecular diffusion are considered. Transverse dispersion is limited as lateral spreading is restricted by the walls of the capillary tube. However, the analysis of a single capillary tube can be adapted to study dispersion in porous media if the medium is regarded as a 'network' of capillaries, randomly orientated, connected to each other by pore throats (e.g., De Josselin de Jong (1958)). The next section shows how this idea was explored by several authors studying dispersion in porous media.

2.2.2 Hydrodynamic dispersion in porous media

The concept of hydrodynamic dispersion in porous media is shown schematically in Figure 2.2. A given amount of tracer is injected into a homogeneous porous medium. The tracer particles spread and occupy an ever-increasing volume of the medium. The tracer tends to spread faster in direction of the main flow than perpendicular to it. The two underlying mechanism causing this phenomenon are (as in dispersion in capillaries) molecular diffusion and mechanical mixing.

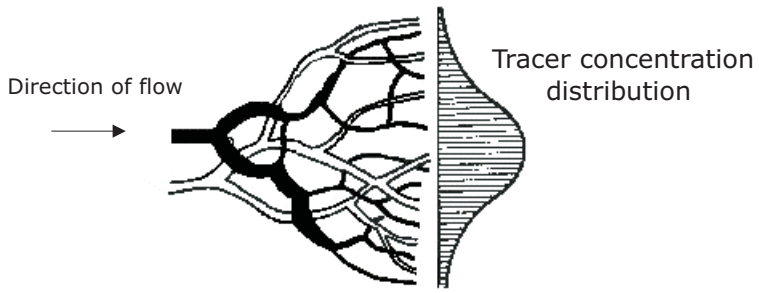

Figure 2.2: The concept of hydrodynamic dispersion.

Dispersion is commonly divided into its longitudinal and transverse component and characterised by their respective longitudinal dispersion coefficient, D_L and transverse dispersion coefficient, D_T. Hence, in general terms a hydrodynamic dispersion coefficient has two components, a diffusion coefficient and a mechanical

mixing coefficient,

$$D_i = D_m + D_{mec} \tag{2.22}$$

The first mechanism, molecular diffusion, can be regarded as the outcome of random motions of the fluid particles (Brownian motion) due to the presence of a concentration gradient (Brown, 1828). Diffusion contributes to the overall dispersion by moving particles forward along the same streamline (axial diffusion) and by moving particles from one streamline to another (radial diffusion). The former mechanism is usually regarded weaker than the latter (Bear, 1969). The molecular diffusion coefficient D_m refers in fact to an 'effective' coefficient. An effective coefficient D_e has to be considered in order to account for the tortuous nature of the pore space. That is, the existence of the porous media reduces the volume over which particles can diffuse. This in turn increases the travel distance (path length) of the particles and hinders solute diffusion. Note that the effective diffusion coefficient defined here differs from that of effective diffusion in capillaries. The effective diffusion coefficient can be defined as,

$$D_e = \frac{D_{mol}}{\tau} \tag{2.23}$$

where τ is the tortuosity factor (Bear, 1972). This factor is a function of the porosity and tortuosity of the medium. In most practical cases porosity is the only parameter that can be measured in a porous medium. Hence, it is common to use empirical functions in terms of porosity alone,

$$D_e = D_{mol}\, n^s \tag{2.24}$$

where s in an empirical coefficient close to the unity (Grathwohl, 1998). Another common approach is to extract D_e from the ratio $\frac{D_e}{D_{mol}}$ reported in dispersion experiments. This ratio is in effect equal to $\frac{1}{\tau}$ and a value of 2/3 has been observed in experiments in unconsolidated media (Fried & Combarnous, 1971; Bear, 1972).

The second dispersive mechanism, mechanical mixing, arises from irregularities of the pore space available for fluids to flow — it creates differences in the flow path and in the flow velocity within the pores. Differences in flow paths allow streamlines to diverge from the mean flow direction and consequently to a variety of travel lengths or travel times. Differences in flow velocity are the result of variations in the pore dimensions and orientation (see Figure 2.3).

2.3 Modelling Dispersion in Porous Media

A common starting point for modelling dispersion in porous media is the use of the macro scale advection-dispersion equation (ADE). The ADE for a non-reactive tracer results from inserting (2.5) into (2.4). Written for a three-dimensional system under uniform velocity field in a homogenous isotropic medium yields,

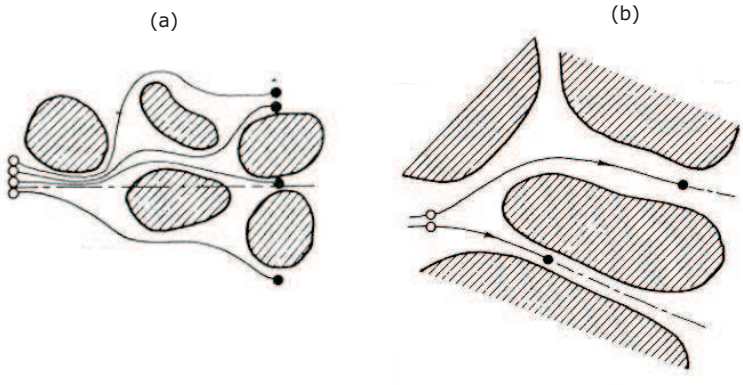

Figure 2.3: Mechanical dispersion as a result of irregularities in the pore spaces.

$$\frac{\partial C}{\partial t} + v\frac{\partial C}{\partial x} = D_L\frac{\partial^2 C}{\partial x^2} + D_T\left(\frac{\partial^2 C}{\partial y^2} + \frac{\partial^2 C}{\partial z^2}\right) \tag{2.25}$$

where D_L and D_T are the longitudinal and transverse dispersion coefficients respectively. There is considerable variation among investigators in prescribing a particular form for D_L and D_T. These coefficients are usually expressed as a product of a dispersivity (a quantity function of the pore geometry) times the fluid velocity, sometimes raised to some power and possibly some other function (Bear, 1972). The obtained expressions vary according to the mathematical procedure used and the assumptions made on the pore structure and on the interacting mechanisms, e.g., molecular diffusion (Bear, 1972). Some of these theoretical models are briefly reviewed below.

2.4 Hydrodynamic Dispersion Models

In the past years a number of theoretical models for describing hydrodynamic dispersion in porous media have been proposed. With a few exceptions like the single capillary model by Taylor (1953) and Aris (1956), most of these models employ statistical approaches to treat dispersion, coupled with a particular way of visualising the porous media structure. From these statistical models, a distinction can be made based on the averaging procedure used.

2.4.1 Statistical models using a continuum approach

Scheidegger (1954) suggested in his analysis of hydrodynamic dispersion in porous media, that the relationship between the dispersion coefficient, D and velocity, v

would depend on the role played by molecular diffusion. Two possibilities were presented: i) $D \propto a'v^2$, where a' is a constant of the porous medium (referred to as dynamic dispersivity) and is the result of mixing taking place by molecular diffusion at each flow channel; ii) $D \propto a''v$ where a'' is also a porous medium constant (called geometric dispersivity) and is the result of not enough molecular diffusion between streamlines. This can be seen in a more general way as the relationship between D and v^n where n varies between 1 and 2. Similar results were concluded by Taylor (1953) for dispersion in capillary tubes. However, no distinction was yet made between longitudinal and transverse dispersion — dispersion was assumed isotropic.

In subsequent works by De Josselin de Jong (1958) and Saffman (1959), statistical techniques are employed to obtain expressions for longitudinal and transversal dispersion coefficients as separate, yet coupled, processes. Both authors based their approach on a more realistic visualisation of the porous structure. For instance, De Josselin de Jong (1958) visualises a porous medium as a series of interconnected straight channels of equal length, uniformly distributed in all directions but randomly orientated, in which average uniform flow takes place. A schematic of this 'random porous structure' is given in Figure 2.4.

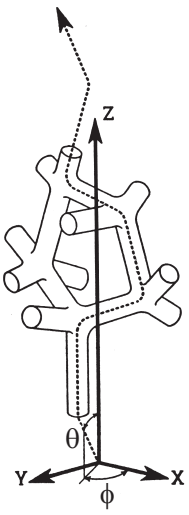

Figure 2.4: Schematics of flow through a random porous medium. Modified from De Josselin de Jong, 1958.

The result of dispersion from the point injection is a Gaussian distribution in three-dimensional space, from which standard deviations in the longitudinal direction σ_L and transverse direction σ_T are obtained. The dispersion coefficients are obtained from the standard deviations,

$$D_L = \frac{{\sigma_L}^2}{2T_o} = \frac{vl(\lambda + \frac{3}{4} - \ln\gamma)}{6}, \tag{2.26}$$

and

$$D_T = \frac{{\sigma_T}^2}{2T_o} = \frac{3vl}{16}, \tag{2.27}$$

where T_o is the arrival time of a maximum number of particles after a given time, travelling in elementary channel of length l, λ is a function of the distance travelled, i.e., the distance travelled in the direction of the mean flow. An interesting observation from (2.26) and (2.27) is that although both coefficients are proportional to the mean velocity only D_L is dependent on the travel distance in the direction of mean flow. D_T is a function of the length l of the elementary channel. This means that the ratio between D_L and D_T is not constant but should increase with travel distance. In practice, it is common to assume a ratio of 1/10 between coefficients.

2.4.2 Models based on volume-averaged techniques

In contrast to the work by Scheidegger (1954), Bear & Bachmat (1967) considered only the case where D is linearly related to v and suggested the following expressions for D_L and D_T,

$$D_L = \alpha_L v \tag{2.28}$$

and

$$D_T = \alpha_T v \tag{2.29}$$

where α_L and α_T are the longitudinal and transverse dispersivity, respectively.

2.5 Factors Influencing Hydrodynamic Dispersion

A number of factors can influence dispersion. For instance, interaction between molecular diffusion and advection, porous media properties, and fluid properties.

2.5.1 Interaction between molecular diffusion and advection

Although hydrodynamic dispersion is the outcome of two basic mechanisms, i.e., molecular diffusion and mechanical dispersion, experimental and numerical studies suggest a much richer interaction depending on the prevailing mechanism. Blackwell (1959) first explained this phenomenon qualitatively by highlighting the role played by molecular diffusion in transporting particles between streamlines. He was in fact the first author to present experimental data in terms of the molecular Peclet number, Pe, and the ratio of the dispersion coefficient (D_L or D_T) to D_{mol}. The molecular Peclet number represents the ratio between the time scale needed

for particles to diffuse the length l, and the time scale needed for particles to travel the same length scale by advection,

$$Pe = \frac{t_d}{t_{con}} = \frac{\frac{l^2}{D_{mol}}}{\frac{l}{v}} = \frac{vl}{D_{mol}}. \tag{2.30}$$

Thus, a small Pe translates into a diffusion-dominated spreading of the particles, and a large Pe into an advective-dominated spreading. Another remark is the choice of l as characteristic length of the porous medium. Although l is a measure of the pore space (a pore length), in practice it is difficult to obtain accurate measurements of the pore space. In the literature, a common practice is to replace l by the grain diameter d, specially if data with different grain sizes and flow velocities have to be compared. Experimental observations by De Josselin de Jong (1958) also confirm that l is a function of the grain size distribution and in the order of the average grain diameter d_{50}. However, some authors argue that d_{10}, i.e. the effective grain diameter is a better representation of the pore space. In this thesis, the molecular Peclet number is based on d_{50}.

Based on experimental data by several authors five different correlations, or *dispersion regimes*, have been inferred for longitudinal dispersion in terms of Pe versus the ratio D_L/D_{mol}. Figure 4.22 shows schematically this behaviour.

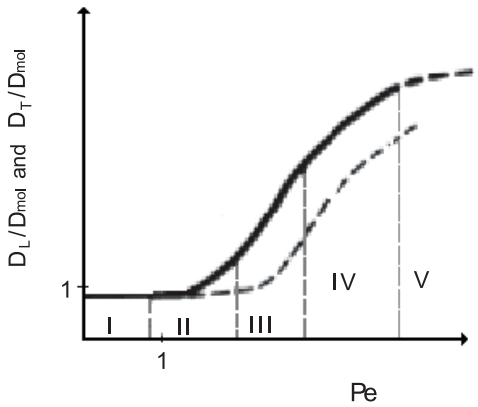

Figure 2.5: Dispersion regimes: behaviour of ratio D_L/D_{mol} and D_T/D_{mol} as a function of the molecular Peclet number. Solid line corresponds to the ratio D_L/D_{mol}, and long-dashed curve corresponds to ratio D_T/D_{mol}. Modified from Bear (1972).

1. Region I. $D_L/D_{mol} \sim 1/F$. In this region molecular diffusion dominates the dispersion process. The variable F is also known as the formation factor. Its value has been found for packs of unconsolidated material to be about

1.5. This means that the ratio D_L/D_{mol} approaches about 0.67 instead of the unity (Bear, 1972). This is a consequence of fact that D_{mol} is the molecular diffusion coefficient in free solution and D_L at $Pe \rightarrow 0$ is in fact the effective molecular diffusion coefficient D_e. For consolidated porous media, e.g. sandstones, F has been found to be much higher than 1.5 (Brigham et al., 1961).

2. Region II. (Pe $\sim$ 0.4 - 5). $D_L/D_{mol} \sim$ not reported. In this region the effects of mechanical dispersion already appear and are considered of the same order of magnitude as molecular diffusion.

3. Region III. (Pe $\sim$ 5 - 300) $D_L/D_{mol} \sim Pe^b$ (where $1 <$ b < 1.3). In this power-law regime, mechanical dispersion is the predominant mechanism but molecular diffusion effects are still visible.

4. Region IV. (Pe $\sim$ 300 - 10^5) $D_L/D_{mol} \sim$ Pe. Here, pure convective or mechanical dispersion dominates the dispersion mechanisms and the dispersion coefficient is linearly related to Pe.

5. Region V. (Pe $> 10^5$) In this region, turbulence effects appear on the dispersion process. The corresponding fluid velocities are rather large and fall outside the validity of Darcy's Law.

Fried & Combarnous (1971) suggest a similar behaviour for transverse dispersion, sifted however, to higher Pe values. This observation will be later corroborated in Chapter 4 where data collected from previous studies and this study are classified in transverse dispersion regimes.

2.5.2 Porous media properties

Porous media properties may promote or limit dispersion (Bear, 1972). If the intrinsic permeability, k, and the porosity, n, of a porous medium varies orders of magnitude within the space domain considered, the medium is said to be macroscopically heterogeneous. Dispersion arising from this type of heterogeneity falls outside the scope of this thesis. On the other hand, if k may be represented by a single (mean) value for the whole domain, the medium may be described as macroscopically homogeneous. It should be noted that the type of homogenous medium considered here may also be regarded as microscopically heterogeneous. This is because even at small-scale (e.g., lab-scale), it is almost impossible to construct a perfectly homogenous medium. Hence, considered here is a medium with a single average value of permeability and porosity but whose pore structure and dimensions intrinsically contain micro-scale heterogeneities. Other porous media characteristics that may influence dispersion are : i) average grain diameter (d_{50}); ii) grain shape (e.g. spherical) and iii) grain size distribution (characterised by the uniformity coefficient, U).

2.5.3 Fluid properties

The properties of the dispersing fluid may also play a role in limiting or promoting dispersion. The most common approach to investigate dispersion processes is to employ a fluid of similar physicochemical properties (e.g., nonabsorbing, nonreactive) and similar density to that of the ambient fluid. The concentration has to be small enough not to influence the density and/or viscosity of the fluid in which the tracer is dissolved. When this is the case, '*tracer conditions*' are established and the flow is assumed unaffected. However, when the concentration of the tracer is higher, the fluid's density and/or viscosity is affected and can induce density-driven and viscosity-driven flow. As a result, a coupling between flow and transport is established and the dispersion mechanisms are now also the result of interaction with other forces such as gravity (Schotting *et al.*, 1999). In this thesis, only variations in fluid's density and their effect on dispersion are investigated. Effects of viscosity variations are mostly disregarded. These property changes are assumed to be only concentration-induced, i.e., temperature-induced changes are not reviewed. Additionally, depending on the position of the denser fluid with respect to the tracer fluid, two configurations can be defined: stable – denser fluid displacing the lighter one, and unstable – denser fluid being displaced. Here only the stable configuration-type of displacement is considered.

2.5.4 Reactivity

When tracer species undergo reaction, the governing ADE given by (2.25) is now added a reaction rate term R_C,

$$\frac{\partial C}{\partial t} + v\frac{\partial C}{\partial t} = D_L\frac{\partial^2 C}{\partial x^2} + D_T\left(\frac{\partial^2 C}{\partial y^2} + \frac{\partial^2 C}{\partial z^2}\right) - R_C. \tag{2.31}$$

The reaction term can take many forms, in the context of this thesis two forms are relevant. These are listed in Table 2.1 and are discussed below.

Type of reaction	*Reaction rate* R_C
First-order decay	$\lambda C;\ \ \lambda = (\ln 2)/t^{(1/2)}$
Instantaneous bimolecular reaction	$R_{AB} = -R_A = -R_B$

Table 2.1: Types of reaction and corresponding rate term for R_C.

First-order decay

The first-order irreversible reaction rate term given in Table 2.1 represents the decay of tracer mass from the dissolved phase, where λ is a first order reaction rate for the dissolved phase and $t^{(1/2)}$ is the half-life of the reactive (or radioactive) solute.

Instantaneous bimolecular reaction

If two reactants A and B instantly react to form a product AB, $r_{AB} = -r_A = -r_B$ expresses the rate of production of AB equal to the rate of consumption of each reactant. The instantaneous reaction model is considered to be a good alternative to more complex multispecies reactive models, e.g., Monod kinetics, when reaction rates are sufficiently fast in relation to flow velocities (Ham *et al.*, 2004).

2.6 Transverse Dispersivity

As reviewed, hydrodynamic dispersion is macroscopic outcome of the combined effects of molecular diffusion and mechanical dispersion. Most of the hydrodynamic dispersion models have in common the use of a dispersion length (or dispersivity) within the dispersion coefficient to quantify the mechanical component of dispersion, e.g., Scheidegger (1961); Bear (1972). In effect, transverse dispersivity or transverse dispersion length (α_T) is defined as a measure of the lateral spreading of a solute due the randomness and heterogeneity of the porous media. A well-known formulation of the transverse dispersion coefficient is

$$D_T = D_e + \alpha_T v, \tag{2.32}$$

Rearranging for transverse dispersivity yields,

$$\alpha_T = \frac{D_T - D_e}{v} \tag{2.33}$$

If molecular diffusion is assumed negligible, α_T is the ratio (linear) between D_T and v. De Josselin de Jong (1958) proposed α_T to be equal to 3/16 of the average grain size, d_{50}. This result was to some extent validated by Grane & Gardner (1961) in their tracer experiment using consolidated-type of porous media. Equally, experiments by Olsson (2005) demonstrated a positive correlation of transverse dispersivity with average grain size. However, these experiments use unconsolidate-type of porous medium (glass beads) and report dispersivity values somewhat smaller than $\frac{3}{16} \cdot d_{50}$.

2.6.1 Effects of fluid velocity

A number of laboratory experiments have reported a decrease in transverse dispersivity with increasing fluid velocity, e.g., Huang (2002); Klenk & Grathwohl (2002). The obtained coefficients seem to better fit a power function of the velocity, rather than the expected linear dependence (see 2.32),

$$D_T = D_e + \alpha_T v^m \tag{2.34}$$

where exponent m has been reported to vary between 0.6 to 0.8 (Olsson & Grathwohl, 2007). Matching the experimental data using a formulation like (2.34) is a

rather empirical approach and does not necessarily explain the physics causing this sub-linear dependence on the fluid velocity. Some attempts to clarify the causes of this behaviour have been proposed by a number of authors, e.g., Klenk & Grathwohl (2002). In that study, the authors propose *incomplete mixing* at the pore spaces to be the cause of such behaviour. In order to match their experimental data, they introduce a 'correction factor' for dispersivity based on the pore size and the mean square displacement for velocities higher than 4 m/day (or equivalent $Pe > 128$). Introducing this correction factor gives very good agreement with experimental data, especially at high velocities. Olsson (2005) carried out a comprehensive experimental study on the effects of grain size, fluid velocity and scale on transverse dispersion. The author proposes an alternative formulation of the dispersion coefficient in terms of the molecular Peclet number (Pe),

$$\frac{D_T}{D_{mol}} = \frac{D_e}{D_{mol}} + 0.28\ (Pe)^{0.72}. \tag{2.35}$$

Expression (2.35) is valid for non-reactive tracers and comparison with existing literature data demonstrates that the expression holds for all investigated Peclet numbers (from $Pe \approx 1$ to 6307). Substituting expression(2.32) in (2.35) and rearranging for α_T yields,

$$\alpha_T = 0.28\ (Pe)^{0.72} \cdot \frac{D_{mol}}{v} \tag{2.36}$$

Equation (2.36) suggests that dispersivity is not only a function of porous media properties such as grain size (contained within the Peclet number) but also of the competition between advective and diffusive processes.

2.6.2 Effects of reactive mixing

There are many examples in the literature of modelling solute transport and reaction in homogeneous porous media, e.g., Prommer *et al.* (2002). A common practice in these modelling studies is to employ in the reactive modelling, parameters (like dispersivity) derived from non-reactive transport. Experimental investigations by Gramling *et al.* (2002), and Huang (2002) suggested that this approach could lead to erroneous estimates of reactive mixing. In the former, one-dimensional experiments were performed in homogeneous porous media where an instantaneous reaction occurred between two mixing solutes. Their results showed that the dispersivity obtained from the conservative experiments had to be decreased in order to match the reactive experiments. Conversely, experiments by Huang (2002) using two-dimensional reactive plumes showed that dispersivity obtained from tracer experiments had to be increased in order to model the reactive experiments. However, in a recent publication by Ham *et al.* (2007) two-dimensional reactive plumes are successfully modelled using dispersivity values derived from conservative experiments. Dispersivity is calculated from a similar

equation to (2.36). This finding contradicts the previous observations. The difference may reside in that the modelling approach used by Gramling and Huang assumed that the linear relationship between the dispersion coefficient and fluid velocity holds, whilst Ham's starting point is the assumption of a non-linear relationship (i.e, expression 2.34).

2.6.3 Effects of variable density

Another deviation from the classical Fickian theory is seen when the dispersive process is affected by large concentration differences between the mixing fluids. In effect, several authors investigating vertical brine transport have concluded that the Fickian theory cannot adequately model the experimental results (Hassanizadeh & Leijnse, 1995; Schotting *et al.*, 1999). In that case, two possibilities have been investigated: the linear form of (2.5) and (2.32) remains valid but the dispersivities are fitted for each experimental run. This implies that dispersivity is not constant and is made function of the prevailing conditions at each experiments in terms of density difference. Another possibility explored by Hassanizadeh & Leijnse (1995) is that the linear relationship between dispersive mass flux and concentration gradient is replaced by a nonlinear equation where additional terms are introduced into (2.5). This topic will be further reviewed in Chapter 3.

2.6.4 Effects of scale and heterogeneity

A quick look at literature values on transverse dispersion shows that neither scale (laboratory/field scale) nor heterogeneity seem to have a big impact on the transverse dispersivity value. Table 2.2 lists some literature data on reported transverse dispersivity for laboratory studies and field data.

Authors	*Description of medium*	d_{50} (mm)	α_T (mm)
Klenk and Grathwohl (2002)	Homogeneous, lab-scale tank (1.5 m)	0.3 – 2	0.25 – 0.6
Olsson (2005)	Homogeneous, lab-scale tank (0.29m and 0.78 m)	0.1 – 2.3	0.02 – 0.3
Rahman et al (2005)	Heterogeneous, medium-scale tank (14 m)	0.1 – 3	0.06
Fiori and Dagan (1999)	Field scale (Borden Site and Cape Cod)	0.1 – 2	≈ 0.5
Prommer et al (2002)	Heterogenous, field scale	–	0 – 4

Table 2.2: Examples of transverse dispersivity values from literature data.

This leads to values of transverse dispersivity for laboratory and field scale varying between 0.02 - 4 mm for homogeneous and heterogeneous media. In con-

trast, numerical studies typically adopt dispersivity values larger by two to three orders of magnitude. This large discrepancy between measured values and adopted modelling values could have an origin in the fact that the ratio $\alpha_T = 1/10 \cdot \alpha_L$ is typically used. This ratio was first proposed by List and Brooks (1967) in their review of lateral dispersion from laboratory data. Most of the data reviewed consisted of experiments in homogeneous media, hence α_L was not significantly larger than α_T. However, at field scale, α_L may be in the range of metres (due to permeability heterogeneity), hence adopted α_T is large.

The observation that transverse dispersivity is not influenced by an increase of scale is in accordance with the work of De Josselin de Jong (1958) (see section 2.4.1). The fact that an increase in heterogeneity does not substantially increase the value of α_T may be explained with the help of Figure 2.6. In this figure, a simplified representation of an heterogeneous aquifer is shown where solute is released at x=0 and travels in parcels (or stream-tubes). The resulting concentration distribution measures the combined effects of macro-dispersion and advection on the solute spreading. This can result in a large longitudinal dispersivity value. However, as reviewed earlier, the mechanisms of transverse dispersion differ to those of longitudinal dispersion. Mixing in the transverse direction implies that the parcels of solute exchange stream tubes perpendicular to the main flow direction. The processes responsible are micro-scale (pore-scale) dispersion and molecular diffusion. Thus, despite a large value of longitudinal dispersivity, $\alpha_T \ll \alpha_L$. Note that micro-scale dispersion and molecular diffusion also contribute to longitudinal dispersion. However, their net effect in the macrodispersion is considered small.

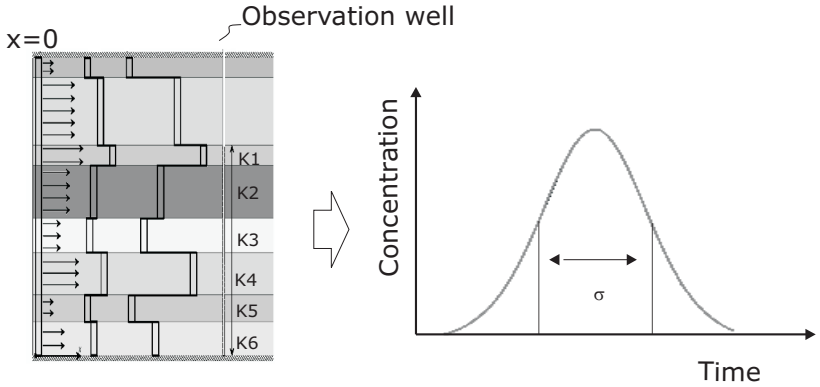

Figure 2.6: Schematics of an heterogeneous aquifer and the effects of advection on solute spreading.

Bibliography

Aris, R., 1956. On the dispersion of a solute in a fluid flowing through a tube. Proc. R. Soc. London, Ser. A 235, 67-77.

Bear, J. Dynamics of Fluids in Porous Media. American Elsevier, New York, 1972.

Bear, J., and Bachmat, T., 1967. A generalized theory on hydrodynamic dispersion in porous media. IASH Symp. Haifa, Publ., 72, 7-16.

Blackwell, R.J., 1959. Experiments on mixing by fluid flow in porous media. Proceedings of Amer. Inst. Chem. Eng. and Soc. Petrol. Eng. 29.

Brown, R., 1828. A brief account of microscopical observations. Philos. Mag. 4, 161-173.

Dagan, G. 1982. Stochastic modeling of groundwater flow by unconditional and conditional probabilities 2: The solute transport. Water Resour. Res. 18, 835-848.

Dagan, G. 1984. Solute transport in heterogeneous porous formations. J. Fluid Mech. 145, 151-177.

de Josselin de Jong, G., 1958. Longitudinal and transverse diffusion in granular deposits. Transactions of the American Geophysical Union 39, 67-74.

Fried, J.J., Combarnous, M.A., 1971. Dispersion in Porous Media. Advances in Hydroscience 7, 169-282.

Gelhar, L.W., Gutjahr, A.L., Naff, R.L., 1979. Stochastic analysis of macrodispersion in a stratified aquifer. Water Resour. Res. 15, 1387-1397.

Gelhar, L.W., Axness, C.L., 1983. Three-dimensional stochastic analysis of macrodispersion in aquifers. Water Resour. Res. 19(2), 161-180.

Gramling, C.M., Harvey, C.F., Meigs, L.C., 2002. Reactive transport in porous media: A comparison of model prediction with laboratory visualization. Environmental Science and Technology 36(11), 2508-2514.

Grane, F.E., Gardner, G.H.F., 1961. Measurements of transverse dispersion in granular media. J. Chem. Eng. Data 6(2), 283-287.

Grathwohl, P., 1998. Diffusion in Natural Porous Media: Contaminant Transport, Sorption/Desorption and Dissolution Kinetics. Kluwer Academic Publishers, Boston, pp 224.

Griffiths, A., 1911. Proc. Phys. Soc. Lond., 23, 190.

Ham, P.A.S., R.J. Schotting, H. Prommer, and G.B. Davis, 2004. Effects of hydrodynamic dispersion on plume lengths for instantaneous bimolecular reactions. Adv. in Water Resour 27(8), 803-813.

Ham, P.A.S., Prommer, H., Olsson, Å.H., Schotting, R.J., Grathwohl, P., 2007. Predictive modelling of dispersion controlled reactive plumes at the laboratory-scale. J. Contam. Hydrol. 93(1-4), 304-315.

Harleman, D.R.F., Rumer, R.R., 1963. Longitudinal and lateral dispersion in an isotropic porous medium. J. Fluid Mech. 16, 385-394.

Hassanizadeh, S.M., and Leijnse, A., 1995. A non-linear theory of high-concentration-gradient dispersion in porous media. Adv. Water Resour., 18, 203-215.

Hellström, G., Tsang, C. F., and Claesson, J., 1988. Buoyancy flow at a two-fluid interface in a porous medium: analytical studies. Water Res. Research, 24(4), 493-506.

Huang, W.E., 2002. The role of transverse mixing of electron acceptors and carbon substrates in natural attenuation. PhD thesis, University of Sheffield, Sheffield.

Johannsen, K., 2003. On the validity of the Boussinesq approximation for the Elder problem. Computational Geosciences, 7(3), 169182.

Klenk, I.D., Grathwohl, P, 2002. Transverse vertical dispersion in groundwater and the capillary fringe. J. Contam. Hydrol. 58, 111-128.

Landman, A.J., 2005. Analysis of physical mechanisms underlying densitydependent transport in porous media, Ph.D. Thesis, Delft University of Technology.

Landman, A.J., and Schotting, R.J., 2007. Heat and brine transport in porous media: the Oberbeck-Boussinesq approximation revisited. Transport in Porous Media, 70, 355-373.

Olsson, Å.H., 2005. Investigation and modelling of dispersion-reaction processes in natural attenuation groundwater. PhD thesis, Eberhard-Karls Universität of Tübingen, Tübingen.

Olsson, Å.H., Grathwohl, P, 2007. Transverse dispersion of non-reactive tracers in porous media: A new nonlinear relationship to predict dispersion coefficients. J. Contam. Hydrol. 92, 149-161.

Perkins, T.K., and Johnston, Q.C., 1963. A review of diffusion and dispersion in porous media. Soc. Petrol. Engrs. J. 3(1), 7086.

Prommer, H., Davis, G.B., Barry, D.A., 2002. Modelling of physical and reactive processes during biodegradation of a hydrocarbon plume under transient groundwater flow conditions. J. Cont. Hydrol., 59, 113-131.

Saffman, P.G., 1959. A theory of dispersion in a porous medium. J. Fluid Mech. 6(3), 321349.

Saffman, P.G., 1960. Dispersion due to molecular diffusion and macroscopic mixing in flow through a network of capillaries. J. Fluid Mech. 7(2), 194-208.

Scheidegger, A.E., 1954. Statistical hydrodynamics in porous media. J. Appl. Phys. 25(8), 994-1001.

Scheidegger, A.E., 1961. General theory of dispersion in porous media. J. Geophys. Res. 66(10), 3273-3278.

Schotting, R.J., Moser, H., Hassanizadeh, S.M., 1999. High-concentration-gradient dispersion in porous media: experiments, analysis and approximations. Adv. Water Resour. Res. 22(7), 665-680.

Taylor, G., 1953. Dispersion of soluble matter in solvent flowing slowly through a tube. Proc. R. Soc. Ser. A 219, 186-203.

Watson, S.J., Barry, D.A., Schotting, R.J., and Hassanizadeh, S.M., 2002. Validation of classical density-dependent solute transport theory for stable, high-concentration-gradient brine displacements in coarse and medium sands. Adv. Water Resour. Res. 25, 611-635.

Chapter 3

Density-dependent dispersion: overview

This Chapter summarises previous work and main findings concerning density-dependent dispersion. Although this thesis is primarily concerned with transverse dispersion, vertical brine transport is reviewed in order to draw general conclusions on the main mechanisms affecting dispersion.

3.1 Background

Problems involving dispersion of a solute with variable density and/or viscosity are commonly found when dealing with flow through porous media. Some examples of which include the intrusion of seawater in exploited coastal aquifers, infiltration of landfill leachate and in general brine transport of pollutants or radionuclides released from a repository salt formations. In these circumstances, knowledge is required of the mixing processes that occur between the fluids. In particular, information should include the role of the density difference and the interplay with porous media characteristics such as permeability and heterogeneity (Landman, 2005).

As discussed in Chapter 2, dispersive mixing is typically modelled using the classical Fick's Law of diffusion, which assumes the dispersive mass flux to be proportional to the concentration gradient,

$$\mathbf{J} = -\mathbf{D} \cdot \nabla C, \tag{3.1}$$

where $\mathbf{J}$ is the dispersive mass flux vector, and $\mathbf{D}$ is the dispersion tensor. According to this equation the dispersion tensor is assumed to be independent of the solute concentration and its gradient. However, it is dependent of fluid velocity, v, following, e.g., Scheidegger (1961),

$$\mathbf{D} = (D_e + \alpha_T v)\mathbf{I} + (\alpha_L - \alpha_T)vv/|v|, \tag{3.2}$$

where D_e is the (effective) molecular diffusion coefficient, α_L and α_T are the medium constants longitudinal and transverse dispersivities, respectively, $\mathbf{I}$ is the unit tensor, and $|v|$ is the magnitude of the fluid velocity vector, v. For almost homogeneous media and tracer conditions, the Fickian dispersion theory seems to give satisfactory results when modelling hydrodynamic dispersion, though shortcomings have been observed. A notorious one is regarding the dependence of the dispersion coefficient on fluid velocity. Analysis of experimental data on tracer dispersion show that for a given range of Peclet values, the longitudinal dispersion coefficient increases roughly linearly with velocity, whereas the transverse dispersion coefficient has a non-linear (< 1) dependence on velocity (Klenk & Grathwohl, 2002). Thus, the dispersivities (longitudinal and transverse) are no longer property of the porous medium but are a function of the flow characteristics. However, this deviation is considered small and often neglected for practical applications. The effects of fluid velocity on transverse dispersivity are further discussed in next Chapter.

Another deviation from the classical Fickian theory is seen when the dispersive process is affected by large concentration differences between the mixing fluids. In effect, several authors investigating vertical brine transport have concluded that the Fickian theory cannot adequately model the experiments results and additional fitting must be introduced (Watson *et al.*, 2002). In this case, two possibilities have been investigated: the linear form of (3.1) and (3.2) remains valid but the dispersivities are fitted for each experimental run. The dispersivity is a function of the density difference and fluid velocity for each experiment. Another possibility explored by Hassanizadeh & Leijnse (1995) is a modified non-linear form of (3.1):

$$(1 + \beta\,|\mathbf{J}|)\mathbf{J} = -\mathbf{D} \cdot \nabla C. \tag{3.3}$$

In this expression, $|\mathbf{J}|$ is the magnitude of the dispersive mass flux, and β is a new additional dispersion parameter. According to Hassanizadeh & Leijnse (1995) the β parameter represents the resistance of the system to disperse the solute due to the existence of a concentration gradient. The non-linear model (3.3) has been validated by Schotting *et al.* (1999), and Watson *et al.* (2002) in their analysis of experimental data of transport in vertical columns.

It should be noted that the kind of deviation from the classical Fick's law imposed by the presence of a high-concentration gradient seems to be far greater than that caused by the effects of fluid velocity and therefore, cannot be easily neglected. As a general rule and for stable displacements, it has been observed that the presence of a large density difference suppresses dispersive mixing. It has also been shown that this behaviour is not caused solely the the presence of a difference in density but also by the interaction with other variables, namely, permeability heterogeneities, and flow velocity (Landman, 2005). In the following, a brief recount of previous experimental and numerical work on vertical brine

transport is given. The aim is to summarise main findings on the mechanisms controlling high-concentration gradient dispersion. The focus is always on stable displacements. Then, prior work concerning transverse brine dispersion is reviewed. This latter has been found to be limited in number and scope. However, main findings are reported in anticipation to the experimental programme presented in a following chapter. The chapter closes with a review of theoretical models for density-dependent dispersion.

3.2 Previous Work on Density-Dependent Dispersion

3.2.1 Longitudinal Dispersion

Several authors investigating the effects of increased density and/or viscosity on vertical transport have concluded that when the displacement is stable, i.e., the heavier fluid displaces the lighter fluid in upward flow, an increase in density leads to a decrease in dispersive transport. Other flow configurations have also been investigated, e.g., upward flow unstable displacement. Because this results in a completely different behaviour, they lie outside the scope of this thesis and will not be further reviewed.

Authors like Hassanizadeh *et al.* (1990); Watson *et al.* (2002) independently performed vertical displacement experiments in homogenous columns in which fresh water is displaced by a high-concentration salt solution (brine). For each experimental programme the number and experimental aims varied. However, they all show consisting results and complementary information could be gathered from each study. In summary:

- The longitudinal dispersion coefficient (and dispersivity) decreases with increasing concentration (density) difference.
- This decrease becomes less pronounced with increasing flow rate.
- If a brine displaces another brine of approximately the same density (difference in density is small), dispersion mechanisms are those of tracer dispersion. This suggests that it is the density difference and not the absolute value of density (or concentration) that plays a role.
- Darcy's Law remains valid for high-concentration transport.
- Fick's Law (linear form) cannot accurately predict high-concentration transport. A nonlinear behaviour becomes evident.

Though consisting general observations could be drawn from each of these experiments, the physical explanation of the underlying mechanisms causing the observed behaviour was not complete. Some initial insights were given by Perkins

& Johnston (1963) and Fried & Combarnous (1971) in their classical reviews of diffusion and dispersion in porous media. Both authors considered the influence of density contrast on dispersion and stabilizing gravity forces are signalled as the underlying physical mechanism. An alternative explanation of the observed behaviour was presented by Hassanizadeh & Leijnse (1995) whom introduced a nonlinear theory of high-concentration-gradient dispersion in porous media (see expression 3.3), and supported by their experimental findings. With this new theory, the authors were able to model the entire set of brine experiments using a fixed (tracer) dispersivity value and the new dispersion parameter, i.e., β in (3.3). It should be noted that although no velocity effects were reported, the experiments were also limited in number and scope. With the introduction of the parameter, β, the authors explain the suppression of dispersion as a result of an increase in resistance to dispersion due to the increase in concentration gradient. However, as stated in Schotting *et al.* (1999) that formulation, 'although formally correct, is not directly linked to the main processes suppressing dispersion'. In a qualitatively analysis of experimental data, Schotting shows the existence of two time-scales during vertical transport, the advective time-scale associated with the average flow in the column given by

$$t_{adv} = \frac{L}{q}, \tag{3.4}$$

where L is the column length. The second time-scale is associated with the action of gravity given by

$$t_g = \frac{\mu\alpha}{\Delta\rho g k}. \tag{3.5}$$

The ratio of these two time-scales is also known as the Rayleigh number, Ra, and is an indication of the significance of the gravity effect

$$Ra = \frac{t_c}{t_g} = \frac{kg\Delta\rho L}{\mu\alpha q}. \tag{3.6}$$

Gravitational forces are present due to the existence of horizontal density gradients. These density gradients are supported by the variations in local velocity which in turn are the result of the inhomogeneities of the porous medium. Even in a macroscopic homogeneous porous media like those of laboratory columns small scale heterogeneities are bound to be present which support these local velocity variations hence supporting mechanical dispersion. If gravity forces have enough time to interact with these velocity fluctuations, the mechanical component of hydrodynamic dispersion will be suppressed.

Whether the interaction between horizontal density gradients and gravity forces is indeed the underlying mechanism causing the decrease in dispersion was a topic of investigation in Landman (2005). In her research, high resolution numerical experiments are carried out mimicking in detail a two-dimensional porous medium. The porous medium used is not entirely homogenous and micro heterogeneities are

introduced in order to recreate what actually occurs in laboratory columns. Figure 3.1 shows an example of a laboratory column system and the numerical set-up used by Landman. Both systems consider stable upward displacement of fresh water by a high-concentrated salt solution entering the medium from the bottom end of the column.

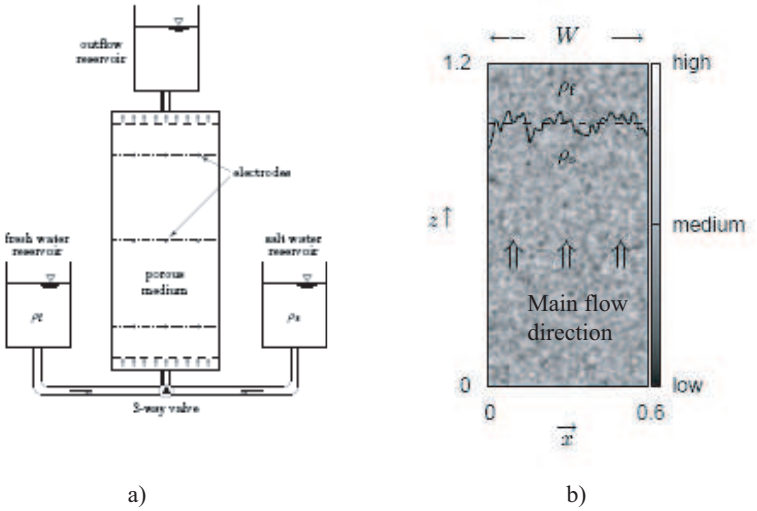

a) b)

Figure 3.1: a) Schematic representation of a set-up used in vertical brine displacement experiments. b) Set-up used in numerical experiments by Landman recreating an homogenous laboratory column with local variations in permeability. Modified from Landman (2005).

The set of plots in Figure 3.2 show the form of the dispersive front at the scale of permeability variations. This is equivalent to "zooming in" to a dispersive front during laboratory experiments in homogeneous columns. Figure 3.2a shows how a dispersive front looks like when there are no density differences, i.e., tracer conditions. If the density is increased, Figure 3.2b shows that the actual shape and size of the front does not vary. However, when gravity is incorporated like in Figure 3.2c there is an smoothing effect of the front to a more piston-like displacement. The net effect is a reduction on the width of the mixing zone, i.e., the vertical distance where concentration changes from 0 to 1 and therefore the dispersion coefficient.

Landman identifies that the parameter controlling the size of the mixing zone is the ratio between the density difference, $\Delta\rho$, and and the mean specific discharge,

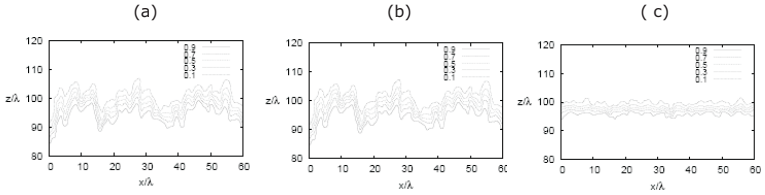

Figure 3.2: Concentration contours for: (a) tracer conditions, (b) increasing the density difference but no gravity effect (i.e., $g = 0$), and (c) tensity differences with gravity incorporated. Modified from Landman (2005).

q, or more specifically the gravity number, Ng,

$$\mathrm{Ng} = \frac{kg\Delta\rho}{\mu q}. \tag{3.7}$$

The gravity number expresses the relative strength of the gravity-induced flow to convection. Note that Ng does not include a characteristic length scale. Keeping k, and μ constant, a small gravity number implies that gravity forces do not have enough time to smooth out the unevenness of the front because the travel velocity is higher. A large gravity number implies a smaller travel velocity and a large density contrast. The strength of the gravity forces may eliminate almost entirely the front unevenness. This result is also supported when comparing the apparent decrease in dispersivity reported in laboratory experiments and the apparent decrease seen in the numerical simulations. Figure 3.3 is a plot of the laboratory-determined dispersivities reported in various studies and the numerical results. As a direct comparison with the absolute dispersivity value is not possible, a plot of the apparent decrease seems more plausible. From Figure 3.3 some interesting conclusions can be drawn: i) the apparent decreases shown by experimental results from homogenous systems could be made function of the gravity number, confirming observations in Landman (2005); ii) the apparent decrease for heterogeneous media is less pronounced compared to that of an homogenous medium. This conclusion is also reported by Landman in her results for media with increasing heterogeneity; iii) dispersivity becomes a function of the gravity number.

These complementary observations have helped building a more complete picture of the specific mechanisms acting during vertical brine transport. It is anticipated that the latter effects, although of similar nature, be quantitatively different for transverse dispersion. This because of the differences in magnitude and direction of the interacting forces.

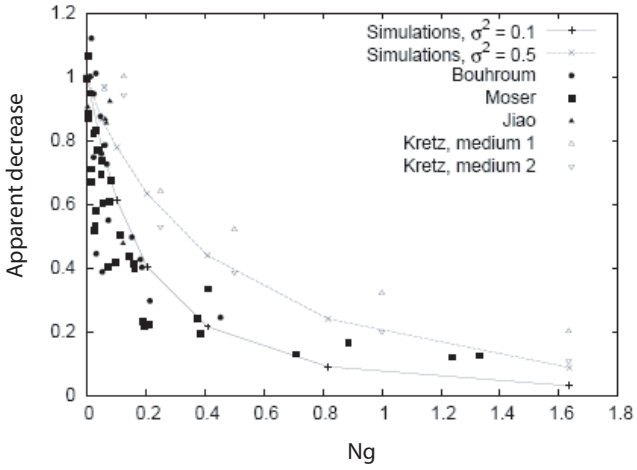

Figure 3.3: Apparent dispersivity decrease. Comparison between laboratory-determined apparent decrease and numerical results from Landman. Solid markers correspond to results from homogenous columns. Open markers correspond to results from heterogenous columns. Modified from Landman (2005).

3.3 Transverse Dispersion

3.3.1 Laboratory experiments

A search through the literature identified only few experimental studies with focus on the effects of density differences on transverse dispersion for horizontal flow conditions. The following briefly reviews these studies, and where possible, results are plotted in terms of dispersivity decrease and Ng. Dispersivity is obtained, unless otherwise stated, following the linear relationship

$$D_T = D_e + \alpha_T v \tag{3.8}$$

where D_e is obtained from $D_e = D_{mol} \cdot n$. It should be noted that these laboratory studies assume that the governing mixing equations for experiments with density contrasts are the same as those for tracer experiments. However, it has been shown that the differences in density influence the degree of dispersion. Therefore the obtained D_T and hence α_T will be an "apparent" value. Equally, velocity effects may play a role in the obtained values. When experimental parameters needed were not directly reported, the appropriate assumptions made to obtain such values are explained.

Grane and Gardner, (1961)

These authors carried out a series of laboratory experiments in homogenous media to investigate the effects of flow velocity and porous media characteristics on transverse dispersion. For most of the experimental runs density differences between fluids were kept low. However, for a set of experiments the density difference is increased and a significant decrease in the amount of mixing is observed. The authors concluded that density differences are important when the permeability of the medium is large. These experiments consisted in keeping a constant fluid velocity, $v = 0.02$ m/s and increasing the difference in density up to 10%. Porosity is reported to be around 40% for an average grain diameter, $d_{50} = 1.5$ mm, $D_{mol} = 1.2 \cdot 10^{-9}$ m^2/s and $\mu = 1.38 \cdot 10^{-3}$ Pa $\cdot$ s. Permeability is calculated using the Carmen-Kozeny relationship yielding $k = 2.2 \cdot 10^{-9}$ m^2. The dispersion coefficient is extracted from Figure 3 in (Grane & Gardner, 1961). In Figure 3.4 the decrease in dispersivity with gravity number is plotted.

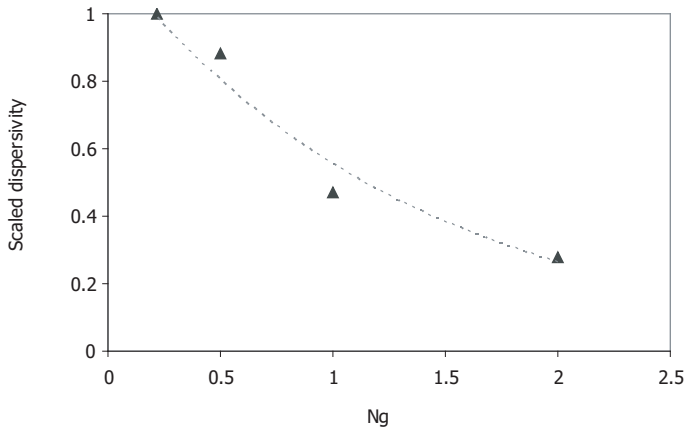

Figure 3.4: Scaled transverse dispersivity as function of gravity number from Grane and Gardner experiments.

Leroy *et al*, (1992)

Tracer dispersion experiments were carried out for stable and unstable upward flow configurations. The effects of small density variations like those occurring during tracer dispersion experiments was investigated using homogeneous and stratified porous media. The authors reported that even when the difference in density is low, extra velocity components appear inducing rotational flows which in turn tend to smooth out the unevenness of the dispersive front. The flows induced by

these small density differences are minute and will only be of significance when the mean flow velocity is also small and if the medium is heterogeneous (Leroy *et al.*, 1992).

Starke and Koch, (2005)

The authors studied the interplay between porous media heterogeneities and density contrast on transverse macrodispersion. A series of intermediate-scale laboratory experiments were carried out in which heterogeneities (in the permeability field) are created using packed sand structures (see Figure 3.5). The fluid system used is that of fresh water - salt water.

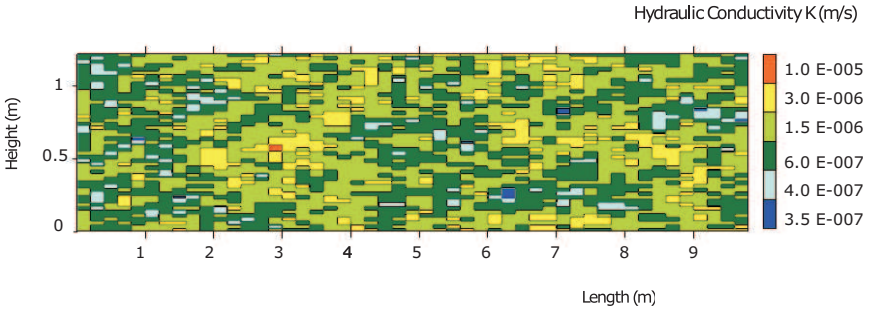

Figure 3.5: Example of a stochastic realization of the hydraulic conductivity field used in experiments by Starke (2005).

The flow configuration is always stable and the density difference is varied from tracer conditions up to a $\Delta\rho = 65$ kg/m^3 for three different fluid velocities. The same series of experiments are repeated using three different degrees of system heterogeneity, referred to in their study as *pack 1*, *pack 2* and *pack 3* respectively. Figure 3.6 shows the experimentally-determined dispersivity as a function of velocity for *pack 2* and *pack 3* (see Starke & Koch (2006)). From these plots a small increase in dispersivity with increasing heterogeneity is observed (σ^2 equals to 1 and 1.5 for pack 2 and pack 3 respectively). For a fixed velocity, both systems show a reduction in dispersivity with increasing density contrast. Another apparent decrease is evident in both systems when the fluid velocity is increased (similar behaviour than observed in homogenous media). However, it appears that this velocity effect becomes less significant for increasing density differences.

Results are now plotted in terms of scaled dispersivity and gravity number (Figure 3.7). Dispersivities, fluid velocities and density contrasts are obtained from Starke (2005). Gravity numbers are calculated with the geometric mean of the permeability using reported values $k_2 = 1.79e^{-10}$ m^2 and $k_3 = 1.91e^{-10}$ m^2, and porosity values $n_2 = 44\%$ and $n_3 = 38\%$, for *pack 2* and *pack 3*, respectively.

In order to obtained the apparent decrease in dispersivity as a function of Ng shown in Figure 3.7, the scaling used in Landman (2005) is also employed here:

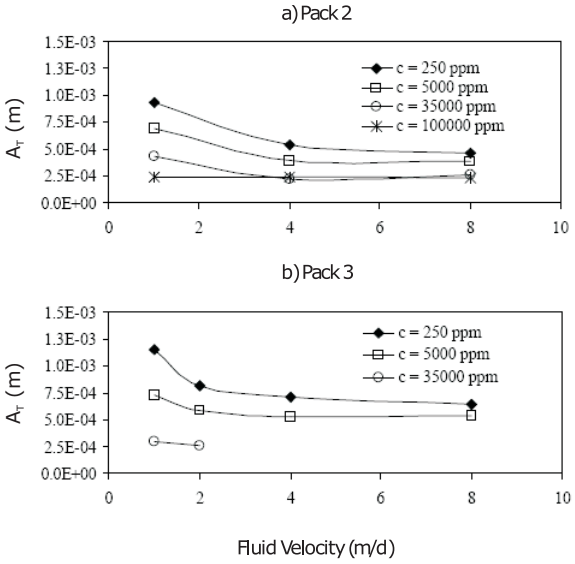

Figure 3.6: Variation of transverse macrodispersivity with fluid velocity for pack 2 and pack 3 systems. Modified from Starke (2005).

dispersivities obtained from brine experiments are scaled by the tracer dispersivity, i.e., the dispersivity obtained from the experiment with the lowest gravity number (see Figure 3.7a). Landman states that it is the apparent decrease that is of interest and not the absolute dispersivity value. Indeed, and recalling Figure 3.3 this scaling was necessary in order to compare her numerical results and the relative decrease seen in laboratory experiments. However, and as opposed to longitudinal dispersion, transverse dispersion experiments have shown that there already exists a relative decrease in dispersivity solely by virtue of increasing fluid velocity (even if density differences are kept to the minimum). This implies that if the scaling is done using the dispersivity from the lowest Ng experiment (i.e, highest velocity), this dispersivity is at an already decreased value and the scaling results in numbers larger that the unity and a larger data scatter as seen in Figure 3.7a. If now the scaling is done using the dispersivity corresponding to the tracer experiment for a fixed velocity (see Figure 3.7b) there is a less scatter of the data and a higher supression is observed. Figures 3.7a and 3.7b also show that an increase in heterogeneity, i.e., increasing σ^2 does not seem to play a role in the apparent decrease.

3.3.2 Numerical Modelling

The benchmark experimental study 'saltpool' problem was initially introduced in Oswald (1999) and more recently in Oswald & Kinzelbach (2004). The experiments

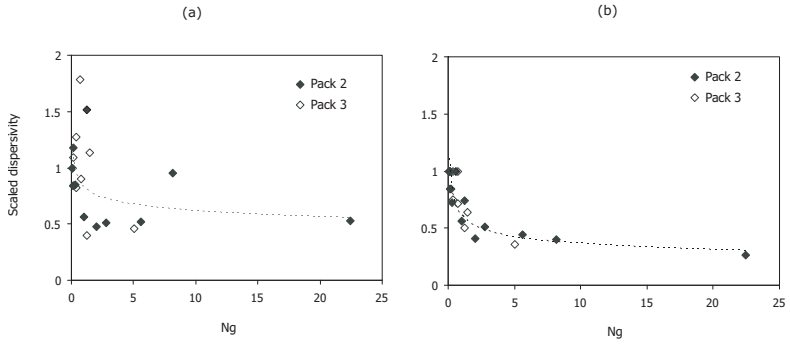

Figure 3.7: Comparison of dispersivity scaling for results from Starke (2005).

resemble the upconing of a saltwater-freshwater interface due to pumping. The system is stable, i.e., the layer of salt is below the layer of freshwater, affected by recharge and discharge of water at the top. Two cases were considered: a low concentration case ($\omega = 1\%$) and a high concentration case ($\omega = 10\%$). A schematics of the experimental set-up used is shown in Figure 3.8.

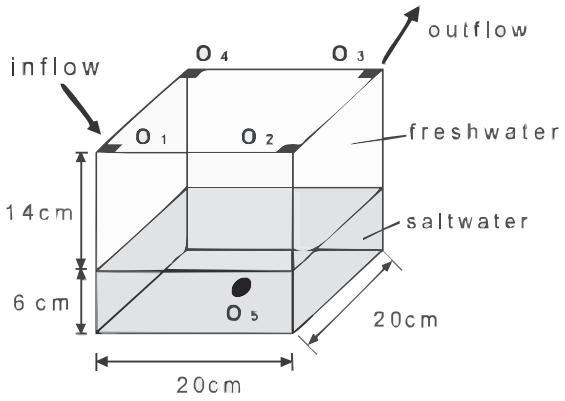

Figure 3.8: A schematic view of the saltpool experimental set-up. Image from Oswald & Kinzelbach (2004).

Breakthrough curves are measured in the outlet of the box and nuclear magnetic resonance (NMR) techniques are used to map the salt concentration distribution in the box, including its time-evolution. Results show that even for the high-concentration case, the interface widens and forms in fact a transition zone between freshwater and saltwater rather that a non-dispersive interface (Oswald & Kinzelbach, 2004).

The saltpool problem was recently modelled by Johannsen *et al.* (2002) using the variable-density flow package d^3f. Due to very small dispersivities and a large density contrast, particularly for the high concentration case, a very high spatial grid resolution was needed in order to better fit the breakthrough curves (up to 16 million grid points with a mesh level up to $l = 8$). Using the Frolkovic-Knabner algorithm for consistent velocity approximation proved essential in order to better approximate the breakthrough curves. In addition, the authors find that three other parameters have to be adjusted for both the low concentration experiment and the high concentration experiment: permeability, porosity, and transverse dispersivity. Concentration-induced changes in viscosity had to also be considered. The main findings of this modelling study are:

1. The minimum mesh level required to model high-concentration gradient conditions is $l = 6$.

2. The use of a consistent velocity approximation was fundamental in the successful modelling of high-concentration case. Small inconsistencies in the velocity field had significant impact in the computed results.

3. In order to achieve a better fit, three parameters had to be adjusted simultaneously for the saltpool 1 and saltpool 2 cases: permeability needed to be increased, transverse dispersivity and porosity had to be reduced. In addition, concentration-induced viscosity variations had to be taken included.

4. The numerical code d^3f used to model the experiments is based on the linear forms of Darcy's and Fick's law as well as commonly used equation of state for concentration-induced density and viscosity variations. This implies that the use of a nonlinear models like in Hassanizadeh & Leijnse (1995) or Schotting *et al.* (1999) did not have to be considered. On the other hand, no attempt was made to model the experiments with the nonlinear model. Thus, discrimination between approaches, i.e., classical linear model vs. nonlinear models could not be concluded at this stage.

An important result from the numerical computations is the apparent decrease in transverse dispersivity, in particular for the high-concentration case. The interplay between high concentration gradients and hydrodynamic dispersion seems to be one of the underlying mechanisms. Other factors could explain the need to adjust the dispersivity values. The transverse dispersivity was in fact inferred from the ratio $\alpha_T = 1/10 \cdot \alpha_L$ and not experimentally determined. The reported value was $\alpha_T = 0.12$ mm. However, the flow velocity used in the saltpool experiments had a relatively high value ($v = 4.8 \cdot 10^{-3}$m/s) for an equivalent Peclet number (Pe = 412). If the nonlinear relation introduced in Chapter 2 is used to account for the effects of velocity in the apparent dispersivity value (see Chapter 2), α_T yields a value of 0.062 mm. This is almost 50% decrease compared to the assumed value in the saltpool experiments.

3.3.3 Theoretical Studies

Non-linear model by Hassanizadeh and Leijnse, 1995

In this work, Hassanizadeh and Leijnse question the applicability of Fick's law for describing hydrodynamic dispersion processes under conditions of high-concentration gradient between the mixing fluids. The authors argue that the assumption of a linear dependency of the dispersive flux on the concentration gradient breaks down when large concentration variations are encountered. As the authors explain, the spreading of the salt from high concentration areas to low concentration areas is opposed by some force, τ^s, which represents the resistance of the porous medium to disperse the salt. This force is assumed to be dependant on fluid flow, $\mathbf{q}$ and may be represented by a Taylor series in terms of the dispersive mass flux, $\mathbf{J}$. Neglecting all terms higher that second order, τ^s is defined as

$$\tau^s = -\mathbf{R}^s(\beta|J| + 1)\mathbf{J} \tag{3.9}$$

where J is the magnitude of $\mathbf{J}$, $\mathbf{R}^s$ is a second-order tensor accounting for the porous medium resistance to solute dispersion, and β is a coefficient accounting for the non-linear effects. Both $\mathbf{R}$ and β are considered to be independent of $\mathbf{J}$ but may still be dependent on $\mathbf{q}$. The resulting nonlinear dispersion equation is given by

$$\mathbf{J}(\beta|J| + 1) = -\mathbf{D}\rho\,\nabla\omega \tag{3.10}$$

where β is a high-concentration coefficient which is porous-medium function and may depend on the flow velocity, $\mathbf{D}$ is the dispersion tensor, and ω is the salt mass fraction which is defined as the salt concentration divided by the fluid density. Expression (3.10) is considered to be valid for a wide range of concentration and concentration gradients. When the dispersive flux is small or when β is zero, (3.10) reduces to the linear Fick's Law.

In Hassanizadeh & Leijnse (1995) the authors supported the validity of equation (3.10) with findings from their series of stable vertical displacement experiments in homogenous porous media. Their results show a consisting decrease of the dispersivity with increasing density difference. Moreover, the authors show that allowing the dispersivity to be a function of the salt concentration would not exhibit a good agreement between simulated and measured profiles. Instead, a single dispersivity value is obtained from the tracer experiments which is fixed and later used to extract the value the parameter β from their brine experiments. With this unique value of β all subsequent high-concentration experiments could be modelled satisfactorily, independently of the concentration difference (or gradient). However, due to the small number of experimental runs no statement could be made on the dependence of β on flow velocity. This was later shown in the experimental results by Moser (1995) and Watson (2002) and the analysis by Schotting *et al.* (1999). Schotting shows that the relationship of β with the

specific discharge q may be of the form

$$\beta = A\, q^{-b} \tag{3.11}$$

where A and b are determined experimentally. This velocity-dependency was obtained by analysis of constant-density experiments in which the concentration difference is kept constant and the flow velocity is varied. Results from these experiment type show that as the flow rate increases, the difference between the tracer dispersion coefficient and the brine dispersion coefficient decreases. That is, the high-concentration dispersion coefficient approaches the value of the tracer coefficient at higher flow rates. This suggests that the physical mechanisms underlying this behaviour are the result of an interplay between convective mechanisms due to local velocity variations and gravity effects as a result of concentration gradients. Moreover, it indicates the existence of two time-scales associated with the former and latter mechanisms (Schotting *et al.*, 1999). Hassanizadeh and Leijnse emphasize that the observed nonlinear effects, i.e, deviations from the classical linear Fick's law, could not be related to the existence of heterogeneities as their study involved the use of homogeneous column systems. However, and as shown by Landman (2005), even in porous media essentially homogenous, small-scale inhomogeneities are always present creating microscale velocity variations that are affected by stabilizing gravity forces.

It should be noted that the proposed model, although in principle applicable for two- or three-dimensional systems, has only been tested under one-dimensional vertical flow conditions. It is one the objectives of this thesis to test the applicability of the proposed nonlinear equation. For transverse dispersion, the experimental observations should verify:

$$\frac{D_{T(B)}}{D_T} = \frac{2}{1 + \sqrt{1 - \ 4\beta\rho D_T \frac{d\omega}{dy}}} \tag{3.12}$$

Solving for β and defining $\theta = \frac{D_{T(B)}}{D_T}$, the expression reads,

$$\beta = \frac{1 - \left(\frac{2}{\theta} - 1\right)^2}{4\rho D_T \frac{d\omega}{dy}} \tag{3.13}$$

Thiele, 1997

The author derives a series of approximated analytical solutions to the transverse mixing in homogeneous porous medium of two fluids flowing parallel to each other varying only in concentration. Within the frames of the boundary layer theory and assuming a constant fluid's diffusion coefficient and constant dispersivity, both stable and unstable flow conditions are analysed. As the latter falls outside the scope of this thesis, it will not be further reviewed here. Moreover, the author utilizes two common dispersion models, the 'Scheidegger' model which assumes a

linear relationship between mechanical dispersion and fluid velocity (Scheidegger, 1961), and a more complicated dispersion model proposed by Bear & Bachmat (1967) which relates the dispersion coefficient to a more complex function of the molecular Peclet number. Adopting the Boussinesq approximation (see Chapter 2) and using the Bear & Bachmat model, the solution for the normalized density-dependent concentration, $\theta = C/C_0$ is given by the following series expansion

$$\theta(\xi,\eta) = \frac{1}{2}\left(1 - \operatorname{erf}\frac{1}{2}\eta\right) - \frac{\beta}{4\sqrt{\pi}}\exp^{\frac{-\eta^2}{4}}\ \operatorname{erf}\frac{1}{2}\eta\cdot\xi\ + ... \tag{3.14}$$

note that the resulting concentration distribution is both a function of the so-called nonsimilarity variable ξ, given by

$$\xi = \frac{Ra_x}{Pe_x^{3/2}} \tag{3.15}$$

and the similarity variable η, given by

$$\eta = \frac{z}{x}Pe_x^{1/2} \tag{3.16}$$

where Ra_x and Pe_x are the x-dependent Rayleigh and Peclet numbers, respectively. These dimensionless groups are defined as

$$Ra_x = \frac{kg\rho(\delta c)x}{\mu D_T} \tag{3.17}$$

and

$$Pe_x = \frac{qx}{D_T} \tag{3.18}$$

The normalized concentration θ is also function of the factor β which represents the mechanical dispersion contribution to the total dispersion. For the Bear & Bachmat model β is given by

$$\beta = \frac{\alpha_T q}{D_{mol} + \alpha_T q} \tag{3.19}$$

Similar to Hassanizadeh & Leijnse (1995), Thiele analyses the effects of density on the transverse dispersion coefficient in terms of an apparent decrease of the density-affected dispersion coefficient, $D_{T\infty}$ in relation to the tracer dispersion coefficient, $D_{T\infty}$. This ratio is defined as

$$\frac{D_T(\rho)}{D_{T\infty}} = \left[\frac{\eta(\theta = 0.8413) - \eta(\theta = 0.1587)}{2\sqrt{2}}\right]^2 \tag{3.20}$$

Equation (3.20) implies that the apparent decrease can be obtained directly from the concentration profiles using the expression (3.14) for any value of the factor

β and nonsimilarity variable ξ. Another implication of this result is that the dispersion coefficient is obtained from the distance between two points, i.e., the 15.87% and 84.13% concentration isolines which also corresponds to twice the standard deviation, σ. This suggests that the resulting density-dependent concentration profile should be rotation symmetrical around the 50% isoline. This condition is observed in tracer experiments but that may not necessary hold for high-concentration experiments, as shown by Landman (2005).

Figure 3.9 shows some of the results in terms of apparent decrease of the coefficient as a function of β and Pe_x. From these plots it can be seen that the density effect is visible for Pe_x values between the unity and 10. For values less than the unity, i.e., in the pure molecular diffusion regime, density effects on the mixing zone are no longer visible. The same seems to hold when Pe_x grows beyond 10 and into the pure mechanical dispersion regime. Again, the density effect on the concentration distribution seem to diminish.

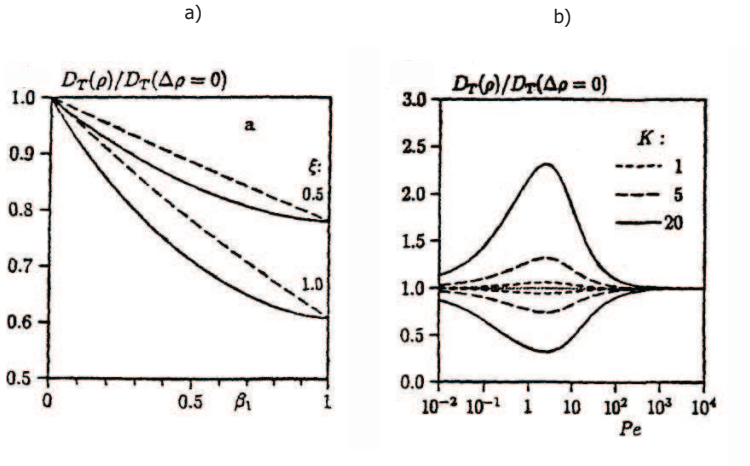

Figure 3.9: Apparent decrease of the dispersion coefficient as a function of: a) β and b) Pe

Homogenization Model of Demidov, 2005

Demidov employs the homogenization theory to analyse density-coupled flow and transport in porous media. Stable vertical and horizontal flow configurations are studied, but here only the horizontal stable situation is reviewed. The homogenization theory consists of a clear separation of scales and is applied at the small-scale (e.g., pore-scale) to derive a set of upscale equations that govern the macro-scale behaviour (i.e., the observation scale). In the following, only the main results of Demidov's work are summarised. A detailed derivation of the equations can be

found in Demidov (2005). In addition, in Chapter 5 a more extended analysis of his results and comparison with experimental data is presented.

The pore structure of the medium considered by Demidov is shown schematically in Figure 3.10.

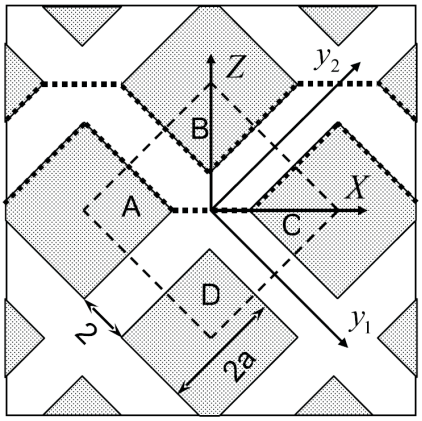

Figure 3.10: Mesh model of porous medium considered by Demidov.

The medium resembles a two-dimensional network of uniform, interconnected pores. Due to the periodicity of the medium, the 'mesh model' is solved only for the section ABCD given in Figure 3.10. The result is a set of macro-scale equations and coefficients containing already information on the microstructure of the porous medium. These coefficients are the effective dispersion coefficient $D_\perp$ and the filtration (permeability) coefficient K^0. Each coefficient exhibits different dependencies: the effective dispersion coefficient depends on the fluid velocity (and hence the Peclet number) and permeability (typically assumed a constant) is made function of the density gradient through the Rayleigh number. Both Peclet and Rayleigh numbers are in fact *local* and defined as:

$$Pe_l = \frac{vl}{d_m} \tag{3.21}$$

and

$$Ra_l = \frac{gl^4}{\mu d_m}\frac{\partial \rho}{\partial z} \tag{3.22}$$

where d_m denotes the molecular diffusion coefficient in free solution, and l refers to a representative pore-scale length, e.g., the pore size. The dependency of $D_\perp$ on Pe_l is given by

$$D_\perp(Pe_l, 0) = \zeta + D^0_\perp(Pe_l); \qquad D^0_\perp(0) = 0 \tag{3.23}$$

where ζ denotes the tortuosity coefficient and $D_\perp^0$ is the tracer dispersion coefficient. It should be noted that $D_\perp$, ζ and $D_\perp^0$ are in fact scaled coefficients, the scaling parameter being the molecular diffusivity d_m. In reference to the terminology used so far, ζ is equivalent to τ and $D_\perp^0$ is the scaled mechanical dispersion coefficient $\frac{D_{mec}}{D_{mol}}$

According to Demidov, density gradients affect both the effective dispersion coefficient and the permeability coefficient. The general form of expression (3.23) holds but in order to account for the density effects, 'correction factors' f_k and $f_\perp$ are introduced for each coefficient respectively. The permeability (filtration) coefficient defined in terms of a correction factor reads,

$$K = K^0 \cdot f_k \tag{3.24}$$

where K^0 is the value of permeability typically assumed constant, and K is the corrected permeability. Next, the correction factor for the dispersion coefficient is given by,

$$f_\perp = \frac{D_\perp - \zeta - D_\perp^\infty}{D_\perp^0 - D_\perp^\infty} \tag{3.25}$$

where $D_\perp^\infty$ denotes the effective dispersion coefficient at $Ra \to \infty$ and equals $\frac{1}{2n}$ with n being the porosity.

Next, the effective dispersion coefficient is obtained as the weighted average between limiting values,

$$D_\perp(\rho) = \zeta + D_\perp^0 \; f_\perp + D_\perp^\infty(1 - f_\perp). \tag{3.26}$$

Note that (ρ) was added to $D_\perp$ to distinguish from $D_\perp$ given by expression (3.23). Note also that in the limit of $f_\perp \to 0$, the tracer dispersion coefficient vanishes and $D_\perp^\infty$ tends to the constant value $1/2n$. In this limit the only mixing mechanism is molecular diffusion.

Demidov's results show that it is in fact the interaction between gravity forces and convective forces that affect the flow and transport at the pore-scale; molecular diffusion does not play a primary role. Hence, the effects can be quantified in terms of the local gravity number,

$$G_l = \frac{Ra_l}{Pe_l} = \frac{gl^3}{\mu v}\frac{\partial \rho}{\partial z}. \tag{3.27}$$

Assuming $\zeta = 0.589$, $n = 0.36$ and hence $D_\perp^\infty = 1.388$ two approximation curves for $f_\perp$ and f_k are as follow:

$$f_\perp = \frac{1 + 0.1\tilde{G}_l}{1 + 0.25\tilde{G}_l^{\,3/2}} \tag{3.28}$$

and

$$f_k = \frac{1 + 0.08G_l}{1 + 0.09G_l + 0.05G_l^{3/2}} \tag{3.29}$$

where $\tilde{G}_l$ is a scaled gravity number defined by $\tilde{G}_l = G_l/D^0_\perp$. According to Demidov, this scaling was necessary in order to group all the results along the same approximation curve. Equations (3.28) and (3.29) are in fact the main practical results of Demidov's work. In Chapter 5 results from laboratory experiments are analysed to assess the applicability of the proposed formulas.

3.4 Summary and Conclusions

An overview of previous experimental, numerical and theoretical work concerning density-dependent dispersion is presented in this Chapter. The main observations reported for longitudinal dispersion are:

1. Whenever high-concentration-gradients are present, gravity forces, acting at the small-scale, stabilise the the dispersion front. For an homogenous media like that of a laboratory column, local micro-heterogeneities in the permeability field cause perturbations (wiggles) in the front. These in turn generate horizontal density gradients in which gravity forces act upon. The result is a 'smoother' dispersive front also reduced in size. As the dispersion coefficient is related to the width of this front, this explains the observed reduction of the dispersion coefficient reported in the brine experiments by Hassanizadeh *et al.* (1990); Schotting *et al.* (1999); Watson *et al.* (2002)

2. Although it holds that for stable displacement, the higher the density difference between the fluids the stronger the stabilizing gravity effect, it also holds that the smaller the flow velocity the larger the gravity effect. Hence, stabilizing conditions are in effect an interplay between density difference and flow velocity. These are represented by the gravity number, Ng.

This Chapter also reviewed previous experimental and theoretical work in the context of density-dependent transverse dispersion. The former was found limited in scope and number, hence supporting the need of additional experimental data. In the following Chapter, transverse dispersion experiments are presented. Results from these experiments are used in Chapter 5 to compare with predictions of two theoretical models of density-dependent dispersion.

Bibliography

Bear, J. Dynamics of Fluids in Porous Media. American Elsevier, New York, 1972.

Bear, J., and Bachmat, T., 1967. A generalized theory on hydrodynamic dispersion in porous media. IASH Symp. Haifa, Publ., 72, 7-16.

Blackwell, R.J., 1959. Experiments on mixing by fluid flow in porous media. Proceedings of Amer. Inst. Chem. Eng. and Soc. Petrol. Eng. 29.

Dagan, G. 1982. Stochastic modeling of groundwater flow by unconditional and conditional probabilities 2: The solute transport. Water Resour. Res. 18, 835-848.

Dagan, G. 1984. Solute transport in heterogeneous porous formations. J. Fluid Mech. 145, 151-177.

de Josselin de Jong, G., 1958. Longitudinal and transverse diffusion in granular deposits. Transactions of the American Geophysical Union 39, 67-74.

Demidov, D., 2005. Upscaling of density-driven flow and transport, Ph.D. Thesis (in Russian), Kazan State University, Kazan, Russia.

Fried, J.J., Combarnous, M.A., 1971. Dispersion in Porous Media. Advances in Hydroscience 7, 169-282.

Gelhar, L.W., Axness, C.L., 1983. Three-dimensional stochastic analysis of macrodispersion in aquifers. Water Resour. Res. 19(2), 161-180.

Grane, F.E., Gardner, G.H.F., 1961. Measurements of transverse dispersion in granular media. J. Chem. Eng. Data 6(2), 283-287.

Hassanizadeh, S. M., Leijnse, A., de Vries, W. J., and Stapper, R. A. M., Experimental study of brine transport in porous media. RIVM Report 728514005, Bilthoven, The Netherlands, 1990

Hassanizadeh, S.M., and Leijnse, A., 1995. A non-linear theory of high-concentration-gradient dispersion in porous media. Adv. Water Resour., 18, 203-215.

Hellström, G., Tsang, C. F., and Claesson, J., 1988. Buoyancy flow at a two-fluid interface in a porous medium: analytical studies. Water Res. Research, 24(4), 493-506.

Johannsen, K., 2003. On the validity of the Boussinesq approximation for the Elder problem. Computational Geosciences, 7(3), 169182.

Johannsen, K., Kinzelbach, W., Oswald, S., and Wittum, G., 2002. The saltpool benchmark problem - numerical simulation of saltwater upconing in a porous medium. Adv. Water Resour. Res., 25(3),335-348.

Klenk, I.D., Grathwohl, P, 2002. Transverse vertical dispersion in groundwater and the capillary fringe. J. Contam. Hydrol. 58, 111-128.

Landman, A.J., 2005. Analysis of physical mechanisms underlying densitydependent transport in porous media, Ph.D. Thesis, Delft University of Technology.

Landman, A.J., and Schotting, R.J., 2007. Heat and brine transport in porous media: the Oberbeck-Boussinesq approximation revisited. Transport in Porous Media, 70, 355-373.

Leroy, C., Hulin, J. P., and Lenormand, R., 1992. Tracer dispersion in stratified porous media: influence of transverse dispersion and gravity. J. Contam. Hydrol., 11:,51-68.

Olsson, Å.H., 2005. Investigation and modelling of dispersion-reaction processes in natural attenuation groundwater. PhD thesis, Eberhard-Karls Universität of Tübingen, Tübingen.

Olsson, Å.H., Grathwohl, P, 2007. Transverse dispersion of non-reactive tracers in porous media: A new nonlinear relationship to predict dispersion coefficients. J. Contam. Hydrol. 92, 149-161.

Oswald, S.E., Kinzelbach, W., 2004. Three-dimensional physical benchmark experiments to test variable-density flow models. J Hydrol, 290(1-2), 22-42.

Oswald, S.E., 1999. Dichteströmungen in porẗ0sen Medien: Dreidimensionale Experimente und Modellierung. PhD Thesis, Schriftenreihe des Instituts für Hydromechanik und Wasserwirtschaft, ETH Zürich.

Perkins, T.K., and Johnston, Q.C., 1963. A review of diffusion and dispersion in porous media. Soc. Petrol. Engrs. J. 3(1), 7086.

Starke, B., 2005. Experimental and numerical investigations of macrodispersion of density-dependent flow and transport in stochastic porous media. PhD Thesis (in german), University of Kassel.

Starke, B., and Koch, M., 2006. Laboratory experiments and monte carlo simuations to validate a stochastic theory of density-dependent macrodispersion. Proceedings of the XVI Conference on Computational Methods in Water Resources, Copenhagen, Denmark.

Scheidegger, A.E., 1954. Statistical hydrodynamics in porous media. J. Appl. Phys. 25(8), 994-1001.

Scheidegger, A.E., 1961. General theory of dispersion in porous media. J. Geophys. Res. 66(10), 3273-3278.

Schotting, R.J., Moser, H., Hassanizadeh, S.M., 1991. High-concentration-gradient dispersion in porous media: experiments, analysis and approximations. Adv. Water Resour. Res. 22(7), 665-680.

Taylor, G., 1953. Dispersion of soluble matter in solvent flowing slowly through a tube. Proc. R. Soc. Ser. A 219, 186-203.

Thiele, M., 1997. Gravity affected lateral dispersion and diffusion in a stationary horizontal porous medium. Transport in Porous Media, 26, 553.

Watson, S.J., Barry, D.A., Schotting, R.J., and Hassanizadeh, S.M., 2002. Validation of classical density-dependent solute transport theory for stable, high-concentration-gradient brine displacements in coarse and medium sands. Adv. Water Resour. Res. 25, 611-635.

Chapter 4

Transverse dispersion: tracer and brine experiments

This Chapter presents the results of a laboratory investigation on transverse dispersion under tracer and high-concentration conditions. Mixing in the transverse direction is studied using a two-dimensional flow-trough tank packed with a homogeneous porous medium. Transverse dispersion coefficients are calculated from data obtained over a range of flow rates, for various density differences using two different types of porous media. Experimental results reported here will be used in Chapter 5 where the applicability of theoretical models on density-dependent dispersion is investigated.

4.1 Introduction

In recent years numerous investigations have been carried out to evaluate the mixing that occurs when a tracer, i.e., a fluid with equal density, equal viscosity to that of the ambient fluid, flows through a homogeneous porous medium. These investigations have helped improving the understanding of how the various microscopic mixing mechanisms can be characterised by the macroscopic dispersion coefficients. However, when the invading fluid exhibits distinct density and/or viscosity compared to the ambient fluid, these property differences can significantly influence the flow and transport through the porous medium (Diersch & Kolditz, 2002). A number of authors have investigated longitudinal dispersion of brine (and other concentrated solutions), see e.g., Hassanizadeh *et al.* (1990); Watson *et al.* (2002). However, transverse dispersion of brine has only occasionally been investigated. Chapter 3 gave a brief summary of some of the experimental studies reported in the literature. It was identified that for homogenous porous media complementary experimental results are needed in order to fully assess the effect of flow velocity and variations in density on the transverse dispersion coefficient.

Hence, the laboratory experiments presented here investigate transverse dispersion mechanisms under conditions of low-concentration gradient (tracer) and high-concentration gradient (brine). The displacement is always stable, i.e., the heavier fluid underlies the lighter fluid. Interaction between flow rate, porous media properties and density differences is investigated, and their effect on the transverse dispersion coefficient is assessed. Following a description of the methodology used, results from the experimental study are presented and analysed to provide an empirical basis to describing tracer and brine dispersion under horizontal flow. The specific physical mechanisms underlying the effects observed on transverse dispersion are not the main focus of this chapter. In Chapter 5, high-concentration transverse dispersion is further discussed where the applicability of recently developed theoretical models of density-dependent transport is investigated.

4.1.1 Laboratory experiments

In order to investigate transverse dispersion mechanisms a series of stable miscible-displacement laboratory experiments were conducted. The system considered here is that of freshwater and a saltwater solution (NaCl). An increase in concentration leads to an increase in fluid's density and viscosity (less significant). The two fluids flow parallel to each other in a uniform horizontal flow field mixing through transverse dispersion. Figure 4.1 depicts the dispersion scenario considered. The porous medium is homogeneous such that it can be characterised by a single (average) value of porosity n, and intrinsic permeability k. In the real laboratory system, this is only true to some extent as small-scale heterogeneities are inherently present due to the type of porous media used and the method of packing. Tracer conditions occur when $\rho_{sw} \approx \rho_{fw}$, i.e., when density differences can be disregarded. Brine conditions occur when $\rho_{sw} \gg \rho_{fw}$ (subscripts sw and fw refer to salt water and fresh water, respectively). The objectives of the experimental programme are two fold:

- To gain a better understanding of transverse dispersion in homogeneous media and the effects of fluid velocity, variable density, and permeability on the dispersion coefficient.
- To obtain a reliable data set for the purpose of testing developed theories on density-dependent dispersion.

4.2 Materials and Methods

4.2.1 Experimental setup

In order to generate the flow and mixing conditions shown in Figure 4.1, a two dimensional flow-through tank was constructed with inner dimensions of 150 cm

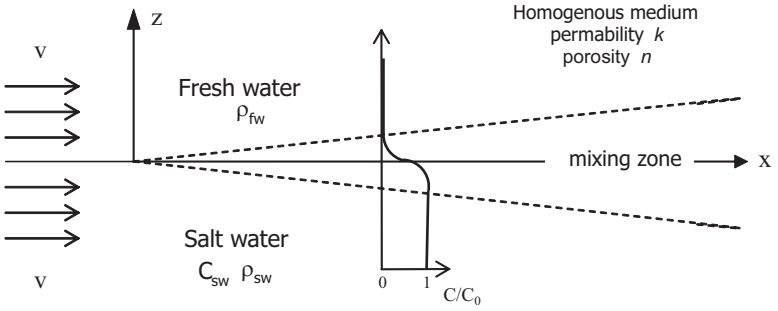

Figure 4.1: Transverse dispersion scenario.

long, 40 cm hight and 1 cm wide, using 1 cm thick Plexiglas. A steel support frame was fitted around the tank to avoid bending of the side walls. Figure 4.2 shows schematically the tank system and photographically in Figure 4.4.

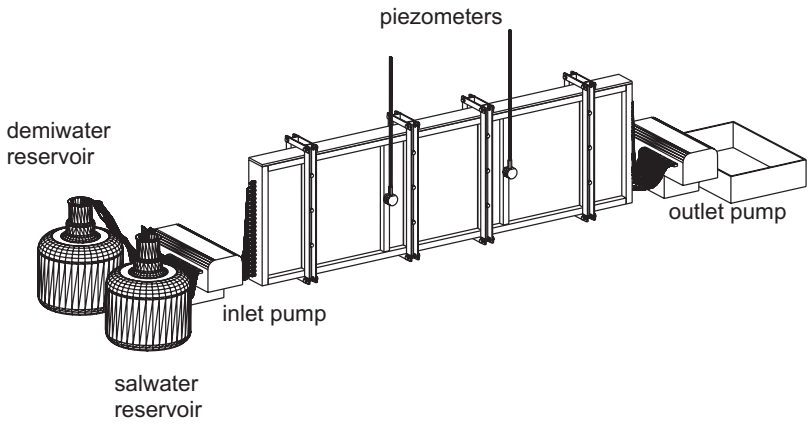

Figure 4.2: Sketch of the experimental setup.

A more detailed plan of the tank dimensions and accessories is shown in the Figure 4.3.

The tank was equipped with 24 inlet and outlet ports respectively, spaced at 1.5 cm intervals. The ports were made with silicone stoppers protruded by stainless steel capillaries. Flow in the tank was controlled by two peristaltic pumps (ISMATEC IP-N 24-channels) that connected to the ports through pump tubing at each end of the tank. In order to avoid possible blockage of the capillaries by the grains, a highly permeable net was fitted in the outlet side of the tank. Preliminary runs showed that this net did not disturbed the flow in the outlet

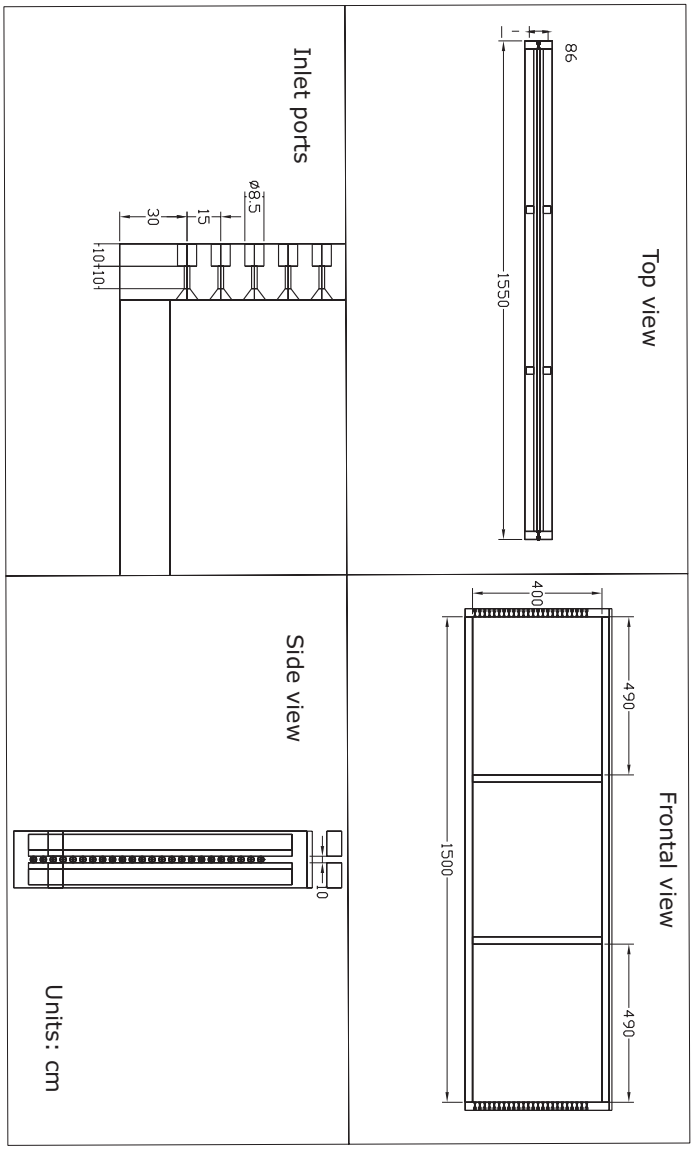

Figure 4.3: Plan of the laboratory tank dimensions.

of the tank. The experiments were carried out in a constant-temperature room where the average temperature was 20°C.

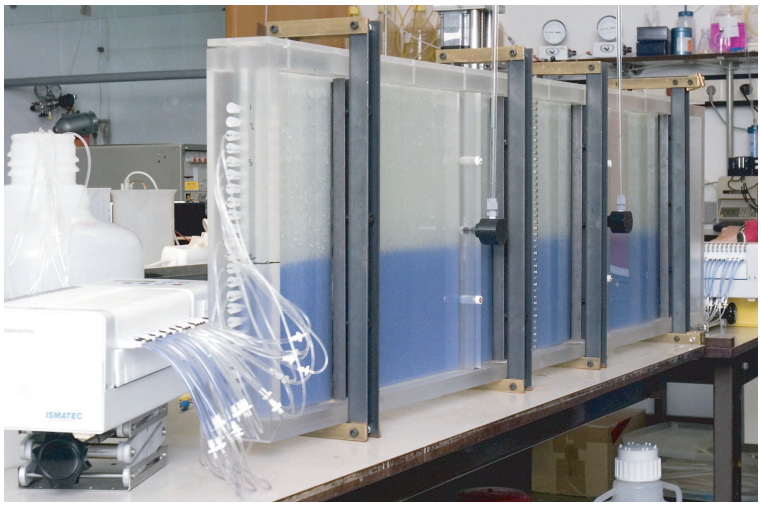

Figure 4.4: Side-view of the laboratory tank.

4.2.2 Porous media

Non-sorbing, chemically inert silica glass beads of three commercially available size ranges (Sigmund-Lidner) were used as porous medium. These porous media are denoted in the remaining of this thesis as *PM1*, *PM2* and *PM3*. The average grain diameters, d_{50}, were 0.36 mm, 0.86 mm and 1.865 mm respectively, and the uniformity coefficients, U, were 1.085, 1.09 and 1.092 respectively. Only results from *PM2* and *PM3* are reported here. Experimental runs using *PM1* were not successful in creating a uniform flow along the tank and did not show reproducibility. This is believed to be due to the low permeability of the medium and the way flow was established in the tank. They were abandoned in favour of porous media with higher permeability. Figure 4.5 shows the grading curves for *PM2* and *PM3*.

Cleaning method

The glass beads were cleaned by letting them soak for 1 hour in a NaClO solution, then thoroughly rinsed with tap water, boiled for another hour and finally rinsed with distilled water. The cleaned glass beads were stored in plastic containers and kept under wet conditions for the whole duration of the experiments.

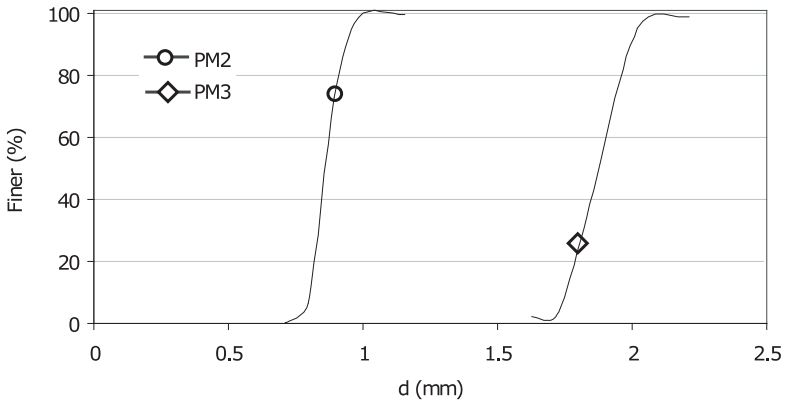

Figure 4.5: *PM2* and *PM3* grading curves.

4.2.3 Packing and homogeneity of the medium

The tank was wet-packed in 10 cm lifts by sprinkling the glass beads into the tank ensuring the beads always stayed under the water level. This prevented trapping of air bubbles. An air hammer was used to sort and compact the glass beads. This process was repeated until the glass beads were about 1 cm from the top edge of the tank and was proved reliable in creating a homogenous medium.
A homogeneous medium is such that properties like dispersivity, permeability and porosity have only small variations along and across the tank. This can be achieved by narrowing the grain size distribution (low uniformity coefficient) and by using a reliable packing method. In these experiments the homogeneity of the medium was checked in the following way. Colour plumes were created by injecting dye fronts through some of the inlet ports. The development of the plumes as well as the shape and size provided a good visual indication of the uniformity of the packed tank. Figure 4.6 shows and example of dye plumes developing. If the dye plumes show no visual differences in size and shape and it would appear that the packing resulted in a fairly homogenous medium. The tank was repacked if visual differences in the size and shape of the plumes existed. Once an homogenous medium was archived, the tank remained packed until all the experimental runs (preliminary and actual experiments) were completed.

4.2.4 Porosity

Porosity for each porous medium was estimated in two ways.

1. Injecting dye fronts through different inlet ports. The average advance rate of the fluid front is a measure of the average fluid velocity, v, within the tank. Since the specific discharge is known from volumetric measurements

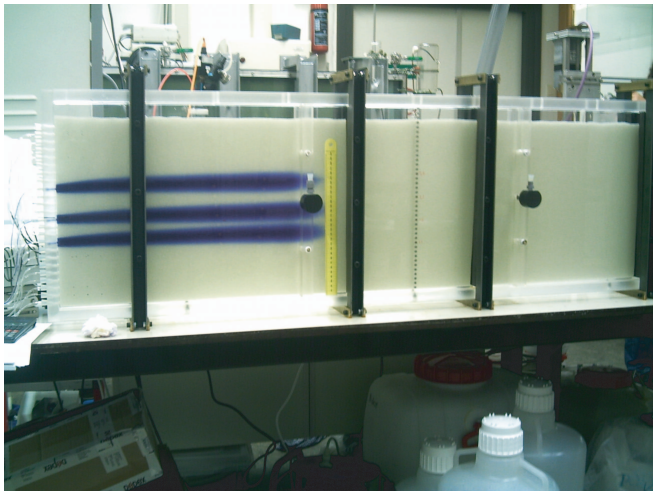

Figure 4.6: Visual confirmation of homogeneity of the porous medium.

then,

$$n = \frac{v}{q} \tag{4.1}$$

The porosity was found to vary locally between 0.38 and 0.40 for both *PM2* and *PM3*.

2. Gravimetrically, by saturating a known volume of porous media and knowing the volume of water that saturated the medium, then,

$$n = \frac{V_{water}}{V_{Total}} \tag{4.2}$$

Results of the porosity measurements from this method gave an average value of 0.38 and 0.39 for *PM2* and *PM3* respectively.

4.2.5 Intrinsic permeability

The tank was equipped with three vertically-spaced sampling ports, located at two transects (6 ports in total) with a spacing of 50 cm between transects (see also Figure 4.3). In these ports, piezometers were fitted to measure the hydraulic head drop Δh at a given specific discharge. For uniform flow, Darcy's Law states that the specific discharge, q, is given by

$$q = KI \tag{4.3}$$

where K is the hydraulic conductivity and I is the hydraulic gradient given by $I = \Delta h/L$. To obtain K it is necessary to know the total flow rate, Q, and the

Parameter	Variable	Units	*PM2*	*PM3*
Average Grain Diameter	d_{50}	mm	0.86	1.865
Uniformity Coefficient	U	-	1.08	1.092
Porosity	n	-	0.38	0.39
Intrinsic Permeability	k	m^2	$5.8 \cdot 10^{-10}$	$3.1 \cdot 10^{-9}$

Table 4.1: Experimental Parameters

head difference Δh, between piezometers. If q is plotted against Δh the slope of the line should be constant and equal to K/L, where L is the distance between piezometers. Results for *PM2* and *PM3* are given in Figures (4.7a) and (4.7b). The plots show measurements of Δh between the two middle ports for various specific discharges, corresponding to tracer experiments reported in next section. Due to the high permeability of *PM3* (larger grain size) only three pressure drops could be measured, corresponding to those runs with a high specific discharge. This is because it was difficult to obtain accurate readings for $\Delta h < 1$ mm corresponding to lower specific discharges. The intrinsic permeability is calculated using

$$k = \frac{K\mu}{\rho g} \tag{4.4}$$

It should be noted that Figures 4.7a and 4.7b not only show that permeability remained constant during the whole duration of the experiments for *PM2* and *PM3* but also confirms the validity of Darcy's law for each of the tracer experiments.

A second method to determine the intrinsic permeability is using the well-known Kozeny-Carman relationship, see Bear (1972). The calculated values are $k_{PM2} = 5.41 \cdot 10^{-10}$ and $k_{PM3} = 3.08 \cdot 10^{-9}$. As expected for these media, i.e., unconsolidate media of uniform grain size, theoretical values closely match the measured values above. Table 4.1 summarises the values used in the experiments for each set of porous media.

4.2.6 Tracer and brine solutions

Tracer and brine solutions used for the experimental runs were prepared with chemically pure NaCl and demineralised water. To prepare a tracer solution a quantity between 2 - 4 g/l of NaCl was added to the demineralised water, thoroughly dissolved and left in the room to achieve an equilibrium temperature of about 20°C. The same procedure was used to prepare the brine solutions except that dissolved quantities of NaCl varied between 25 g/l up to 200 g/l. Additionally, both tracer and brine solutions contained a small amount of a non-conducting, non-absorbable colour indicator (Reazurin) to allow for visual study of the behaviour of the front and the fluid interface.

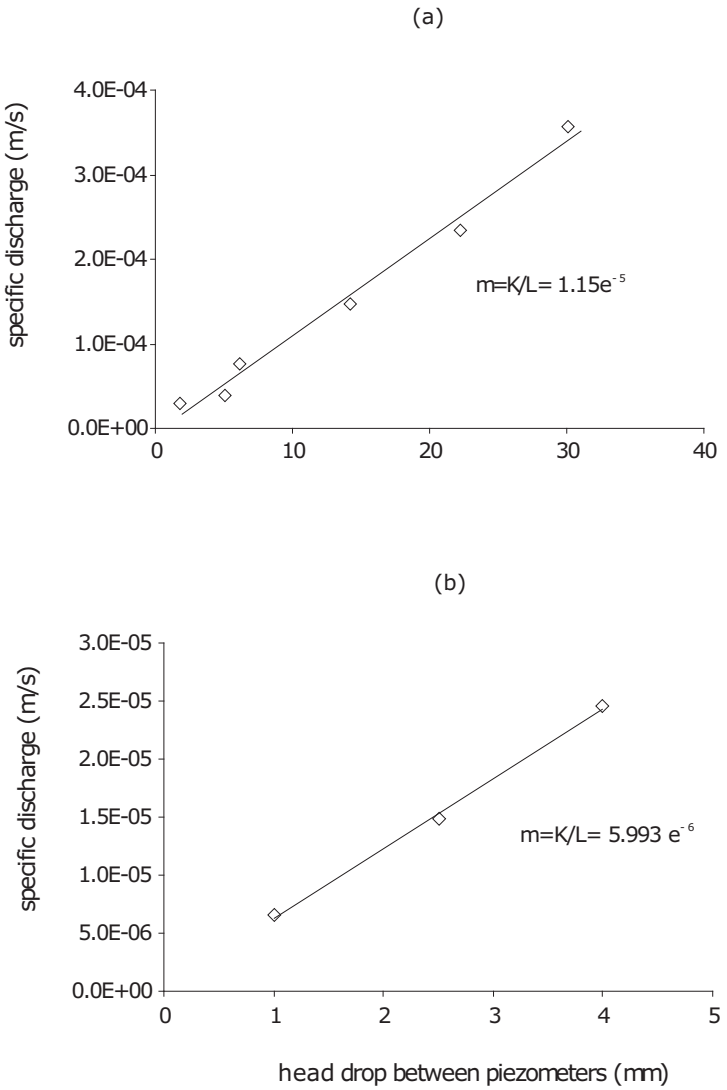

Figure 4.7: Determination of intrinsic permeability for a) *PM2* and, b) *PM3*. Confirmation of Darcy's Law for tracer runs.

4.2.7 Flow regulation and measurement

Flow through the tank was controlled by two 24-channels peristaltic pumps located at the inlet and outlet sides respectively, and connected to the tank through tubing and capillaries. Two reservoirs were connected to the inlet pump. One reservoir provided the freshwater and the other reservoir the saltwater fluid (NaCl solutions) that varied for tracer experiments from 2 to 4 g/l, and for brine experiments from 25 up to 200 g/l. This meant that the inlet pump injected with 11 channels demineralised water into the top half of the tank and 11 channels the tracer solution into the bottom half. In contrast, at the outlet side the second 24-channel pump discharged with 23 channels into a common reservoir. The outlet pump was adjusted to match the inlet flow rate. This procedure allowed an unsaturated zone to exist near the top of the tank and was proven successful to achieving a uniform and horizontal flow field along the tank. This is shown in Figure 4.8 where dye plumes develop in horizontal uniform flow conditions. Due to practical limitations on the pump delivery capacity it was necessary to use two different sizes of tubing (1.02 mm and 3.17 mm id.) to generate the desire range of flow rates. Additionally, for this pump model (IP-N) calibration curves needed to be generated.

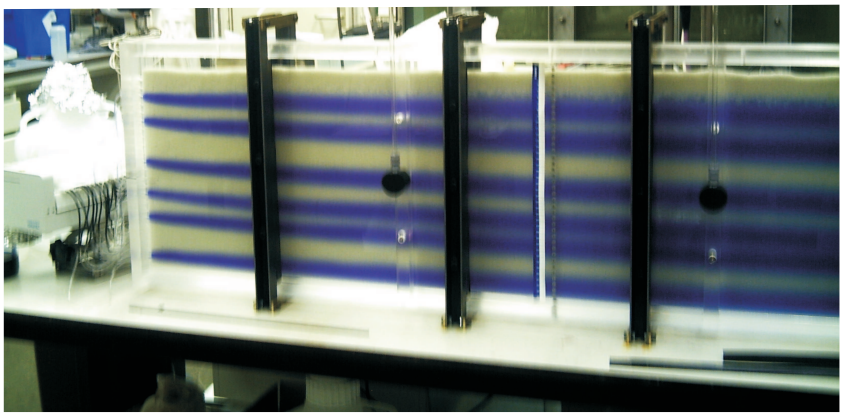

Figure 4.8: Dye plumes developing under conditions of uniform horizontal flow.

To ensure the prescribed initial and boundary conditions of constant and uniform flow rate in the inlet and outlet of the tank, the following series of tests were carried out for both pumps and then compared against each other:

- Pump curve - relationship between RPM (revolutions per minute) v. flow rate, for both inlet and outlet pumps. Two curves were generated for each pump, one corresponding to tubing of 1.02 mm i.d. and another one corresponding to tubing of 3.17 mm i.d. respectively.

- Tubing performance assessed after days of use.
- Relationship between RPM and flow rate/per channel (salt water at different mass fraction)
- Inlet and Outlet pumps working with the two fluids together.

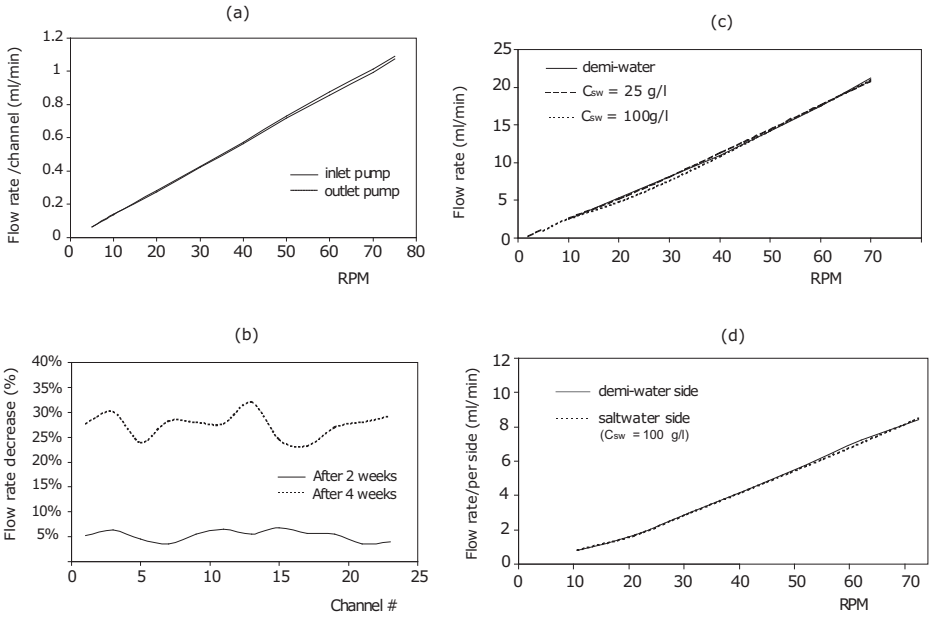

Figure 4.9: Pump tests: a)comparison of inlet and outlet pump curve (curve shown for tubing 1.02 mm i.d.); b)tubing performance after weeks of usage; c)example of flow rate delivered using demi-water only, a salt solution of up to 25 g/l and salt solution containing up to 100 g/l; d) flow rate delivered by pump connected to two reservoirs, one containing demi-water and the other containing a salt solution.

From the above-mentioned tests, the following could be concluded:

- Although same type of pump (model) and same type of tubing used, each pump was run with its own individual calibration curve.
- The inlet and outlet pumps show no major differences in delivered flow when working with half of the channels pumping demi-water and the remaining channels pumping salt water.
- Tubing had to be replaced after two-weeks of continuous use in order to avoid differences higher than 5% in flow rate delivered per channel.

4.2.8 Fluid velocity

The average fluid velocity for each experiment was calculated by measuring volumetrically the total effluent fluid, Q, for a given time lapse and using the following relationship:

$$v = \frac{Q}{A_s\, n} \tag{4.5}$$

where A_s refers to the crossectional area of saturated flow at the outlet of the tank. Because this saturated area varied between experiment depending on the specific discharge and Δh, A_s was measured for each individual experimental run.

4.2.9 Measurement of salt concentration profile

Electrical conductivity measurements were carried out using a Consort multichannel analyser (model R305) connected to a 3-pole conductivity electrode. Previous to the conductivity measurements a calibration curve for the conductivity meter and probe was generated to allow determination of the salt concentration. The calibration procedure was as follows: a number of salt solution samples were prepared with known salt concentration ranging from 0.5 g/l to 200 g/l. To prepare the sample a carefully-weighted amount of chemically pure NaCl was dissolved in 250 ml of demineralised water. The samples were left to achieve room temperature (20°C). Conductivity measurements were recorded and a plot of salt concentration vs. electrical conductivity was prepared (see Figure 4.10). The calibration procedure was repeated in a number of occasions throughout the duration of the experimental programme in order to check the stability of the instrumentation. Figure 4.10 shows the calibration curve for the conductivity meter and probe when first calibrated and the last calibration run. It can be seen that the meter and probe remained fairly stable.

The tank outlet was the chosen location to determine a salt concentration profile. The outlet profile was sampled by connecting glass sample vials to the outlet ports (see Figure 4.11). Electrical conductivity readings were obtained by inserting directly the conductivity probe into the vials.

4.2.10 Steady-state conditions

Preliminary runs were carried out for both tracer and brine experiments in order to to determine when stationary conditions were achieved. Conductivity measurements were obtained from the effluent stream at various pore volumes (PV), namely at 1, 1.5, 2, 3, 4 and 5 PV. When constant values of conductivity were observed, it was assumed that the steady state had been reached. For tracer experiments this happened soon after 1 PV as subsequent pore volume measurements showed no change in the conductivity readings. This was also corroborated by numerical simulations of the experimental runs (Duijster, 2007). However, for brine

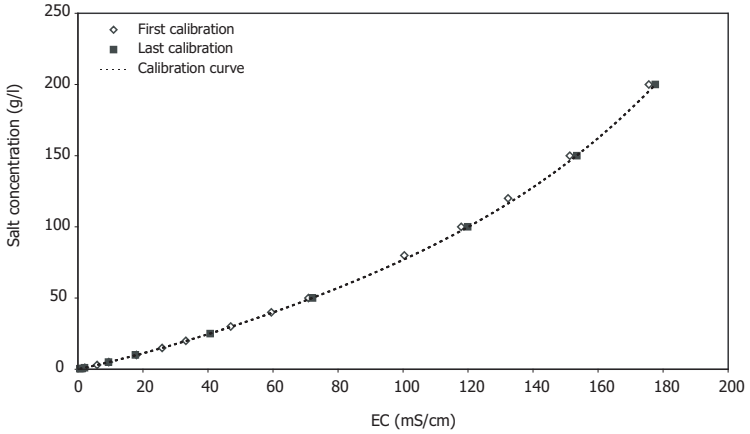

Figure 4.10: Calibration curve for conductivity meter and probe.

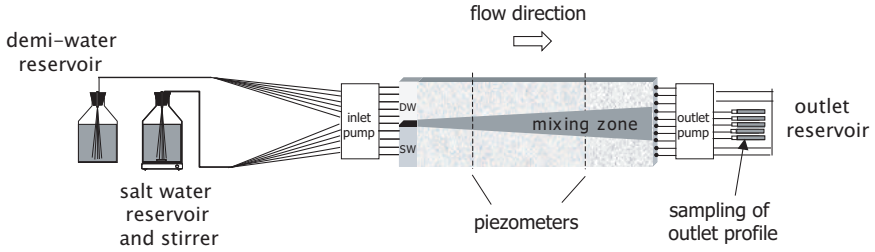

Figure 4.11: Schematics of sampling method for outlet concentration profile.

experiments stationary conditions varied between 3 and 4 PV depending on the flow rate and concentration difference between fluids.

4.2.11 Reproducibility of experiments

Reproducibility of the experimental method was tested by emptying the tank, repacking and repeating an equal-velocity, equal-concentration experiment. Figure 4.12 is a plot of two experimental runs from the first and second tank packings, respectively. The plot gives an example of a two tracer runs at a fluid velocity of 3.3 m/day using *PM2* for the initial packing and after repacking the tank. The same procedure was followed for *PM3*. In addition to the tracer runs, reproducibility was also tested for brine experiments showing again a very good agreement.

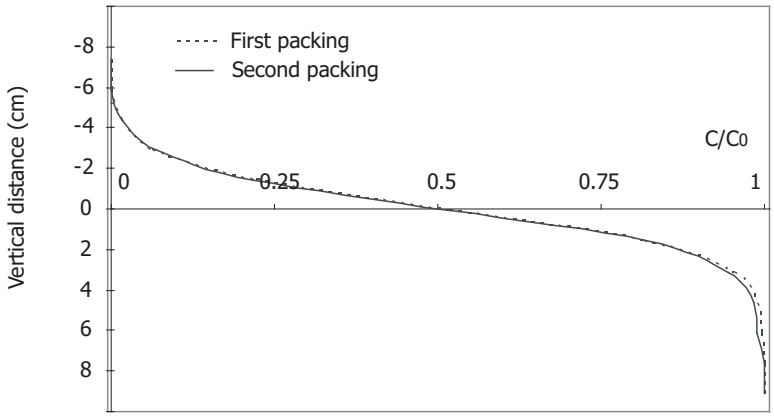

Figure 4.12: Concentration profiles generated with initial packing and after emptying and repacking tank. The experiments correspond to a fluid velocity of 3.3 m/day

4.2.12 Experimental errors

Experimental errors can be associated with electrical conductivity measurements and flow rate measurements. The error associated with conductivity measurements and the obtained calibration curve have a direct effect on the obtained salt concentration profile measured at the tank outlet. In Section 4.2.9 it was shown that the calibration curves and conductivity meter used are reliable and cover the full spectrum of salt concentrations used during the experiments. A maximum total error associated with the salt concentration measurements was estimated to ranged in $\pm 0.5\%$

The errors associated with the flow rate have an effect on the flow field established in the tank and the obtained fluid velocity. In Section 4.2.7 it was described how the flow rate was regulated by using the same pump tubing no longer than 2 weeks and by visually monitoring the development of the injecting fluid. This help to ensure a uniform and constant flow field in the tank. The maximum error associated with the the flow rate measured at the tank outlet was in the range $\pm 2.5\%$.

4.3 Experimental Results

The laboratory experiments assume that: *i)* the porous medium is homogenous and can be characterised by a single (average) value of porosity, permeability and

dispersivity; *ii)* the values of the transverse dispersion coefficients correspond to asymptotic values as the length scale of the system is of meters and stationary conditions are achieved before measuring the concentration profile; *iii*) for each porous media (i.e., *PM2* and *PM3*) the two varying parameters are initial salt concentration, C_0, and fluid velocity, v.

It should be noted that although the main difference between the two porous media is the value of the average grain size, this sole condition allowed to investigate a wide range of Peclet numbers (which is function of the grain size), and gravity numbers (which is function of permeability). Moreover, the Reynolds number in the experimental runs was kept between the Darcy's law validity range, i.e., $0 \leq \text{Re} \leq 1$. The following gives a general description of the experiments carried out for each porous media pack.

***PM2* series**. Seven tracer experiments with added salt ranging between between 2 g/l to 4 g/l and considered small enough not to cause any gravitational effects due to density differences. Fluid velocities were varied between 2 m/day and 81 m/day. For each fluid velocity a corresponding brine or experiment was performed. The salt concentration for these experiments ranged between 100 g/l to 200 g/l. A total of 14 dispersion experiments were carried out with *PM2*.

***PM3* series**. Seven tracer experiments (similar to *PM2* series) for which the fluid velocity ranged between 1.4 m/day to 26 m/day. For the first four fluid velocities, namely 1.4 m/day, 3.3 m/day, 5.5 m/day and 8.3 m/day, three subsequent brine experiments were performed increasing the salt concentration from 20 g/l, up to 110 g/l. For the remaining three fluid velocities only one subsequent brine experiment was conducted for which the salt concentration was approximately $\simeq$ 110 g/l. A total of 22 dispersion experiments were performed using *PM3*.

The details of the experimental runs are given in Table 4.2; an explanation of the different data columns is: *Column 1* gives the run number of the experiment. The first three letters refer to the porous media set, the fourth and fifth letters refer to the fluid velocity used, and the T and B refer to a tracer or a brine experiment, respectively. *Column 2* gives the average fluid velocity through the saturated porous medium and is the total flow rate through the tank divided by the cross-sectional area measured at the outlet of the tank times the average porosity. It was observed that measured outflow velocities for tracer experiments and subsequent brine experiments showed discrepancies in value not higher than 2% in all cases (this is in line with test runs described in Section 4.2.7). Thus, it is assumed that all experimental runs can be classified as constant flow rate experiments in which only the density is varied and the fluid velocity remains constant. *Column 3* gives the density difference between the mixing fluids, i.e., between freshwater and salt water. Density is calculated using the relationship (2.10) as given in Chapter 2. The salt concentration is obtained from conductivity measurements and using the calibration curve shown in Figure 4.10.

Experiment Number	**Fluid Velocity** (m/s)	**Density Difference** (kg/m^3)
PM2 Series		
PM2V1T	$2.39 \cdot 10^{-5}$	1.8
PM2V1B	$2.39 \cdot 10^{-5}$	66
PM2V2T	$5.75 \cdot 10^{-5}$	2.2
PM2V2B	$5.75 \cdot 10^{-5}$	120
PM2V3T	$1.29 \cdot 10^{-4}$	2.1
PM2V3B	$1.29 \cdot 10^{-4}$	98
PM2V4T	$3.2 \cdot 10^{-4}$	2.2
PM2V4B	$3.2 \cdot 10^{-4}$	120
PM2V5T	$3.76 \cdot 10^{-4}$	2.4
PM2V5B	$3.76 \cdot 10^{-4}$	98
PM2V6T	$6.44 \cdot 10^{-4}$	2.1
PM2V6B	$6.44 \cdot 10^{-4}$	99
PM2V7T	$9.41 \cdot 10^{-4}$	2.2
PM2V7B	$9.41 \cdot 10^{-4}$	99
PM3 Series		
PM3V1T	$1.68 \cdot 10^{-5}$	1.5
PM3V1B1	$1.68 \cdot 10^{-5}$	18
PM3V1B2	$1.68 \cdot 10^{-5}$	36
PM3V1B3	$1.68 \cdot 10^{-5}$	69
PM3V2T	$3.81 \cdot 10^{-5}$	2.2
PM3V2B1	$3.81 \cdot 10^{-5}$	19
PM3V2B2	$3.81 \cdot 10^{-5}$	35
PM3V2B3	$3.81 \cdot 10^{-5}$	70
PM3V3T	$6.41 \cdot 10^{-5}$	1.8
PM3V3B1	$6.41 \cdot 10^{-5}$	17.5
PM3V3B2	$6.41 \cdot 10^{-5}$	35
PM3V3B3	$6.41 \cdot 10^{-5}$	68
PM3V4T	$9.61 \cdot 10^{-5}$	1.8
PM3V4B1	$9.61 \cdot 10^{-5}$	18
PM3V4B2	$9.61 \cdot 10^{-5}$	36
PM3V4B3	$9.61 \cdot 10^{-5}$	68
PM3V5T	$1.84 \cdot 10^{-4}$	1.6
PM3V5B1	$1.84 \cdot 10^{-4}$	69
PM3V6T	$2.41 \cdot 10^{-4}$	1.7
PM3V6B1	$2.41 \cdot 10^{-4}$	70
PM3V7T	$3.06 \cdot 10^{-4}$	1.9

Table 4.2: Experimental Parameters

4.3.1 Experimental profiles

Tracer experiments — PM2 and PM3 – series

First, experimental results are given for tracer experiments of both the *PM2* and *PM3* series. Figures 4.13a through 4.14b show the experimentally-determined concentration profiles across the fluid interface, i.e., where the scaled concentration changes from $C/C_0 = 1$ to $C/C_0 = 0$. It is first plotted as a function of vertical distance along the tank, and secondly, as a function of relative distance regarding location of the 50% concentration isoline. Tracer profiles corresponding to both *PM2* and *PM3* series show that the vertical position of the interface remained fairly constant for each of the tracer runs (see Figures 4.13a and 4.14a). Another behaviour visible from Figures 4.13b and 4.14b is the decrease of the interface width with increasing fluid velocity for both experimental sets.

Brine experiments — PM2 series

Concentration profiles of *PM2* brine experiments are presented in Figure 4.15. The top panel shows the brine concentration profiles plotted as a function of the vertical position along the tank. It can be seen that the location of interface remained relatively constant in all cases. The bottom panel shows the same brine experiments plotted together with the tracer experiments of the same series. A slight shift of the vertical position with respect to the tracer runs can be observed for all the brine experiments. This behaviour has also been reported in previous experiments by Spitz (1985) and more recently by Starke (2005). Next, Figure 4.16 shows all the brine experiments plotted as a function of relative distance to the 50% concentration isoline. There appears to be a reduction in the width of the interface as velocity increases. However, this reduction could also be the result of an increase in the salt concentration (hence density difference). As a consequence a decreasing trend with increasing velocity is not as evident as in the tracer-only experiments.

To better illustrate the effects of density difference, Figure 4.17 shows two pairs of constant flow rate experiments, tracer and brine runs, corresponding to fluid velocities of 2 m/day and 4.9 m/day, respectively. Both profiles show that the profile becomes steeper with an increase in density. An interesting observation is that the brine profile corresponding to the lowest velocity (PM2V1B) exhibits a larger decrease (with respect to the tracer profile) than the brine run PM2V2B, although the density difference was higher in the latter ($\Delta\rho = 66$ kg/m^3) than in the former ($\Delta\rho = 120$ kg/m^3). The overall effect on the steepness of the profile appears to be the result of an interplay between density differences and flow velocity. Note from both brine runs, PM2V1B and PM2V2B, the concentration profile is not symmetrical around $C/C_0 = 0.5$, as opposed to what is observed in tracer runs. The brine profiles tend to be steeper at the saltwater side where the concentration is higher. These observations are further investigated in the *PM3* experimental series.

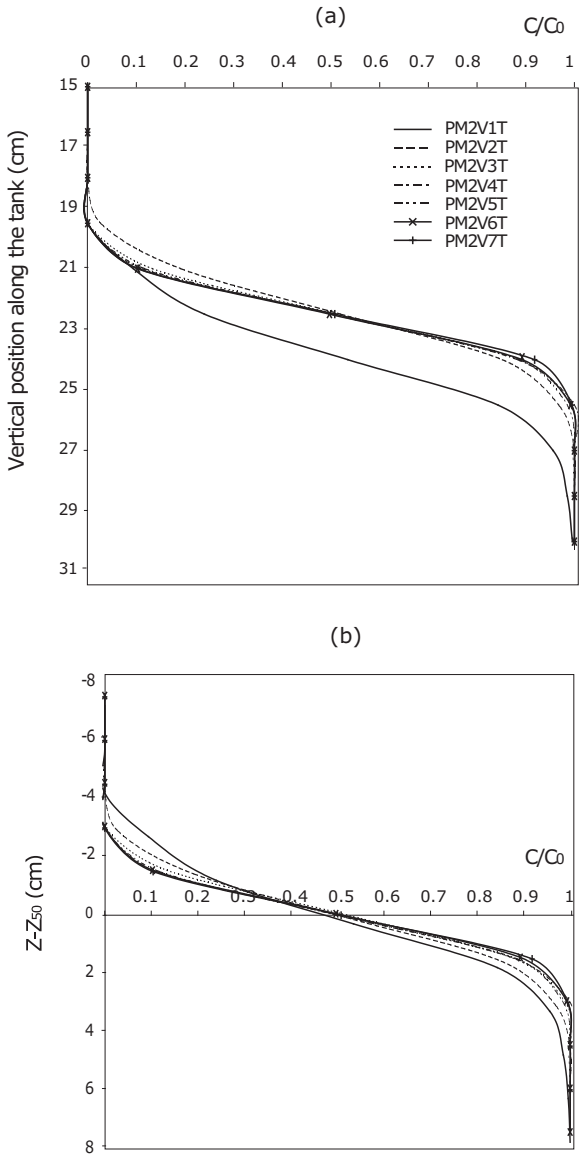

Figure 4.13: Experimentally obtained concentration profiles at the tank outlet for *PM2* series. (a) profiles of normalized concentration as a function of vertical location along the tank. (b) profiles of normalized concentration as a function of relative height.

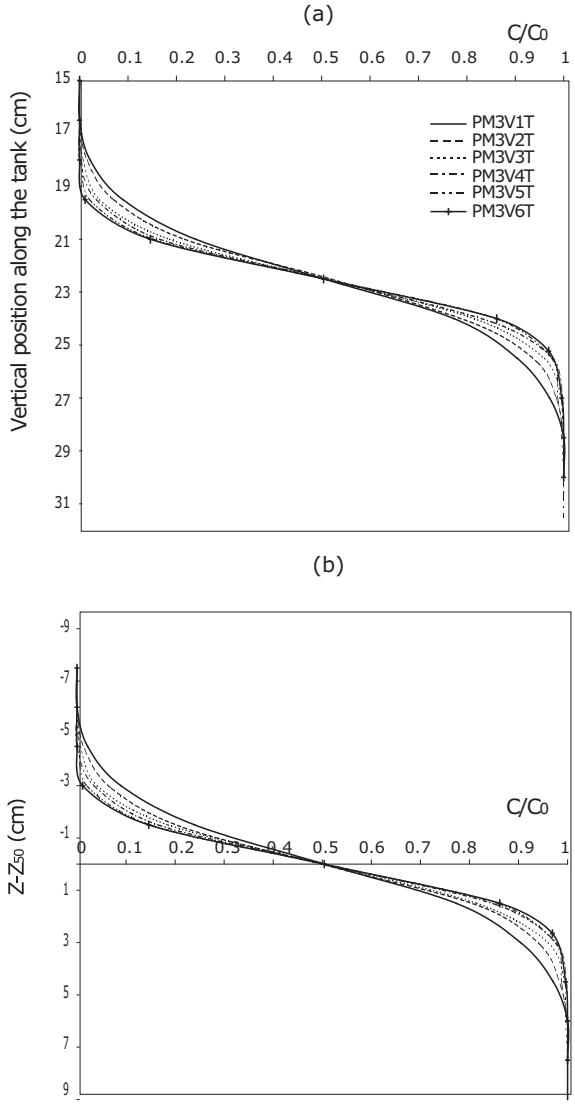

Figure 4.14: Experimentally obtained concentration profiles at the tank outlet for *PM3* series. (a) profiles of normalized concentration as a function of vertical location along the tank. (b) profiles of normalized concentration as a function of relative height.

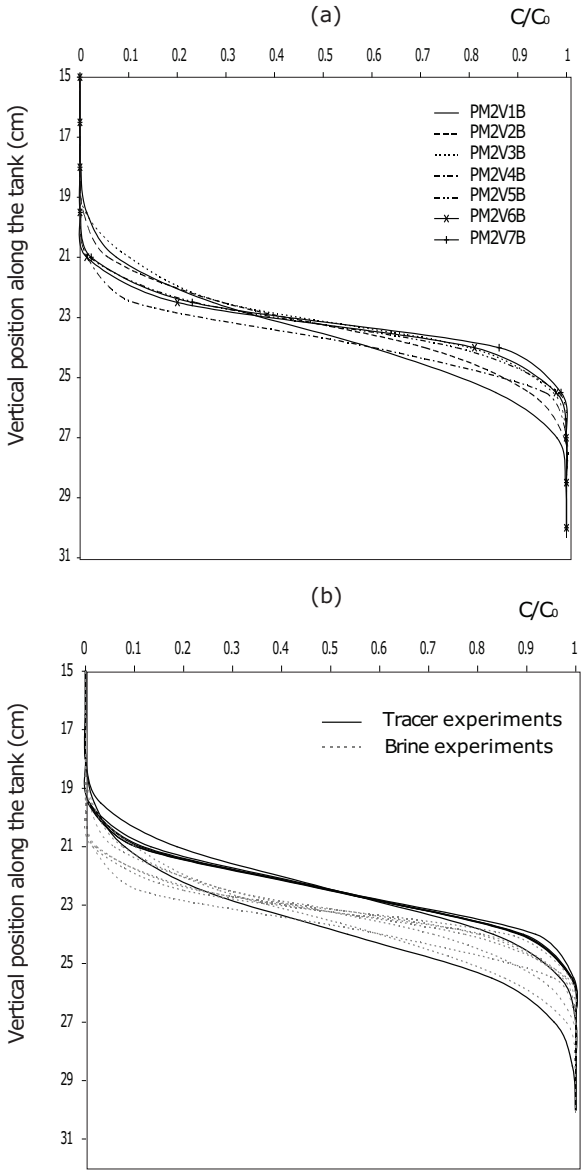

Figure 4.15: Concentration profiles of *PM2* series experiments. (a) profiles of normalized concentration plotted as a function of vertical location along the tank. (b) profiles of all tracer and brine experiments as a function of vertical position in the tank.

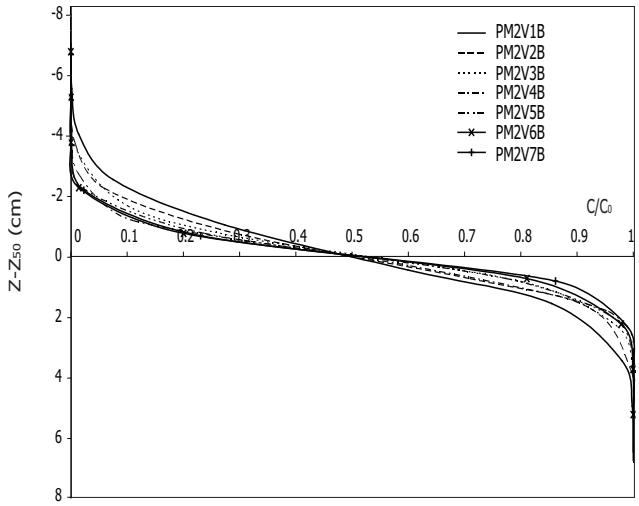

Figure 4.16: Normalized concentration as a function of relative distance to $C/C_0 = 0.5$.

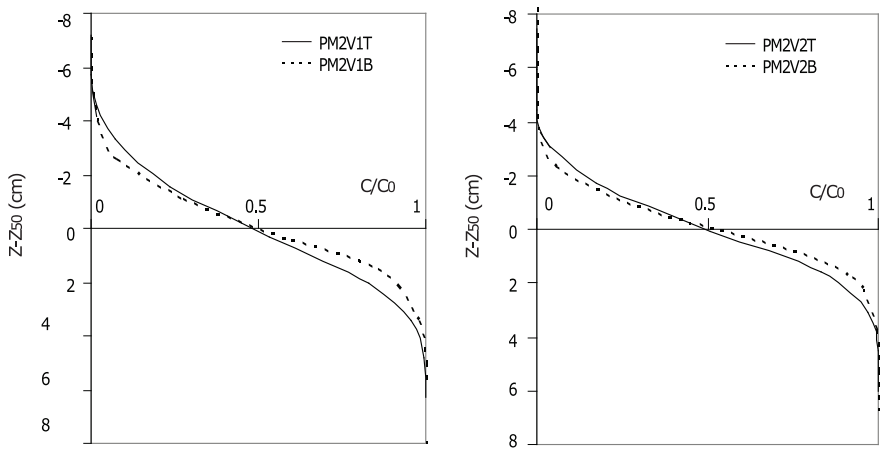

Figure 4.17: Concentration profiles for pair of experiments, tracer and brine, for fluid velocities V1= 2 m/day (LHS plot) and V2= 4.9 m/day (RHS plot), respectively.

Brine experiments — PM3 series

Profiles associated to some of the brine experiments from the *PM3* series are shown in Figures 4.18 and 4.19. These pairs of plots correspond to four constant flow rate experiments for which the fluid velocity is kept constant and the salt concentration is increased for a total of four experimental runs per fluid velocity. LHS plots in Figures 4.18 and 4.19 show the vertical location of the interface along the tank. Again, and as seen in runs from the *PM2* series, the vertical position of the interface for all the brine runs appears slightly shifted downward with respect to the tracer case. However, no systematic sinking of the interface with increasing salt concentration (hence density difference) is observed. The RHS plots show the normalized concentration as a function of relative distance to $C/C_0 = 0.5$. There is a clear evidence that an increase in density leads to a steeper profile in each set of constant velocity experiments. The previous remarks on the concentration profiles are also observed here: brine profiles corresponding to the V1 set, i.e., PM3V1B1, PM3V1B2, PM3V1B3, are steeper that the tracer run of the same set, i.e., PM3V1T. This reduction increases with increasing concentration. The same holds in the V2, V3 and V4 experimental sets. The overall degree of reduction of the interface zone appears again to be the result of the interplay between density difference and fluid velocity as the decrease is not the same in all the experimental sets even for similar density difference. Also, and as previously observed in Figure 4.17, brine profiles tend to be steeper in the high concentration side, hence non-symmetrical around $C/C_0 = 0.5$. This latter behaviour was also observed by Landman (2005) in her numerical results of brine concentration profiles.

4.3.2 Determination of the transverse dispersion coefficient

As reviewed in Chapter 2, the transverse dispersion coefficient, D_T, is commonly determined by measuring the steady state concentration profile at a given transect, x_i, along the flow field. The dispersion problem in this study considers the mixing of two horizontal streams flowing at the same velocity, v, in an infinite medium. The corresponding initial conditions are $C/C_0 = 1$ at $x = 0$ and $C = 0$ at $x > 0$. The boundary conditions are $C/C_0 = 1$ at $z \to -\infty$ and $C/C_0 = 0$ at $y \to \infty$. At steady state, the governing mixing equation of an ideal tracer is

$$\frac{\partial C}{\partial x} = \frac{\partial}{\partial y}\left(D_T \frac{\partial C}{\partial y}\right) \tag{4.6}$$

The transverse dispersion coefficient can be determined by using an approximate analytical solution to (4.6) given by

$$\frac{C}{C_0} = \frac{1}{2}\,\mathrm{erfc}\left(\frac{z - z_{50}}{\sqrt{4D_T \frac{x}{v}}}\right) \tag{4.7}$$

where C is the solute concentration at a point with coordinates (x, z), C_0 is the initial tracer concentration at the inlet, and z_{50} is the z value at which $C/C_0 = 0.5$.

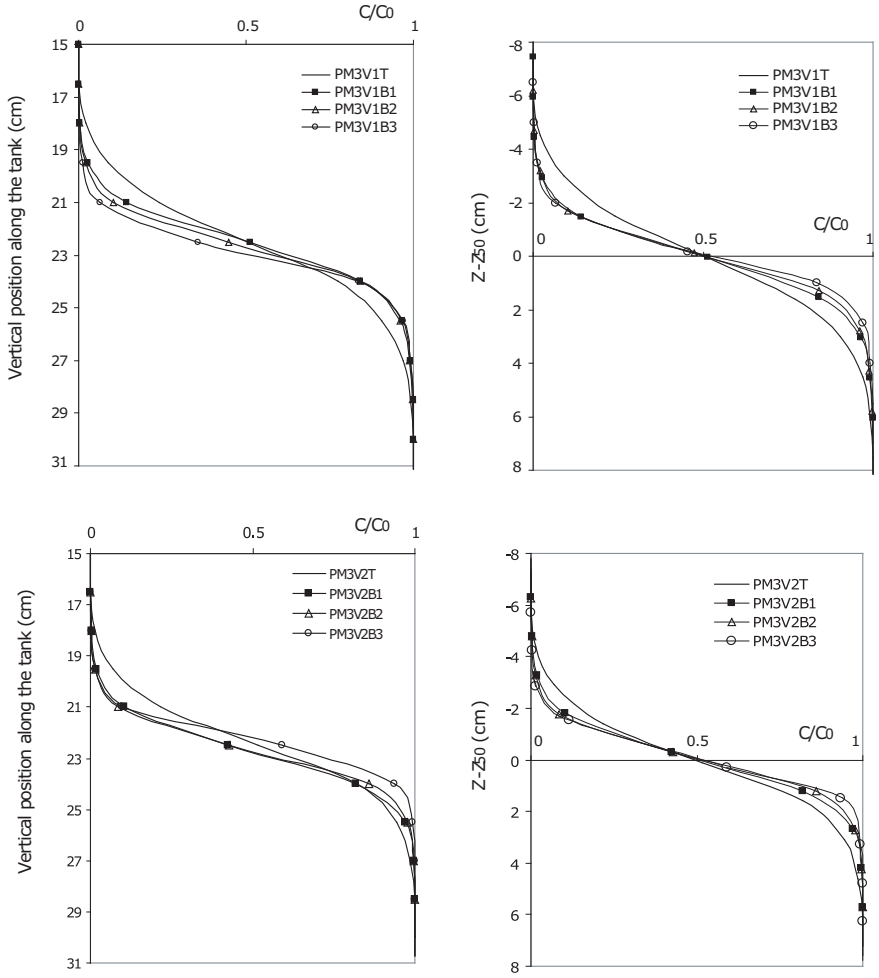

Figure 4.18: Concentration profiles for runs at fluid velocities V1=1.4 m/day (top figures) and V2=3.3 m/day (bottom figures), respectively. *PM3* series. LHS figures correspond to plots of normalized concentration as function of vertical location in the tank. RHS plots correspond to concentration as a function of relative distance to $C/C_0 = 0.5$

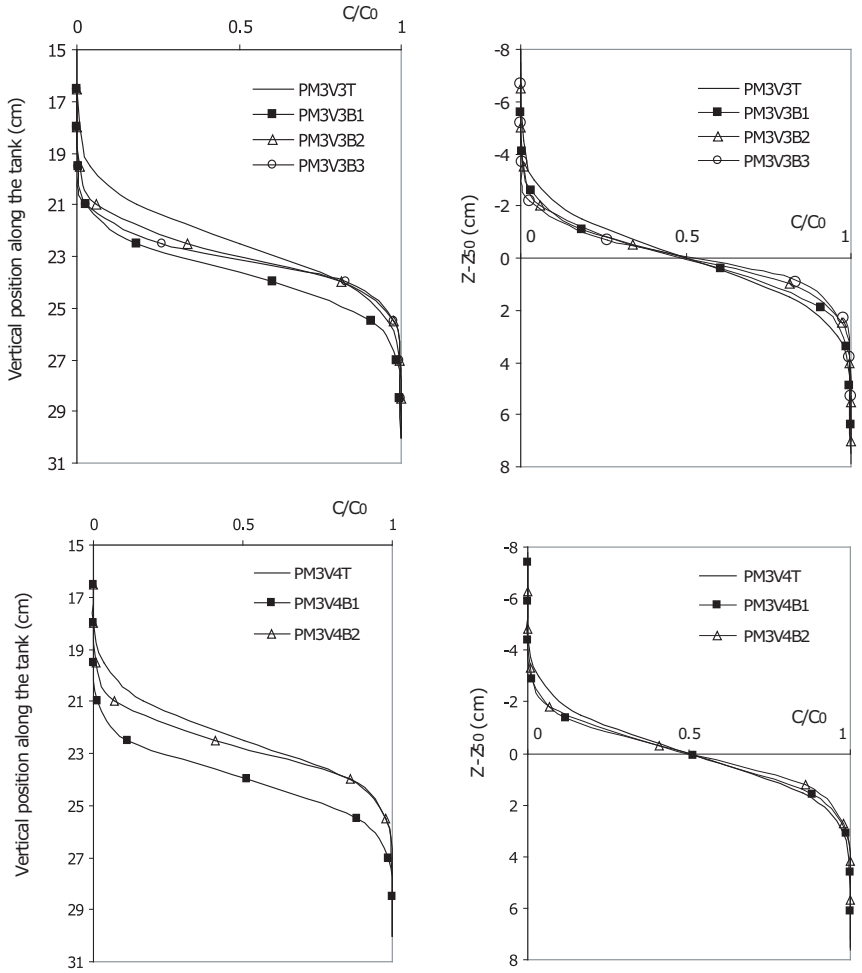

Figure 4.19: Concentration profiles for runs at fluid velocities V3=5.5 m/day (top figures) and V4=8.3 m/day (bottom figures), respectively. LHS figures correspond to plots of normalized concentration as function of vertical location in the tank. RHS plots corresponds to concentration as a function of relative distance to $C/C_0 = 0.5$.

An optimization routine was used to determine the value of the D_T , which best fitted the experimental tracer data and (4.7). In obtaining the dispersion coefficient for brine experimental runs it was assumed that the governing mixing equation (4.6) still holds and that D_T can be determined by fitting the analytical solution (4.7) through the concentration profile. However, density differences influence the degree of dispersion and therefore the obtained D_T will be an "apparent coefficient" as is a bulk representation of the influence of brine properties on the mixing. Additionally, an apparent value of the transverse dispersivity, α_T was also obtained. Dispersivity values are calculated following the linear combination of effective diffusion and mechanical dispersion (see Chapter 2),

$$D_T = \frac{D_{mol}}{\tau} + \alpha_T v \tag{4.8}$$

assuming $D_{mol} = 1.24 \cdot 10^{-9}$ m^2/s and τ =3/2 for the experimental conditions encountered in this study (Bear, 1972). The computed dispersion coefficient and dispersivity values are listed in Table 4.3.

4.4 Discussion

4.4.1 Transverse dispersion — effects of fluid velocity

Results of the tracer experiments are shown in Figure 4.20 in terms of the molecular Peclet number and the ratio between the apparent dispersion coefficient D_T and the molecular diffusion coefficient D_{mol}. Here, the molecular Peclet number, defined as

$$Pe = \frac{d_{50} v}{D_{mol}} \tag{4.9}$$

ranged between $\approx$ 17 to $\approx$ 650 for the *PM2* experiments and between $\approx$ 25 to $\approx$ 460 for the *PM3* runs. Additionally, Figure 4.20 compares the tracer results with literature data. A general observation from previous experimental studies is that the commonly assumed linear dependence of the dispersion coefficient on the fluid velocity, e.g., expression (4.8), does not hold for tracer experiments. Therefore it is common to describe the experimental data by a relationship of the form

$$\frac{D_T}{D_{mol}} = \frac{D_e}{D_{mol}} + b\,(Pe)^m. \tag{4.10}$$

where the ratio $\left(\frac{D_e}{D_{mol}}\right)$ can be extracted from experimental data (indicated by the arrow in Figure 4.20 and approximately equal to 2/3. Coefficients b and m are determined experimentally. A curve fitting through the experimental tracer data (plotted in Figure 4.20), reveals a similar dependency as given by expression (4.10),

Experiment Number	D_T (mm^2/s)	α_T (mm)
PM2 Series		
PM2V1T	2.81	0.098
PM2V1B	2.59	0.085
PM2V2T	4.63	0.072
PM2V2B	3.88	0.055
PM2V3T	7.08	0.051
PM2V3B	6.83	0.048
PM2V4T	13.8	0.041
PM2V4B	11.1	0.033
PM2V5T	15.8	0.041
PM2V5B	13.5	0.031
PM2V6T	25.9	0.04
PM2V6B	16.9	0.025
PM2V7T	36.6	0.038
PM2V7B	22.8	0.024
PM3 Series		
PM3V1T	2.71	0.133
PM3V1B1	1.2	0.043
PM3V1B2	1.03	0.033
PM3V1B3	0.837	0.001
PM3V2T	4.47	0.105
PM3V2B1	2.29	0.047
PM3V2B2	2.02	0.04
PM3V2B3	1.47	0.026
PM3V3T	6.29	0.092
PM3V3B1	3.92	0.055
PM3V3B2	2.97	0.04
PM3V3B3	2.12	0.027
PM3V4T	7.61	0.074
PM3V4B1	5.17	0.049
PM3V4B2	4.51	0.042
PM3V4B2	3.2	0.028
PM3V5T	12.7	0.066
PM3V5B1	4.78	0.023
PM3V6T	15.6	0.063
PM3V6B1	6.71	0.026
PM3V7T	19.8	0.063

Table 4.3: Computed values of apparent transverse dispersion coefficients and transverse dispersivity.

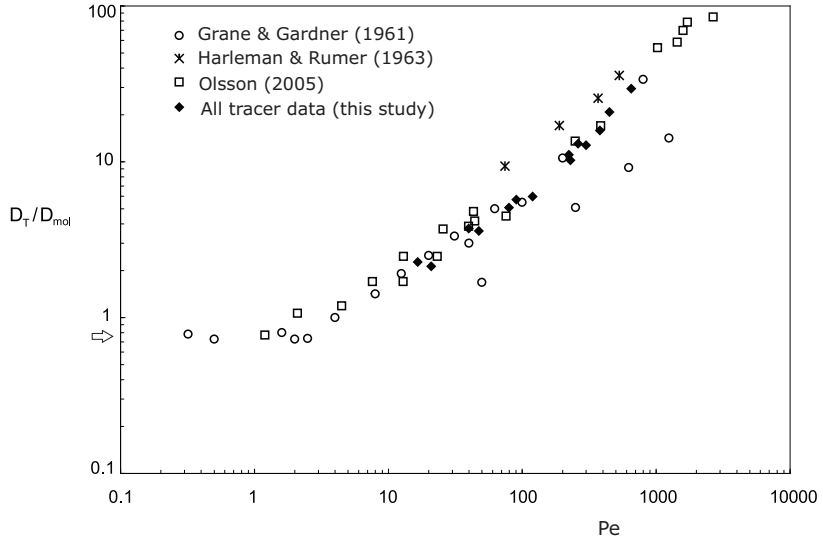

Figure 4.20: Results from tracer experiments compared to reported data from previous experimental studies.

$$\frac{D_T}{D_{mol}} = \frac{D_e}{D_{mol}} + 0.26\ (Pe)^{0.68}. \tag{4.11}$$

Similar values of the coefficients b and m have been reported by e.g., Harleman & Rumer (1963); Olsson & Grathwohl (2007). The form of equation (4.11) suggests that: i) the transverse dispersion coefficient exhibits a weaker (sub-linear) dependence on the flow velocity; ii) molecular diffusion plays a stronger role in transverse dispersion as D_T varies inversely proportionally to ${D_{mol}}^{1.47}$ (assuming $m = 0.68$). Data taken from Olsson (2005) corroborates the latter. Figure 4.21 shows experimental results using three tracer fluids (in the same porous medium), namely, Fluorescein at room temperature, Fluorescein at 4°C, and Bromide. The reported molecular diffusion coefficients were $6.48 \cdot 10^{-10}$ m^2/s, $3.57 \cdot 10^{-10}$ m^2/s and $2.08 \cdot 10^{-9}$ m^2/s, respectively. The range of fluid velocities was very similar for the three experimental sets.

It is evident from Figure 4.21 that dispersion is greater for the fluid with the largest diffusion coefficient (i.e., Bromide) compared to the fluid with the smallest diffusion coefficient (Fluorescien at 4°C). Although this behaviour may be intuitive, when longitudinal dispersion is considered, functional relationships of similar form to Eq. (4.10) have been reported, e.g., Schotting *et al.* (1999). However, values of m range between 1.1 and 1.3. This means longitudinal dispersion coefficients that are inversely proportional to ${D_{mol}}^{0.8}$ (assuming $m = 1.2$) which in turn means that a larger molecular diffusivity suppresses longitudinal dispersion.

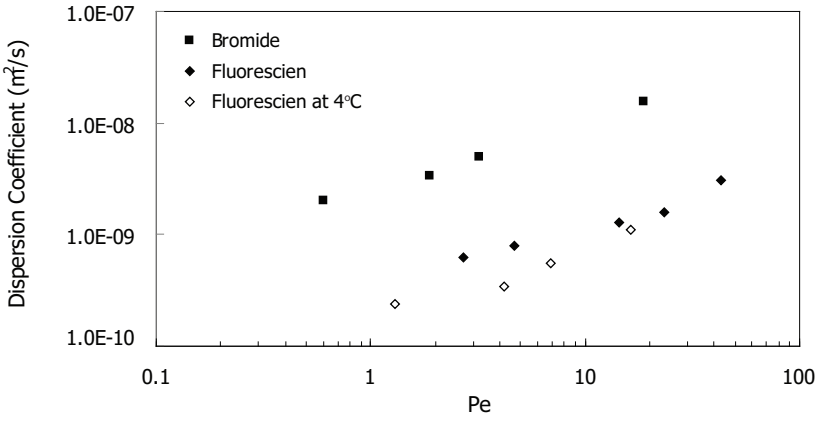

Figure 4.21: Effects of molecular diffusion coefficient on transverse dispersion. Experimental data taken from Olsson (2005) (d_{50}= 0.18 mm).

The physical causes behind the non-linear relation of the transverse dispersion coefficient and Pe have been addressed by a number of authors, e.g., Perkins & Johnston (1963); Klenk & Grathwohl (2002). In both publications *incomplete mixing* at the pore spaces due to insufficient residence time is said to be the cause. In a recent experimental investigation with pore networks, Gaganis *et al.* (2005) confirms that transverse dispersion is indeed greatly affected by pore-scale phenomena such as partial mixing at the pore junctions. Their results also exhibit an apparent decrease in α_T with increasing flow velocity (or Pe) already at the pore-scale. Other authors such as Sahimi *et al.* (1986) and more recently Bijeljic and Blunt (2007) have also demonstrated, using pore-network modelling approaches, that the linear dependence of the dispersion coefficient on the fluid velocity is only observed when complete mixing at the pore spaces is assumed. The nonlinearities arise in the modelling when including velocity profiles in the pores and allowing particles to 'jump' between (and along) streamlines thus imitating to some extent a molecular diffusion process. The main result appears to be incomplete equalization of the concentration at the pore spaces as velocity increases.

This non-linear dependence had already been postulated in the early theoretical work by Taylor (1953). Taylor shows that in the lower range of Pe (where diffusion dominates) the dispersion coefficient is independent of fluid velocity. In the upper Pe range where advection dominates dispersion mechanics the coefficient is linearly related to the fluid velocity. But at intermediate ranges of Pe, i.e., when dispersion results from the interplay between molecular diffusion and advection, the coefficient is a power function of the fluid velocity. The values of m varies between 1 - 2. Longitudinal dispersion experiments in the intermediate Pe

range have revealed a dependence in the order of ∼1.2 as opposed to the extreme value of 2 suggested by Taylor. Although Taylor's work was limited to longitudinal dispersion in capillary tubes, a similar behaviour can be expected for dispersion in the transverse direction in a porous medium. To verify this, Figure 4.22 reproduces the complete data sets as given in Figure 4.20 into subplots distinguishing three ranges of Pe for describing the ratio D_T/D_{mol}. The top panel shows the lower Pe range where the ratio is linearly related to Pe. It can be seen that as Pe decreases, the ratio tends to a constant value equal to the tortuosity factor, τ, and thus independent of the fluid velocity. In this lower range molecular diffusion is the dominant dispersion mechanism. The middle panel shows an intermediate range of Pe values varying between 10 and 300 where a non-linear dependency is evident from the fitted curves. Values of coefficients b and m vary only slightly in magnitude revealing a consisting sub-linear dependence on Pe. At this intermediate Pe range, dispersion is the result of the interplay between diffusion and advection. The bottom panel shows experimental data for a range of $Pe > 300$ where the ratio D_T/D_{mol} appears to be proportional to Pe. Two curves fitted to the experimental data yielded coefficients with no significant difference. This Pe range corresponds to the purely mechanical dispersion regime.

It should be noted that the prescribed Pe ranges in these sub-plots are only approximate values as they were derived experimentally. They do not necessarily imply a universal distinction of the ratio D_T/D_{mol} and may vary for other porous media, e.g., consolidated media. The intention is to show a qualitative dispersion behaviour that arises in a range of Pe values of practical interest and that differs markedly from classical descriptions of transverse dispersion. If the experimental observations at this intermediate Pe range are indeed caused by incomplete mixing at pore spaces, this can be explained as follows:

in laminar flow (i.e., in the absence of turbulence) diffusion is the only mechanism acting towards mixing and equalizing concentration at the pores spaces. When the velocity increases there is less residence time at the interstices and insufficient time for diffusion to act. In transverse dispersion, these two mechanisms can be regarded as competing processes, that is, advection acting along the main flow direction and diffusion in the direction of the concentration gradient, i.e., perpendicular to flow. If incomplete mixing at the pore spaces occurs, it implies that the solute moves onto subsequent pore spaces with only a fraction of the total amount of possible mixing. Macroscopically, this results in a smaller mixing zone which size is related to the dispersion coefficient.

Transverse dispersivity

Another feature arising from the form of Eq. (4.11) is that transverse dispersivity, typically given by the ratio between D_T and v, is not constant but decreases with Pe (i.e., velocity). Figure 4.23 shows the computed dispersivities (see Table 4.3) as a function of fluid velocity. Dispersivity increases with grain diameter but decreases with fluid velocity. These two observations have also been reported in

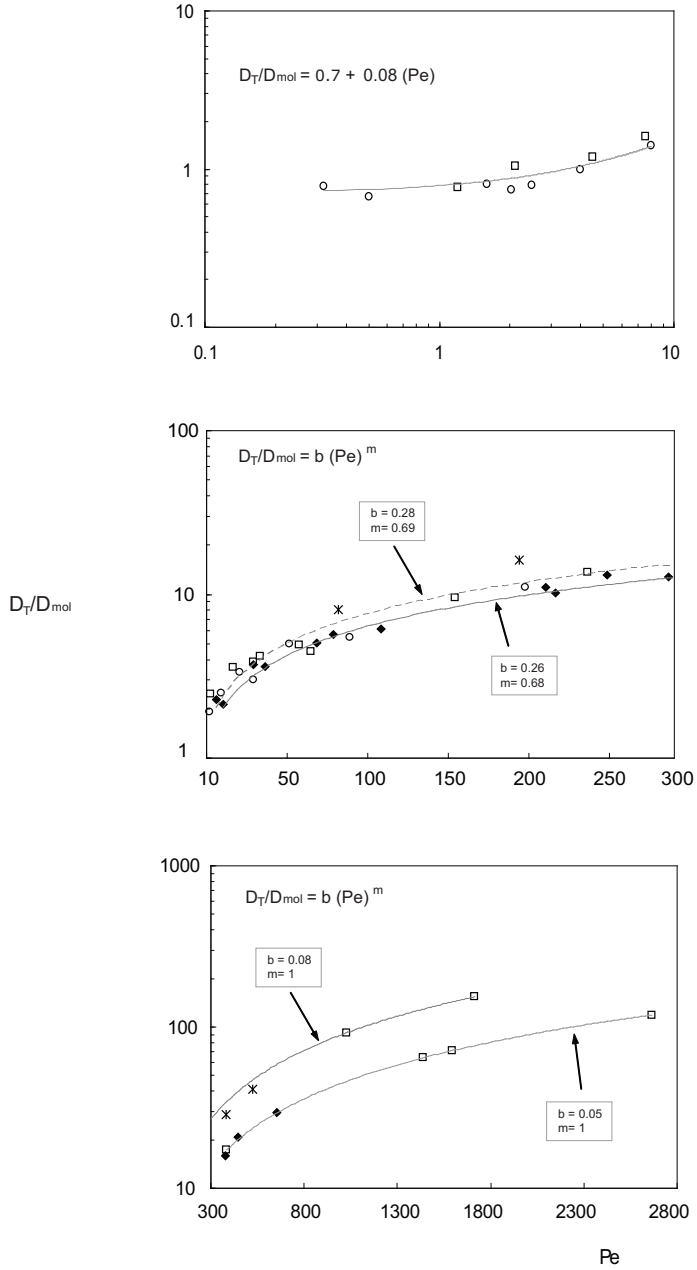

Figure 4.22: Transverse dispersion regimes inferred from experimental data.

previous experimental studies (Olsson & Grathwohl, 2007). Theoretical descriptions of transverse dispersivity approximate α_T to $\sim 3/16\ d_{50}$ (De Josselin de Jong, 1958). However, this expression usually yields slightly larger dispersivity values than those found in laboratory experiments and assumes that dispersivity is independent of fluid velocity.

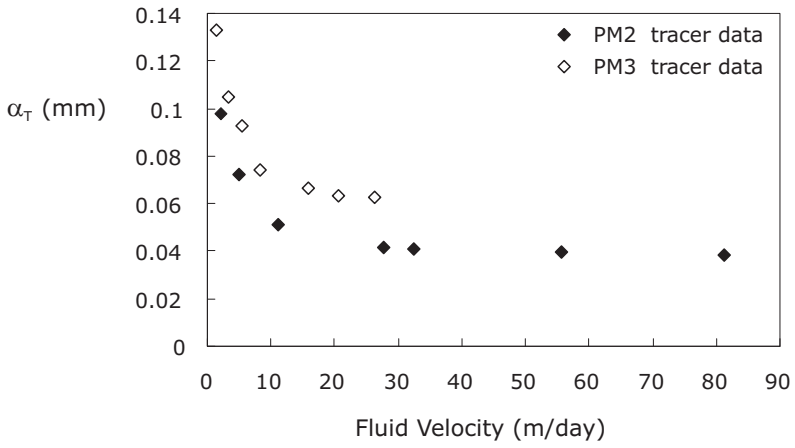

Figure 4.23: Transverse dispersivity as function of fluid velocity obtained from *PM2* and *PM3* tracer experiments. The average grain diameters are 0.86 mm and 1.86 mm for PM2 and PM3 respectively.

An additional observation from Figure 4.23 is that the apparent decrease in dispersivity reaches a constant value for velocities higher than 10 m/day (or equivalent Pe >200). Figure 4.24 compares tracer results with literature data plotted in terms of apparent dispersivity decrease as a function of Pe. A similar trend of decreasing dispersivity with increasing Pe is observed for all sets of tracer experiments. Although the overall degree of reduction depends on the porous medium type, there appears to be a critical value of Pe after which a constant dispersivity value is attained. This critical value may be related to the onset of the purely mechanical dispersion regime and thus varies from porous medium to porous medium. Note that the scaling shown in Figure 4.24 was obtained dividing by the largest dispersivity value reported.

To account for the observed nonlinear dependence a modified form of the apparent transverse dispersivity is obtained by substituting equation (4.8) in (4.11), yielding an expression for dispersivity that depends on molecular diffusivity, fluid velocity and grain size,

$$\alpha_T = 0.26(Pe)^{0.68} \cdot \frac{D_{mol}}{v}. \tag{4.12}$$

The validity of expression (4.12) should be confined to a range of Peclet numbers

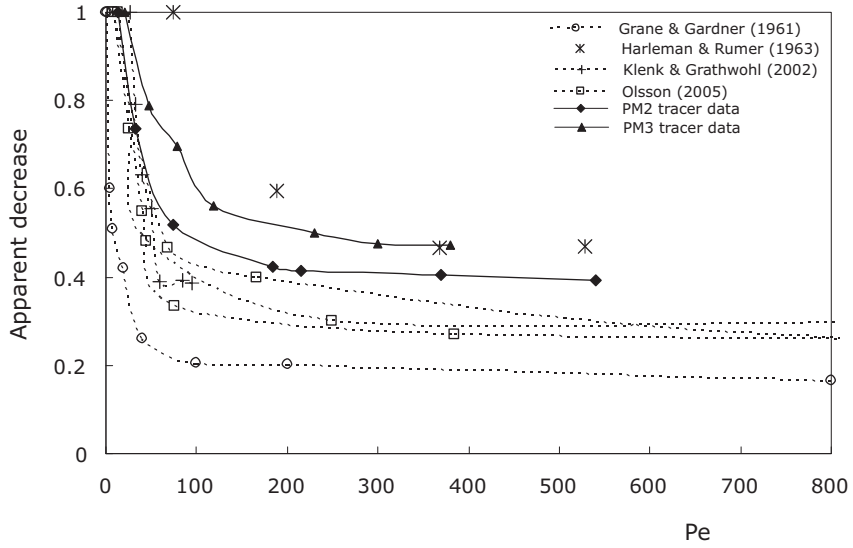

Figure 4.24: Apparent decrease of transverse dispersivity as function of Peclet number. Plotted data correspond to previous experiments and this study.

between ≈ 15 to ≈ 300 (in this study). For $Pe > 300$, a constant dispersivity assumption (although at a reduced value) seems appropriate. The latter is consistent with the observations arising from Figure 4.22.

4.4.2 Transverse dispersion — effects of density differences

Ideal tracer conditions

Tracer experiments are in fact carried out by adding a small amount of tracer and properties of the fluid such as density or viscosity are not significantly altered. However, Leroy *et al.* (1992) showed that in vertical transport, even if the density differences are small, for low-enough flow rates additional velocity components become significant leading to a suppression of dispersion. In order to investigate the impact of small density differences on the transverse coefficient, Figure 4.25 shows the ratio D_T/D_{mol} as a function of the density difference. From this, the value of the ratio D_T/D_{mol} is extracted (indicated by the arrows). It is equivalent to the asymptotic limit $\Delta\rho = 0$. Data sets used correspond to the first 4 velocities of the PM3-series. The estimated difference between the ratio D_T/D_{mol} under ideal tracer conditions and for the density differences used in the tracer experiments lies between 3% and 5%. Thus, it can be concluded that the small $\Delta\rho$ imposed on the tracer experiments does not affect the outcome of the experiments significantly.

Next, results from all the brine experiments from both PM2 and PM3 series

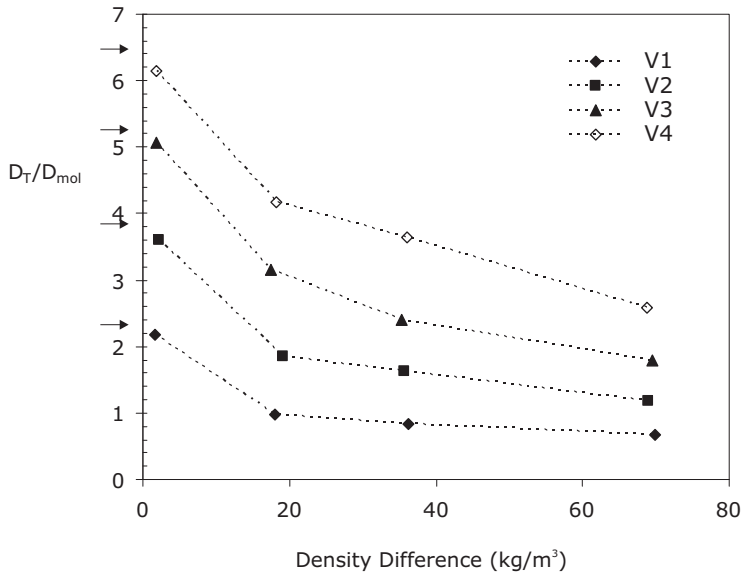

Figure 4.25: Effect of density difference on D_T/D_{mol} ratio. Results plotted correspond to experiments from PM3-series. Arrows indicate the extrapolated value of D_T/D_{mol} at $\Delta\rho$=0.

are plotted in Figure 4.26 in terms of the ratio D_T/D_{mol}. While tracer data is a function of Pe only (as seen in Figure 4.20), brine data does not correlate exclusively with Pe. Moreover, the relation of D_T/D_{mol} with Pe is not unique for every imposed $\Delta\rho$. To better explains this, selected brine runs from the PM3 series for three density differences and the corresponding tracer runs are plotted in Figure 4.27 as a function of ratio D_T/D_{mol} and Pe. Curve fitting through the data is applied using the non-linear relationship between D_T/D_{mol} and Pe given by equation (4.11). It can be observed that the value of the coefficient m tends to the unity with increasing density difference. Recalling that in the previous section the lower value of the coefficient m was the result of the effects of fluid velocity on D_T/D_{mol}. It appears that the presence of a high density contrast counteracts this nonlinear behaviour.

Next, in Figure 4.28 brine experimental data is plotted as function of the gravity number, Ng,

$$\mathrm{Ng} = \frac{kg\Delta\rho}{\mu q}, \tag{4.13}$$

and it indicates the competition between gravity-induced flow (due to the existence of a $\Delta\rho$) and forced convection (due to the fluid flow). It can be observed that all brine data follows the same trend: for gravity number $>$ 150 the ratio

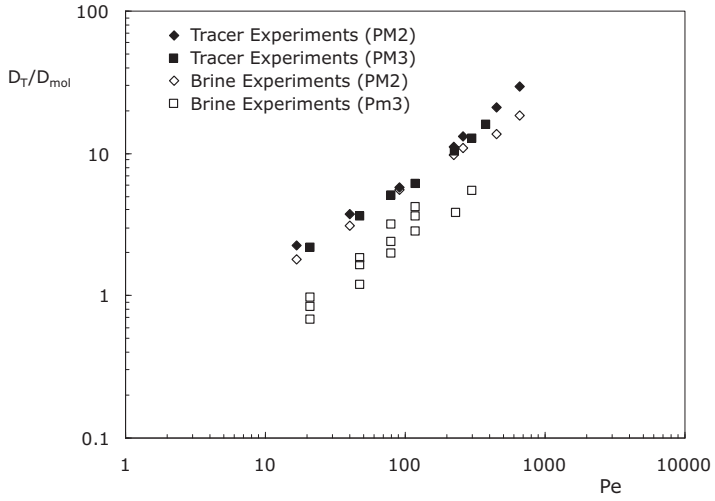

Figure 4.26: Ratio of computed apparent dispersion coefficient to the molecular diffusion coefficient as a function of the Peclet number.

D_T/D_{mol} decreases and appears to reach a constant value (hence independent of Ng). This constant value is approximately equal to the tortuosity factor 2/3 which also corresponds to the ratio $\frac{D_e}{D_{mol}}$ when $Pe \to 0$. This implies that when gravity effects are large, it leads to a complete suppression of mechanical mixing. At this point, molecular diffusion is the only mixing mechanism. To emphasize this behaviour Figure 4.28 is now plotted on a semi-log scale with values of the x-axis inverted.

Curve fitting the experimental data yields the following relationship,

$$\frac{D_T}{D_{mol}} = \frac{D_e}{D_{mol}} + R \cdot (\mathrm{Ng})^p. \tag{4.14}$$

where the coefficients R and p take the value of 25 and 0.64 respectively. Note that the gravity number can also be seen as the ratio between the critical vertical velocity q_c (defined in Chapter 2),

$$q_c = \frac{kq\Delta\rho}{\mu_f}. \tag{4.15}$$

and the specific discharge q, i.e., $\mathrm{Ng} = q_c/q$. Or in terms of the fluid velocity if $v_c = q_c/n$. With this definition, the gravity number represents competition between a vertical velocity component induced by gravity and the horizontal velocity component. The effect of this interaction appears to be the cause of the suppression of dispersion observed in the experiments.

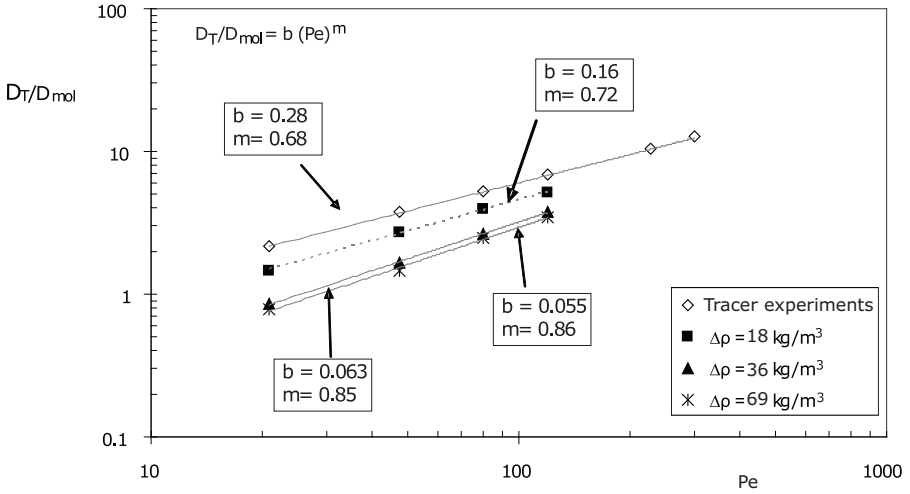

Figure 4.27: Effect of $\Delta\rho$ on the ratio D_T/D_{mol}. The data corresponds to the tracer and brine runs of the PM3 series.

Transverse dispersivity

Transverse dispersivity exhibits a decrease in value with increasing $\Delta\rho$. However, the decrease is not the same for all the constant-velocity experiments even if the imposed density differences were approximately the same. It is possible to merge all the curves if the apparent dispersivity decrease is plotted as a function of the gravity number (see Figure 4.30). The scaling is done by diving the dispersivity obtained from the brine experiments by the corresponding tracer dispersivity for each imposed velocity. This scaling is necessary as transverse dispersivity from tracer experiment exhibits a decrease with increasing velocity alone. If the scaling is done as in Landman (2005), i.e., scaling all dispersivities by the lowest Ng experiment, it will result in a large scatter of the data. Curve fitting through the data yields a power-law function for the scaled dispersivity with the gravity number:

$$\frac{\alpha_{T(\rho)}}{\alpha_T} = S \cdot (\mathrm{Ng})^{-a} \tag{4.16}$$

where $\alpha_{T(\rho)}$ denotes the dispersivity corresponding to a brine experiment, α_T is the tracer dispersivity, and coefficients S and a have values of 2.5 and 0.47, respectively. If the ratio $\frac{\alpha_{T(\rho)}}{\alpha_T}$ is used as a 'correction factor' for the effects of brine properties on the tracer dispersivity, substituting equation (4.16) in (4.12) yields,

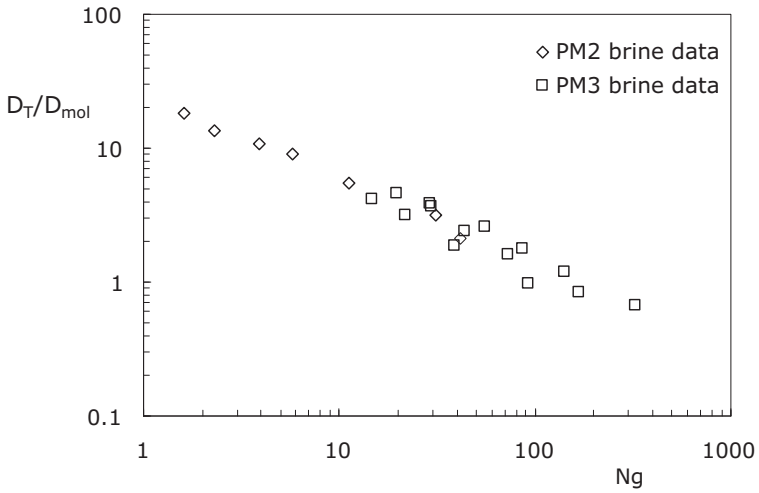

Figure 4.28: Ratio of transverse dispersion coefficient to molecular diffusion coefficient as a function of gravity number. Log-log scale.

$$\alpha_T = 0.65\ (Pe)^{0.68} \cdot \frac{D_{mol}}{v} \cdot \frac{1}{(\mathrm{Ng})^{0.47}} \tag{4.17}$$

This expression confirms that indeed dispersivity is not constant but depends on both porous media properties and fluid properties. Comparing literature values for longitudinal dispersivity with transverse dispersivity values, it is noticed that the magnitude of the gravity number has to be substantially higher for α_T than for α_L in order to observe a suppression effect. Taking for instance a gravity number of 1.5, this would lead to a reduction of the longitudinal dispersivity of up to 80% (see Landman (2005), Fig. 7.15). In comparison, transverse dispersivity would only exhibit a reduction of around 2% of its initial (tracer) value.

4.5 Summary and Conclusions

This Chapter presented the results of laboratory experiments on transverse dispersion in homogeneous porous media. The effects of varying fluid velocity, density differences and porous media characteristics on the transverse dispersion coefficient, D_T and transverse dispersivity, α_T were assessed. New empirical relationships to describe the behaviour of D_T and α_T are proposed in terms of the Peclet number, Pe and the gravity number, Ng. The main findings are summarised below.

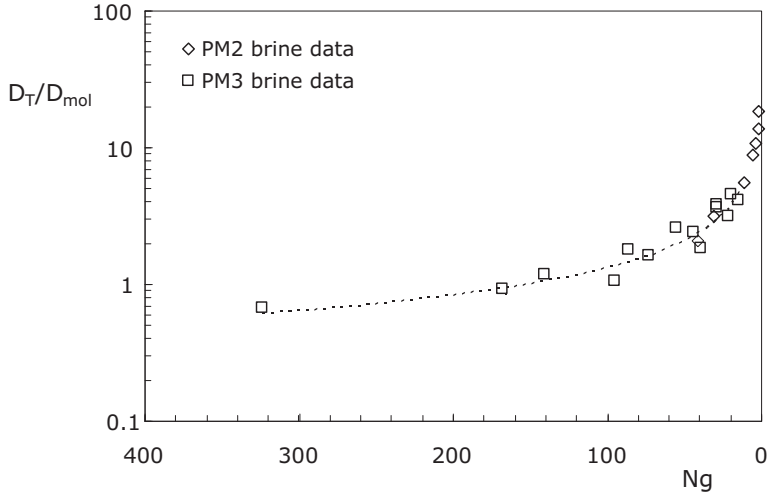

Figure 4.29: Ratio of transverse dispersion coefficient to molecular diffusion coefficient as a function of the Gravity number. Semi-log plot with x-axis inverted values.

1. Results from the tracer experiments confirm previous experimental observations that the transverse dispersion coefficient has a non-linear relationship with the Peclet number. This nonlinear relationship holds mainly in an intermediate range of Pe numbers, namely $300 > Pe > 10$. In this range, transverse dispersion is the result of the interplay between molecular diffusion and advection.

2. Further comparison with literature values showed that two other dispersion regimes could be inferred from the behaviour of D_T with Pe. For $Pe << 10$ the transverse dispersion coefficient is virtually independent of Pe and tends to a constant value equivalent to the tortuosity factor, τ. This regime is diffusion-dominated. For $Pe > 300$ a linear dependence of D_T on Pe was observed. This ranges corresponds to the purely mechanical dispersion (advection-dominated) regime.

3. The cause of the non-linear behaviour in the intermediate Pe range may be attributed to incomplete mixing at the pore-spaces due to insufficient residence time. The observed sublinear function of D_T with Pe indicates not only that diffusion cannot effectively even out the concentration variations within the interstices but also that dispersion is less than if complete mixing is assumed.

4. The presence of a density difference between the mixing fluids leads also to

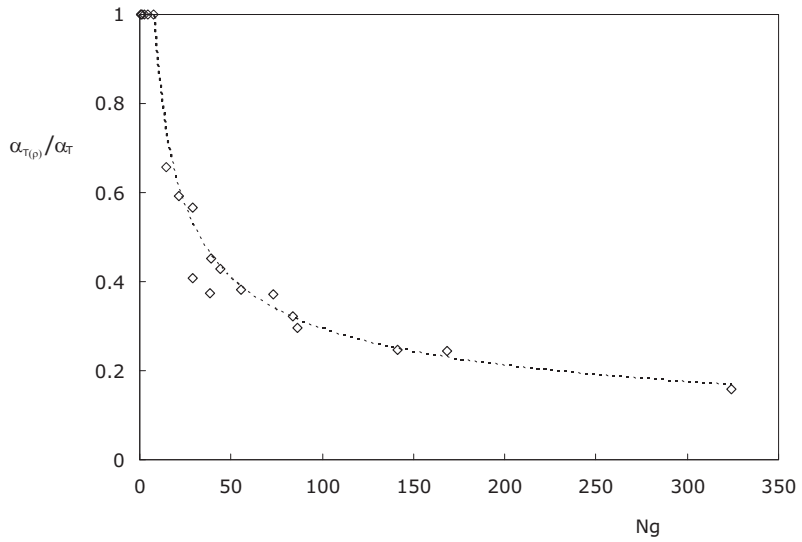

Figure 4.30: Apparent decrease of transverse dispersivity as function of Gravity number. The dashed line is the best-fit curve. Plotted data correspond only to PM3-series experiments .

non-linearities in the dependence of D_T on Pe. Results from the brine experiments showed that an increase in the density difference yielded a reduction in the transverse dispersion coefficient.

5. However, it is in fact the interaction between the density difference and the fluid velocity that determines the net effect on D_T. Hence, the behaviour of D_T in brine experiments can be directly related to the gravity number, Ng.

6. The relation between D_T and Ng points at the physics underlying the reduction in transverse dispersion: competition between gravity forces and advective forces.

7. Transverse dispersivity is also affected by changes in fluid velocity and density differences. These effects were quantified by means of an apparent decrease. Curve fitting of the experimental data yielded non-linear relationships of α_T with Pe for tracer conditions, and in terms of Ng for brine conditions.

8. These empirical expressions show that transverse dispersivity cannot be considered a constant property of the porous medium but has to be made function of both the Peclet number and the gravity number for a better representation of its behaviour.

When looking at theoretical models of transverse dispersion (tracer), although the obtained expressions vary according to the assumptions made on the geometry of the porous medium and the interaction with the velocity field, the interaction of molecular diffusion with mechanical mixing is overlooked. Complete mixing at the pore space is always assumed. Though, this appears to be the cause of discrepancies between the theoretical expression and experimental results. Specially in an intermediate range of Peclet values varying between 10 and 300 as observed in the experiments. Another interesting remark is that these theoretical models are often given in terms of a constant property of the porous media, i.e., the dispersivity. Hence, the analysis of experimental data focuses mainly on proving the existence of dispersivity. However, there already exists a wealth of experimental evidence showing that the classical definition of dispersivity as a medium constant fails to hold. In the following Chapter, the experimental results are used to assess the applicability of theoretical models on density-dependent transport.

Bibliography

Bear, J. Dynamics of Fluids in Porous Media. American Elsevier, New York, 1972.

Bear, J., and Bachmat, T., 1967. A generalized theory on hydrodynamic dispersion in porous media. IASH Symp. Haifa, Publ., 72, 7-16.

Bijeljic, B. and Blunt, M., 2004. Pore-scale modelling of transverse dispersion in porous media. Water Resour. Res. 40, W12S11, doi:10.1029/2006WR005700.

de Josselin de Jong, G., 1958. Longitudinal and transverse diffusion in granular deposits. Transactions of the American Geophysical Union 39, 67-74.

Diersch, H.J., and Kolditz, O., 2002. Variable-density flow and transport in porous media: approaches and challenges. Adv. Water Resour. 25(812), 899944.

Fried, J.J., Combarnous, M.A., 1971. Dispersion in Porous Media. Advances in Hydroscience 7, 169-282.

Gaganis, P., Skouras, E.D., Theodoropoulou, M.A., Tsakirogloua, C.D., and Burgano, V.N., 2005. On the evaluation of dispersion coefficients from visualization experiments in artificial porous media. Journal of Hydrology, 307, 79-91.

Grane, F.E., Gardner, G.H.F., 1961. Measurements of transverse dispersion in granular media. J. Chem. Eng. Data 6(2), 283-287.

Ham, P.A.S., R.J. Schotting, H. Prommer, and G.B. Davis, 2004. Effects of hydrodynamic dispersion on plume lengths for instantaneous bimolecular reactions. Adv. in Water Resour 27(8), 803-813.

Ham, P.A.S., Prommer, H., Olsson, Å.H., Schotting, R.J., Grathwohl, P., 2007. Predictive modelling of dispersion controlled reactive plumes at the laboratory-scale. J. Contam. Hydrol. 93(1-4), 304-315.

Harleman, D.R.F., Rumer, R.R., 1963. Longitudinal and lateral dispersion in an isotropic porous medium. J. Fluid Mech. 16, 385-394.

Hassanizadeh, S. M., Leijnse, A., de Vries, W. J., and Stapper, R. A. M., Experimental study of brine transport in porous media. RIVM Report 728514005, Bilthoven, The Netherlands, 1990

Hassanizadeh, S.M., and Leijnse, A., 1995. A non-linear theory of high-concentration-gradient dispersion in porous media. Adv. Water Resour., 18, 203-215.

Huang, W.E., 2002. The role of transverse mixing of electron acceptors and carbon substrates in natural attenuation. PhD thesis, University of Sheffield, Sheffield.

Johannsen, K., 2003. On the validity of the Boussinesq approximation for the Elder problem. Computational Geosciences, 7(3), 169182.

Klenk, I.D., Grathwohl, P, 2002. Transverse vertical dispersion in groundwater and the capillary fringe. J. Contam. Hydrol. 58, 111-128.

Landman, A.J., 2005. Analysis of physical mechanisms underlying densitydependent transport in porous media, Ph.D. Thesis, Delft University of Technology.

Landman, A.J., and Schotting, R.J., 2007. Heat and brine transport in porous media: the Oberbeck-Boussinesq approximation revisited. Transport in Porous Media, 70, 355-373.

Leroy, C., Hulin, J. P., and Lenormand, R., 1992. Tracer dispersion in stratified porous media: influence of transverse dispersion and gravity. J. Contam. Hydrol., 11:,51-68.

Olsson, Å.H., 2005. Investigation and modelling of dispersion-reaction processes in natural attenuation groundwater. PhD thesis, Eberhard-Karls Universität of Tübingen, Tübingen.

Olsson, Å.H., Grathwohl, P, 2007. Transverse dispersion of non-reactive tracers in porous media: A new nonlinear relationship to predict dispersion coefficients. J. Contam. Hydrol. 92, 149-161.

Perkins, T.K., and Johnston, Q.C., 1963. A review of diffusion and dispersion in porous media. Soc. Petrol. Engrs. J. 3(1), 7086.

Sahimi, M., B. D. Hughes, L. E. Scriven, and H. T. Davis, 1986, Dispersion in flow through porous media. 1. One-phase flow, Chem. Eng. Sci., 41, 21032122.

Scheidegger, A.E., 1961. General theory of dispersion in porous media. J. Geophys. Res. 66(10), 3273-3278.

Schotting, R.J., Moser, H., Hassanizadeh, S.M., 1999. High-concentration-gradient dispersion in porous media: experiments, analysis and approximations. Adv. Water Resour. Res. 22(7), 665-680.

Spitz, K., 1985. Dispersion in porous media: influence of inhomogeneities and density variations. PhD Thesis (in German), University of Stuttgart.

Starke, B., 2005. Experimental and numerical investigations of macrodispersion of density-dependent flow and transport in stochastic porous media. PhD Thesis (in German), University of Kassel.

Taylor, G., 1953. Dispersion of soluble matter in solvent flowing slowly through a tube. Proc. R. Soc. Ser. A 219, 186-203.

Watson, S.J., Barry, D.A., Schotting, R.J., and Hassanizadeh, S.M., 2002. Validation of classical density-dependent solute transport theory for stable, high-concentration-gradient brine displacements in coarse and medium sands. Adv. Water Resour. Res. 25, 611-635.

Chapter 5

Density-dependent transverse dispersion: comparison with theoretical models

This Chapter compares the results of the laboratory investigation presented in Chapter 4 with predictions of two theoretical models for density-dependent transport. The models are assessed based on their ability and limitations to reproduce the experimental observations.

5.1 Introduction

Saltwater intrusion is a widespread environmental problem in freshwater aquifers. Intrusion of saltwater occurs primarily from seawater in coastal aquifers, but the salinity may also come from other sources like deep saline aquifers, salt domes, leaching of shallow salt deposits, and of course anthropogenic sources. The quantitative assessment and prediction of saltwater intrusion in many applications relies on numerical modelling. However, modeling of density-dependent flow and transport has proven to be particularly challenging (Johannsen *et al.*, 2002). Changes in fluid's properties such as density or viscosity, e.g., induced by temperature of concentration changes, creates non-linearities in the coupling between flow and transport. In addition, the interaction with heterogeneities adds to the complexity of the problem. These heterogeneities can exists even in assumed homogenous system like laboratory columns (Landman, 2005).

Laboratory experiments on homogeneous vertical columns revealed that the presence of density differences influences the degree of hydrodynamic dispersion.

If the displacement is stable, a reduction of the longitudinal dispersion coefficient has been observed (Hassanizadeh *et al.*, 1990; Schotting *et al.*, 1999; Watson *et al.*, 2002). The phenomenon causing this suppression has been explained as follows. In a homogeneous laboratory column heterogeneities are present at the small scale. These micro-heterogeneities cause irregularities in the permeability distribution of the porous medium. This causes, in turn, horizontal density gradients in the displacing front. Gravity forces act on these density gradients, stabilizing and reducing the width of the dispersive front. This leads to a reduction of the dispersion coefficient.

Whether these phenomena are also observed for transport in the transverse direction was one of the aims of the experimental study presented in Chapter 4. The laboratory results showed that transverse dispersion is indeed affected by the presence of density differences between the resident fluid (fresh water) and the invading fluid (salt water). For a stable displacement, a reduction of the transverse dispersion coefficient is observed and depends not only on the density difference but also on the flow velocity. In this Chapter the results from the experimental investigation presented in Chapter 4 are compared with numerical and theoretical predictions. First, results from a numerical investigation on the effects of density variations on transverse dispersion are discussed. This is followed by a comparison of the experimental observations with theoretical ones. Two theoretical models of density-dependent transport are reviewed. The first model is the nonlinear model by Hassanizadeh & Leijnse (1995), so far only tested for longitudinal dispersion. The second model is an theoretical model by Demidov (2005) derived from homogenization principles. Both models are assessed in their abilities (and limitations) to reproduced the experimental observations.

5.2 Numerical study on transverse brine dispersion

In a recent publication by Nick *et al.* (2008) the effects of variable density on transverse dispersion are numerically investigated. A series of high resolution numerical simulations are conducted using the variable-density flow package d^3f. This code had previously been used in Johannsen (2003); Johannsen *et al.* (2002) to model density-dependent flow problems, and in Landman (2005) to investigate density-affected longitudinal dispersion.

5.2.1 Numerical experiments

Numerical experiments are carried out to investigate the effects of brine properties on transverse dispersion. Equally, the effects of medium heterogeneity are also studied. The model set-up is comparable to that of the laboratory experiments presented in Chapter 4. The two fluids, fresh water and salt water, flow parallel to each other in a uniform horizontal flow field mixing through transverse dispersion.

The displacement is miscible and stable. Figure 5.1 shows the dispersive zone that develops between the fluids. Tracer conditions correspond to a gravity number, Ng=0. The degree of heterogeneity is equal to σ^2 =0.1.

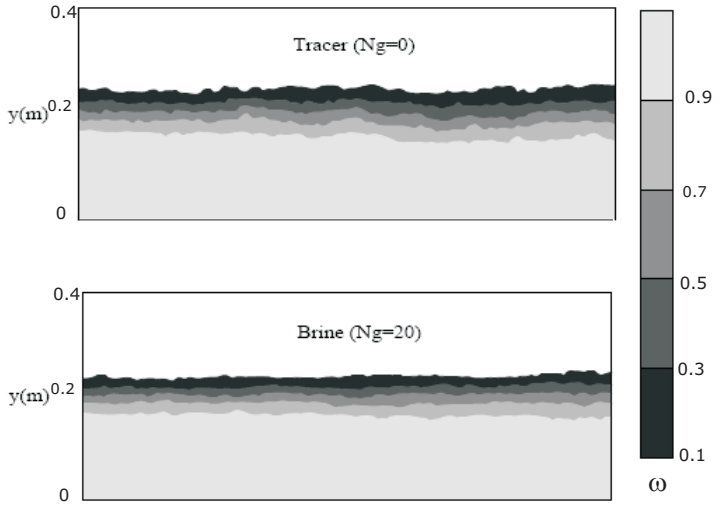

Figure 5.1: Computed mixing zone. Top panel: tracer conditions. Bottom panel: brine conditions

The mixing zone width is defined by the vertical distance where the mass fraction changes between 0 and 1. The perturbations (wiggles) in mixing zone are the result of micro-scale heterogeneities. These heterogeneities generate local variations in velocity and horizontal density gradients. Gravitational forces act upon them generating a smoother and smaller mixing zone. The transverse dispersion coefficient (and hence the transverse dispersivity) is related to the width of this mixing zone. Figure 5.1 illustrates that an increase in the gravity number results in a reduction in the width of the mixing zone.

In order to quantify the degree of suppression of transverse dispersion, Nick *et al.* (2008) plots de decrease of the apparent transverse dispersivity, i.e., the ratio between the tracer dispersivity (Ng=0) and the dispersivity at a given Ng. Note that for Ng >10 there is no further effect on the apparent decrease. This means a maximum degree of reduction in the order of 10% for a medium with an heterogeneity of σ^2 =0.1. However, if the degree of heterogeneity is increased (i.e., a larger σ^2) this leads to a higher reduction (for the same gravity number). This is illustrated in Figure 5.2.

Some of the main findings of this modelling study are:

- Individual changes in flow rate, density difference and permeability cannot

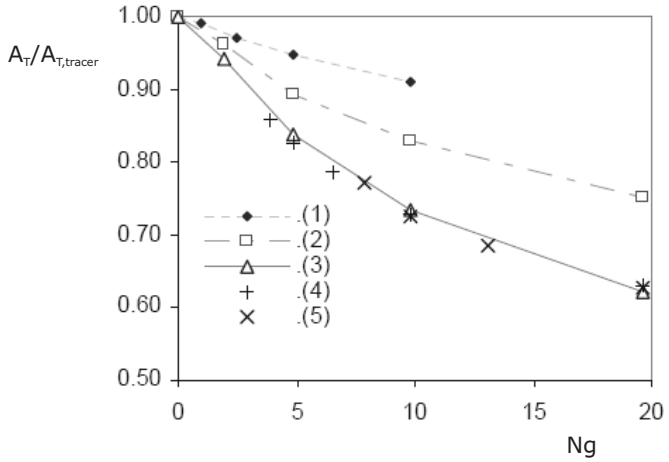

Figure 5.2: Scaled transverse dispersivity as a function of the gravity number for different heterogeneities. (1) $\sigma^2 = 0.1$.; (2) $\sigma^2 = 0.25$; (3) $\sigma^2 = 0.5$; (4) $k = 2 \cdot 10^{-10}\,\mathrm{m}^2$; (5) $k = 4 \cdot 10^{-10}\,\mathrm{m}^2$. From (Nick *et al.*, 2008)

be directly related to the reduction of dispersion. The controlling variable is the gravity number which contains all those variables.

- The decrease of the apparent transverse dispersivity is hence the result of the action of gravity forces which act upon the horizontal density gradients. This reduces the width of the mixing zone and thus the transverse dispersivity.
- The amount of decrease in the apparent dispersivity is a function of the heterogeneity of the medium. The more heterogeneous a medium is, the higher the achievable reduction (for the same gravity number).
- For a medium with an heterogeneity comparable to that found in homogeneous laboratory models (i.e. $\sigma^2 = 0.1$), the apparent decrease reached up to 10%.
- When compared to observations for longitudinal dispersivity, the magnitude of the gravity number has to be substantially higher for a decrease in the transverse dispersivity to be observed.

5.2.2 Comparison with experimental observations

A feature arising from Figure 5.2 is that the stronger the heterogeneity the stronger the gravity effect. Figure 5.3 compares the results from the experiments reported in Chapter 4 corresponding to experiments in weakly heterogenous media with

results from Starke (2005) corresponding to experiments in media with stronger heterogeneity. This comparison confirms observations by Nick *et al.* (2008). In effect, for a given Ng, the observed decrease in the apparent dispersivity is higher in a medium with stronger heterogeneity.

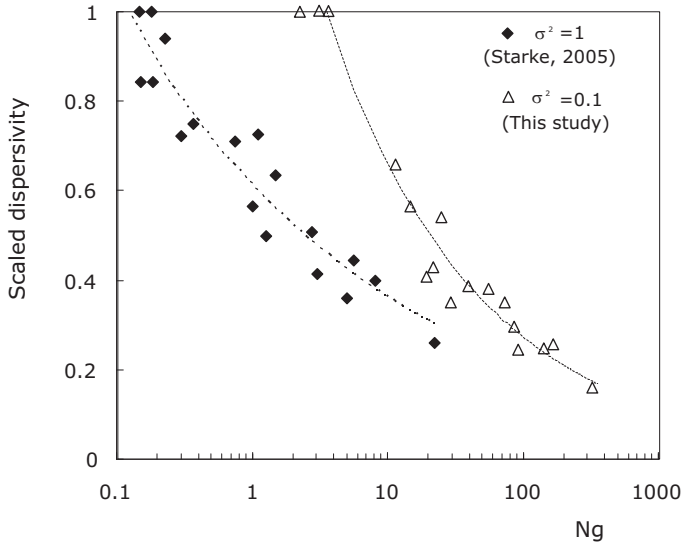

Figure 5.3: Scaled transverse dispersivity as a function of the medium heterogeneity. Solid symbols correspond to a medium with strong heterogeneity (Starke, 2005) and empty symbols correspond to a medium with weak heterogeneity (this study).

It follows from Figure 5.2 that in a medium with a weak heterogeneity (equivalent to homogeneous laboratory models) a maximum decrease in the apparent dispersivity is around 10%. However, the laboratory experiments in this study showed that transverse dispersivity is in fact suppressed up to 80% (as observed in Figure 5.3). In order to explain the difference between numerical results and laboratory results two possibilities may be explored: i) The computer code d^3f used in the numerical computations is based on the classical (linear) form of Fick's law and valid at the Darcy average scale. Consideration of other alternative forms of the Fick's Law like the nonlinear model by Hassanizadeh & Leijnse (1995) may be able to better represent the observed experimental behaviour. ii) Other physical processes have to be taken into account. However, these mechanisms would have to occur at a different scale, e.g., the scale of pores. The homogenization model of Demidov is derived starting from the pore-scale level and the obtained upscaled coefficients reflect the physical processes that occur at this scale. Note the fact that transverse dispersion is strongly affected by mechanisms occurring

at the pore scale has already been suggested in Chapter 4, i.e., incomplete mixing at the pore spaces.

5.3 Non-linear model of Hassanizadeh and Leijnse

As discussed in Chapter 2, dispersion in porous media is typically modelled using linear Fick's Law of diffusion, which assumes the dispersive mass flux to be proportional to the mass fraction gradient,

$$\mathbf{J} = -\rho \mathbf{D} \cdot \nabla \omega, \tag{5.1}$$

where $\mathbf{J}$ is the dispersive mass flux vector, $\mathbf{D}$ is the dispersion tensor, and the solute mass fraction ω, defined by $\omega = C/\rho_f$. The symbols C and ρ_f denote the solute concentration and fluid's density respectively. According to equation (5.1), the dispersion tensor is assumed to be independent of the solute mass fraction and its gradient. However, it is dependent of fluid velocity, v, following, e.g., Scheidegger (1961),

$$\mathbf{D} = (D_e + \alpha_T v)\mathbf{I} + (\alpha_L - \alpha_T) vv/|v|, \tag{5.2}$$

where D_e is the (effective) diffusion coefficient, α_L and α_T are the medium constants longitudinal and transverse dispersivities, respectively. $\mathbf{I}$ is the unit tensor, and $|v|$ is the magnitude of the fluid velocity vector, v. For homogeneous media and tracer conditions, the Fickian dispersion theory seems to give satisfactory results when modelling hydrodynamic dispersion. However, Hassanizadeh & Leijnse (1995) argue that the applicability of linear Fick's Law breaks down in the presence of high-concentration gradients. The experiments reported in (Hassanizadeh *et al.*, 1990) showed that dispersivity did not remain constant but decreased with increasing density difference. That is, the apparent dispersivity became a function of the salt concentration (or density difference between the fluids) and hence not a porous media constant only. However, Hassanizadeh & Leijnse (1995) also showed that adjusting the dispersivity value for each brine experiment would not match fully the experimental curves. Instead the authors proposed a modified nonlinear dispersion equation of the form

$$\mathbf{J}(\beta|J| + 1) = -\rho \mathbf{D} \cdot \nabla \omega \tag{5.3}$$

where β is a high-concentration dispersion coefficient which is porous-medium function and may depend on the flow velocity. The applicability of (5.3) has been confirmed for one-dimensional vertical columns in Schotting *et al.* (1999); Watson *et al.* (2002). These conclusions were based on the modelling of the experimental breakthrough curves and the subsequent determination of the non-linear coefficient β as a fitting parameter. In addition, complementary information of the dependence of β on other parameters like flow rate has been presented.

Here, the non-linear theory by Hassanizadeh & Leijnse (1995) is tested against experimental data on transverse brine dispersion. However, instead of attempting to model the experimental profiles, a simpler approach is presented. The starting point is the assessment of the properties assigned for β in Hassanizadeh & Leijnse (1995):

- β is independent of fluid properties.
- β is a function of the flow velocity.
- β is isotropic (independent of direction).

According to Hassanizadeh & Leijnse (1995) the significance of the non-linear parameter β can be assessed by defining the reduction in the dispersion coefficient in terms of an apparent decrease. For a two-dimensional horizontal flow domain, the equation for dispersive flux in the transverse direction is given by

$$J_y = -\rho D_{T(\rho)} \frac{\partial \omega}{\partial y} = \frac{-1 + \sqrt{1 - 4\beta\rho D_T \frac{\partial w}{\partial y}}}{2\beta} \tag{5.4}$$

where $D_{T(\rho)}$ denotes the apparent dispersion coefficient as it is a function of the brine properties, and differs from the 'ideal' or tracer dispersion coefficient given by D_T. The mass fraction gradient $\frac{\partial w}{\partial y}$ has to be negative so the square root results in a real value. Next, the ratio between the apparent and the ideal coefficient defines the apparent decrease as follows,

$$\frac{D_{T(\rho)}}{D_T} = \frac{2}{1 + \sqrt{1 - \ 4\beta\rho D_T \frac{d\omega}{dy}}} \tag{5.5}$$

Solving for β and denoting the apparent decrease by $\theta = \frac{D_{T(\rho)}}{D_T}$ the expression reads,

$$\beta = \frac{1 - \left(\frac{2}{\theta} - 1\right)^2}{4\rho D_T \frac{d\omega}{dy}} \tag{5.6}$$

Equation 5.6 shows that β can be inferred from experimental data on the mass fraction gradient $\left(\frac{d\omega}{dy}\right)$ and the observed reduction in the dispersion coefficient θ.

5.3.1 Comparison with experimental results

The experimental results presented in Table 5.1 correspond only to experiments from the PM3-series. These experiments are of constant flow rate-type in which for a fixed flow velocity three different density contrasts are imposed. The same density difference was applied in subsequent experimental runs whilst varying the flow velocity. In practice, there were slight differences in the density contrast

Experiment	q (m/s)	θ	ϕ	$\Delta\rho$ (kg/m^3)	β (s m^2/kg)
PM3V1T	$6.54 \cdot 10^{-6}$	1	1	1.5	0
PM3V1B1	$6.54 \cdot 10^{-6}$	0.44	0.32	18	35973
PM3V1B2	$6.54 \cdot 10^{-6}$	0.39	0.25	36	51131
PM3V1B3	$6.54 \cdot 10^{-6}$	0.3	0.16	69	73515
PM3V2T	$1.48 \cdot 10^{-5}$	1	1	2.2	0
PM3V2B1	$1.48 \cdot 10^{-5}$	0.51	0.45	19	13874
PM3V2B2	$1.48 \cdot 10^{-5}$	0.45	0.39	35	18644
PM3V2B3	$1.48 \cdot 10^{-5}$	0.33	0.25	70	33857
PM3V3T	$2.45 \cdot 10^{-5}$	1	1	1.8	0
PM3V3B1	$2.45 \cdot 10^{-5}$	0.62	0.59	17.5	5192
PM3V3B2	$2.45 \cdot 10^{-5}$	0.47	0.43	36	10935
PM3V3B3	$2.45 \cdot 10^{-5}$	0.35	0.3	68	20152
PM3V4T	$3.74 \cdot 10^{-5}$	1	1	1.8	0
PM3V4B1	$3.74 \cdot 10^{-5}$	0.68	0.66	18	2794
PM3V4B2	$3.74 \cdot 10^{-5}$	0.6	0.56	36	4438
PM3V4B2	$3.74 \cdot 10^{-5}$	0.42	0.38	69	10094
PM3V5T	$7.2 \cdot 10^{-5}$	1	1	1.6	0
PM3V5B1	$7.2 \cdot 10^{-5}$	0.37	0.35	69	7520
PM3V6T	$9.4 \cdot 10^{-5}$	1	1	1.7	0
PM3V6B1	$9.4 \cdot 10^{-5}$	0.42	0.41	70	4432

Table 5.1: Experimental parameters from PM3-series brine runs.

between experimental sets. However, this variation is only minor and therefore assumed not to influence the analysis.

In order to obtain the β-values from each experimental profile, an optimization routine was used to extract the value of $\left(\frac{d\omega}{dy}\right)$. The mass fraction gradient corresponds to the experimental profile measured at the end of the experimental tank described in Chapter 4, i.e., at x =1.5 m. The mass fraction gradient is not constant over the whole profile and therefore for the calculations of β the maximum slope was used (attained at $\omega/\omega_0 = 0.5$). Table 5.1 lists the obtained β-values from the brine experiments. Values of θ are obtained by scaling the brine dispersion coefficient with the corresponding tracer experiment. In addition, a similar apparent decrease is defined for the transverse dispersivity given by $\phi = \alpha_{T(\rho)}/\alpha_T$. For the tracer experiments (experiments with a small $\Delta\rho$) the β-value corresponds to zero as θ equals 1.

Dependence of β on density difference and flow rate

Table 5.1 shows that for a fixed flow rate, the higher the density contrast the larger the value of β. This indicates that β is dependent on $\Delta\rho$ and a single value of the parameter β cannot be obtained for the experimental runs. This is in disagreement with reported behaviour of β in longitudinal dispersion experiments (Schotting *et al.*, 1999; Watson *et al.*, 2002). However, when looking at the variation of β with q, increasing the flow rate decreases the non-linear effects and hence the value of β. This is in accordance with results from aforementioned studies.

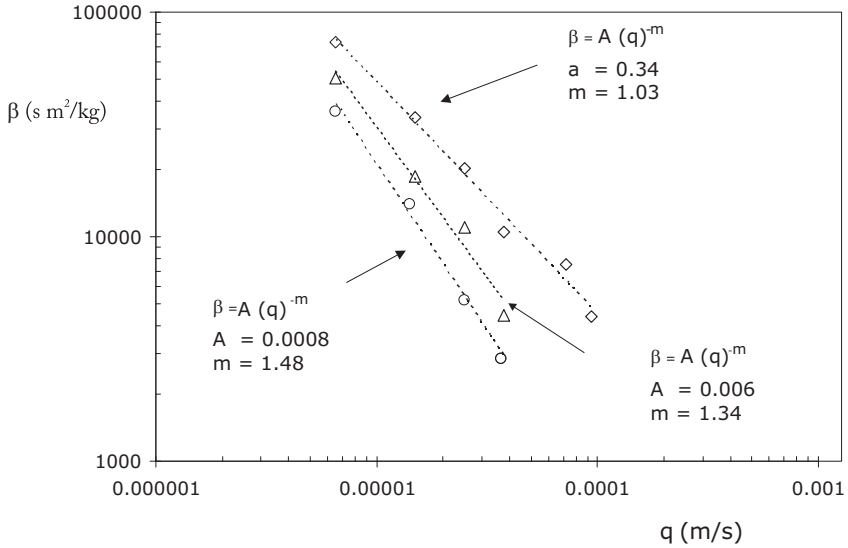

Figure 5.4: Experimental β-values as a function of flow rate. The three data sets plotted correspond to:($\diamond$) $\Delta\rho = 69$ kg/m^3, ($\triangle$) $\Delta\rho = 36$ kg/m^3 and ($\circ$) $\Delta\rho = 18$ kg/m^3. Dashed lines correspond to the least squares approximation.

The flow rate dependence of β is plotted in a log-log scale in Figure 5.4. For the three data sets, a least square curve fitting yields an expression of the following form,

$$\beta = A\, q^{-m} \tag{5.7}$$

where A and m are fitting coefficients. As observed in longitudinal dispersion experiments, transverse dispersion experiments also show that the nonlinear effects decrease with increasing flow rate. However, Figure 5.4 also reveals that it is in fact an interplay between flow rate and density difference what determines the nonlinear effects. The values obtained for m, 1.48, 1.34 and 1.03 suggest that an increase in $\Delta\rho$ results in a weaker flow rate dependence of β. Dependence of β

on $\Delta\rho$ suggests that in effect β cannot be considered as a property of the porous medium but has to be made function of the density contrast. Conversely, the dependence on q following expression (5.7) is in accordance with the premise that β is a function of flow velocity.

Transverse dispersivity

The relationship between the non-linear term β and the transverse dispersivity is assessed in terms of the apparent dispersivity decrease as defined by ϕ (see Table 5.1). This apparent decrease is plotted in Figure 5.5. The apparent decrease tends to a constant value below which it is independent of β.

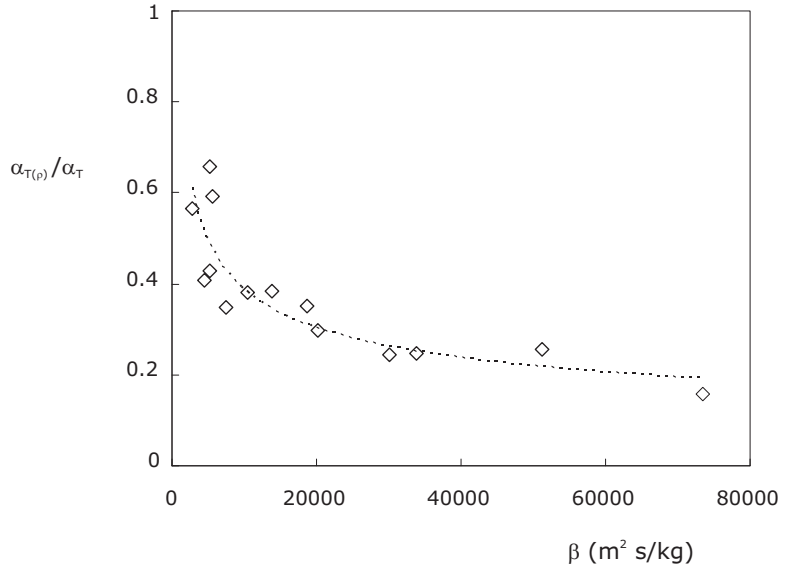

Figure 5.5: Scaled transverse dispersivity ($\phi = \alpha_{T(\rho)}/\alpha_T$) as a function of experimental β-values. Dashed line correspond to the approximation curve.

Dependence of β on J

Figure 5.6 compares the values of β for longitudinal dispersion and transverse dispersion experiments. The comparison is based using the data reported in Schotting *et al.* (1999) and in Watson *et al.* (2002) for the constant density difference experiments. The density difference in experiments by Schotting *et al.* (1999) was $\Delta\rho = 64$ kg/m^3 and in Watson *et al.* (2002) was $\Delta\rho = 200$ kg/m^3. The transverse dispersion experiments plotted correspond to $\Delta\rho = 69$ kg/m^3,

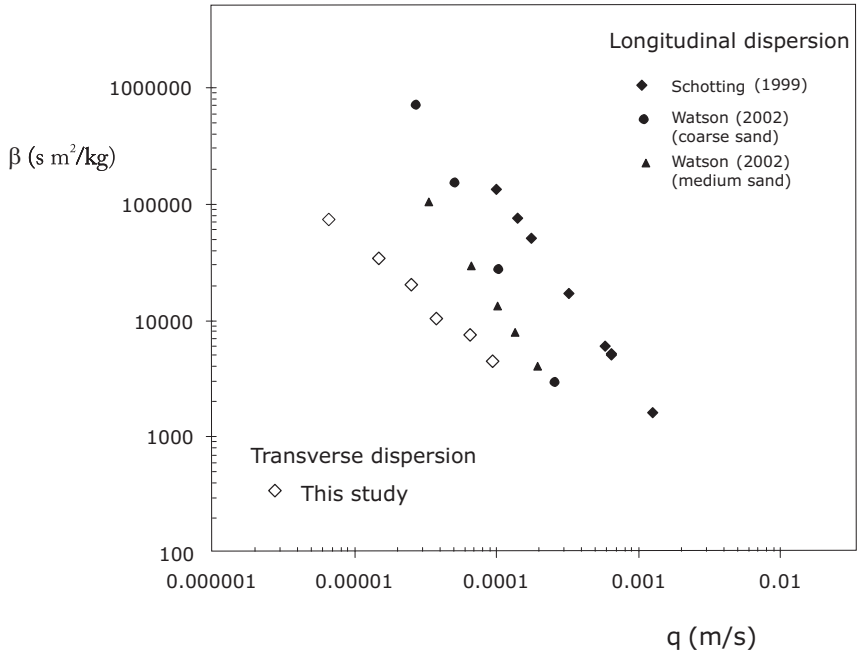

Figure 5.6: Behaviour of β as a function of flow rate for longitudinal and transverse dispersion experiments.

Although the imposed $\Delta\rho$ is not the same for all the experimental data, the comparison shown in Figure 5.6 may be regarded as only illustrative. However, considering that for longitudinal dispersion β is not affected by $\Delta\rho$ but only by q, the conclusions from this comparison are not necessarily only descriptive. The β-values obtained from the transverse dispersion experiments are smaller than those reported in longitudinal dispersion experiments. This means that β in fact depends on the direction of the displacement (i.e., longitudinally or transversally to the main flow direction) and cannot be considered an isotropic parameter. This is a similar conclusion as reported in Nick *et al.* (2008)

5.3.2 Discussion

Coefficient β as a function of the gravity number

The form of expression (5.5) indicates that the apparent decrease in the dispersion coefficient observed in the brine experiments is a function of the non-linear parameter β. Hassanizadeh & Leijnse (1995) explain that this parameter represents the opposition of the porous medium to disperse a solute and that this resistance in-

creases when the density gradient is larger. This in turn causes the deviation from the classical, linear Fick's Law. Hence, β is assumed to be a medium's property.

However, the observed dependencies of β on $\Delta\rho$ and q suggest differently. Not only β is a function of the fluid properties but also an underlying physics can be attributed to this coefficient. This is demonstrated as follows: it is possible to group all the experimental points in Figure 5.4 into a single curve if β is plotted as a function of Ng. The corresponding gravity numbers vary between 14 and 325.

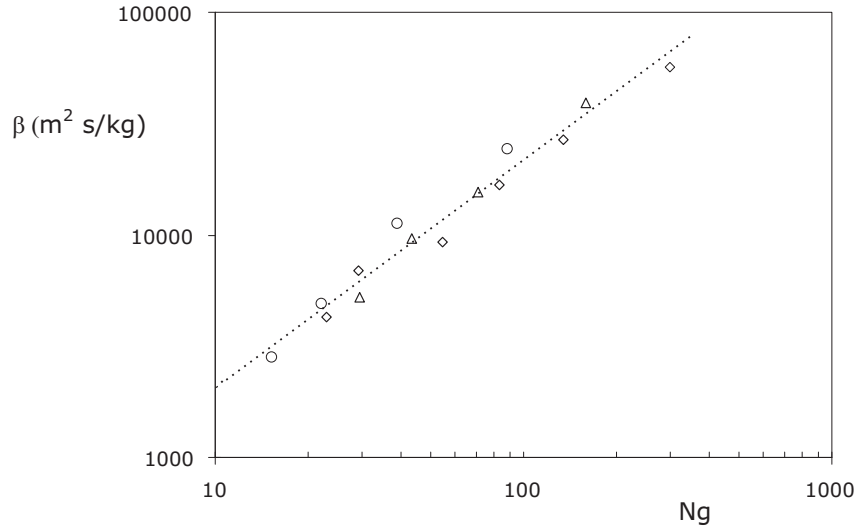

Figure 5.7: Experimental β-values as a function of the gravity number. The three data sets correspond to :($\diamond$) $\Delta\rho$ = 69 kg/m^3; ($\triangle$) $\Delta\rho$ = 36 kg/m^3; ($\circ$) $\Delta\rho$ = 18 kg/m^3. Dashed line correspond to the least squares approximation.

A least square curve fitting of the experimental points yields the the following linear relation (in a log-log scale) between β and Ng,

$$\beta = R \cdot \mathrm{Ng} \tag{5.8}$$

where $R = 257$. According to Hassanizadeh & Leijnse (1995), the presence of large density gradients induces also a large dispersive mass flux (larger than in tracer conditions). The opposition of the medium to disperse a fluid increases as a consequence. The non-linear dispersion equation (5.3) has to be employed in order to account for this effect. However, expression (5.8) shows that β can be directly related to physical mechanisms such as gravitational forces.

5.4 Homogenization Model of Demidov

As already introduced in Chapter 3, Demidov analyses density-coupled flow and transport in porous media using the concepts of homogenization. Stable vertical and horizontal flow configurations are studied, but here only the horizontal stable situation is reviewed. The homogenization theory consists of a separation of scales and is applied at the microscale to derive a set of upscaled equations that govern the macro-scale behaviour. In Demidov's analysis, the microscale corresponds to the pore-scale and the macroscale corresponds to one scale above referred to as the Darcy scale. Demidov's results are thus applicable to e.g., laboratory experiments in homogeneous porous media.

The resulting set of upscaled equations is used to describe the macroscale characteristics of the porous medium. These characteristics are in turn taken into account through dependencies of the coefficients in the various processes taking place. Demidov's analysis is given in terms of two coefficients: the permeability (filtration) coefficient K, and the effective transverse dispersion coefficient $D_\perp$. In the classical models, the permeability coefficient is commonly considered a medium constant. It is usually a function of a representative length of the pore space l such as the pore size or the grain size (Bear, 1972). Hence,

$$K = K^0 \tag{5.9}$$

where K^0 is constant the medium's permeability coefficient. Equally, the transverse dispersion coefficient $D_\perp$ is commonly defined in terms of a dependency with the Peclet number,

$$D_\perp(Pe_l, 0) = \zeta + D_\perp^0(Pe_l) \tag{5.10}$$

where ζ denotes the tortuosity coefficient and $D_\perp^0$ is the tracer dispersion coefficient. Note that although $D_\perp^0$ is explicitly a function of the Peclet number, its functional form is not given. Note also that $D_\perp$, ζ and $D_\perp^0$ are in fact scaled coefficients. The scaling parameter is the molecular diffusion coefficient D_{mol}. Consistent with the terminology used in previous chapters, the scaled Eq. (5.10) is equivalent to

$$\frac{D_T}{D_{mol}} = \frac{1}{\tau} + \frac{D_{mec}}{D_{mol}} \tag{5.11}$$

where D_{mec} denotes the mechanical mixing coefficient. However, Demidov's analysis shows that not only $D_\perp$ but also K are in fact depending on the local Peclet and Rayleigh numbers, i.e., $D_\perp(Pe_l, Ra_l)$, and K (Pe_l, Ra_l). The local Peclet and Rayleigh numbers defined by Demidov read,

$$Pe_l = \frac{vl}{D_{mol}} \tag{5.12}$$

and

$$Ra_l = \frac{gl^4}{\mu D_{mol}} \frac{\partial \rho}{\partial z}. \tag{5.13}$$

This implies that both, the permeability and dispersion coefficients are dependent on the fluid velocity v, through the Peclet number, and the density gradient $\left(\frac{\partial \rho}{\partial z}\right)$ through Ra_l.

5.4.1 Macroscopic coefficients

In order to determine the specific dependencies of K and $D_\perp$ on Pe_l and Ra_l, information of the microstructure of the porous medium has to be considered. To analyse horizontal transport, Demidov constructs a two-dimensional model referred to as the 'mesh model'. This model is shown schematically in Figure 5.8.

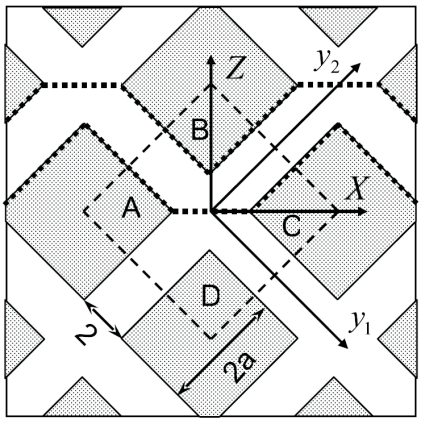

Figure 5.8: Mesh model of the porous medium considered by Demidov.

In the absence of density gradients (i.e., $Ra_l = 0$), the tracer coefficient $D^0_\perp(Pe_l, 0)$ grows monotonically with Pe up to a constant value approximately equal to 16 when $Pe \to \infty$. Figure 5.9 shows the dependency of $D^0_\perp$ on Pe.

Demidov explains that the behaviour $D^0_\perp(Pe) \to$ constant is the result of a stabilization of the density fields. This phenomenon is depicted in Figure 5.10 where concentration lines for $Ra = 0$ and small to large values of Pe are shown. Figure 5.10 shows the concentration isolines through the pore junction bounded by the area ABCD depicted in Figure 5.8. As the model is symmetrical, computations are carried out for half of the domain.

It can be observed that the concentration lines at $Pe = 10$ start only to spread over a part of the flow domain (left panel). With further growth of Pe (right panel) these lines are already spread (and stabilised) over the whole domain, hence $D^0_\perp$ comes to a constant value.

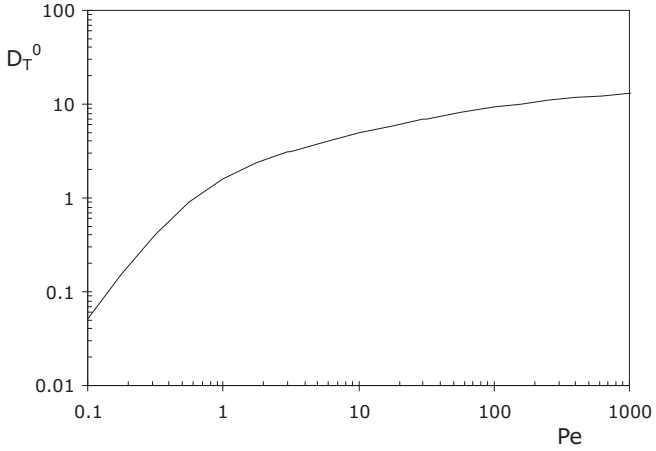

Figure 5.9: Dependence of the tracer dispersion coefficient on Pe

Next, the effect of density gradients (i.e., $Ra > 0$) on the flow structure is shown in Figure 5.11. It can be observed that under conditions of growing Ra there appears a re-arranging of the flow lines creating a zone of vortices (returning currents).

As these vortex cells grow, the area available for flow decreases. The consequences are two-fold: i) the permeability of the porous medium is reduced and thus no longer constant; ii) the diffusive exchange between the flow lines is also lowered which in turn decreases the dispersive mixing. Another observation from Figure 5.11 is that the evolution of the vortices zone is not only linked to changes in the Ra_l number but also to the Pe_l number. This implies that it is in fact the local gravity number G_l that controls this behaviour. Demidov defines the local gravity number by,

$$G_l = \frac{Ra_l}{Pe_l} = \frac{gl^3}{\mu v}\frac{\partial \rho}{\partial z}. \tag{5.14}$$

which reflects the competition between gravity forces (due to the existence of a density gradient) and the advective forces (due to flow). With these interesting results, Demidov makes a direct link to the physical processes underlying the observed decrease of dispersion (and permeability): the appearance and evolution of reversing currents (vortices) under the influence of gravity.

Correction for density effects

To account for the effect of density variations, Demidov introduces 'correction factors' for both the permeability and the dispersion coefficients. The general

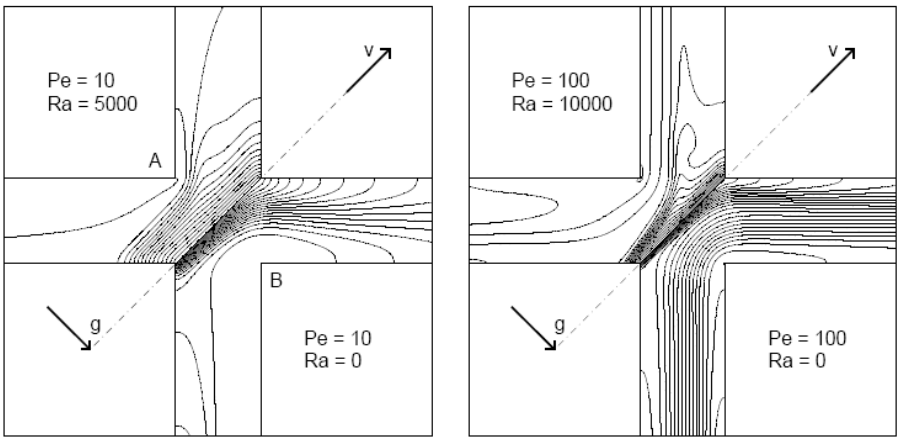

Figure 5.10: Concentration lines at $Ra = 0$ (lower-half in both panels)

form of equations (5.9) and (5.10) holds but the correction factors f_k and $f_\perp$ now modify the coefficients. The permeability (filtration) coefficient defined in terms of f_k reads,

$$K = K^0 \cdot f_k \tag{5.15}$$

The scaled transverse dispersion coefficient in terms of the correction factor reads,

$$D_\perp = \zeta + D_\perp^0 \, f_\perp + D_\perp^\infty (1 - f_\perp). \tag{5.16}$$

where $D_\perp^\infty$ denotes the effective dispersion coefficient at $Ra \to \infty$, equal to $1/2n$ with n being the porosity. Note that in the limit of $Ra \to \infty$, the correction factor, $f_\perp$ tends to 0, hence $D_\perp = \zeta + 1/2n$.

In this limit the only dispersion mechanism is molecular diffusion. If no density gradients are present and in the limit of mechanical mixing vanishing, $D_\perp$ approaches ζ only. However, in the presence of density gradients, dispersion (of diffusion) will always be higher. Rewriting equation (5.16) for the correction factor $f_\perp$ yields,

$$f_\perp = \frac{D_\perp - \zeta - D_\perp^\infty}{D_\perp^0 - D_\perp^\infty} \tag{5.17}$$

Note that the correction factor varies between 1 and 0. This factor can also be interpreted as the apparent decrease of the tracer dispersion coefficient due to density effects. Figure 5.12 shows for various Pe numbers the dependence of f_k and $f_\perp$ on the local gravity number and scaled gravity number, respectively. This scaled gravity number is necessary in order to merge all the curves corresponding to the different Pe into a single curve. To do this, Demidov normalizes G_l by the tracer dispersion coefficient $D_\perp^0$, that is $\tilde{G}_l = G_l / D_\perp^0$

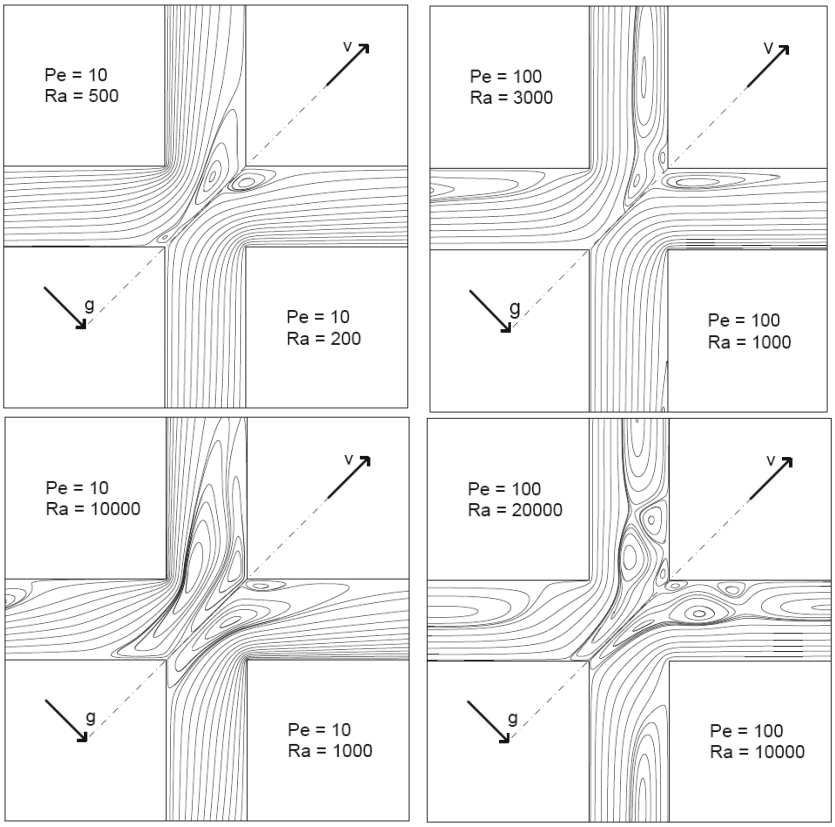

Figure 5.11: Flow lines with growth of Pe and Ra

The approximation curves shown in Figure 5.12 for f_k and $f_\perp$ obtained by Demidov read

$$f_k = \frac{1 + 0.08G_l}{1 + 0.09G_l + 0.05G_l^{3/2}} \tag{5.18}$$

and

$$f_\perp = \frac{1 + 0.1\tilde{G}_l}{1 + 0.25\tilde{G}_l^{\,3/2}} \tag{5.19}$$

In the next section the applicability of these formulas is compared with experimental observation. As no experimental data is available to assess the effects on the permeability coefficient, only the dispersion coefficient is assessed.

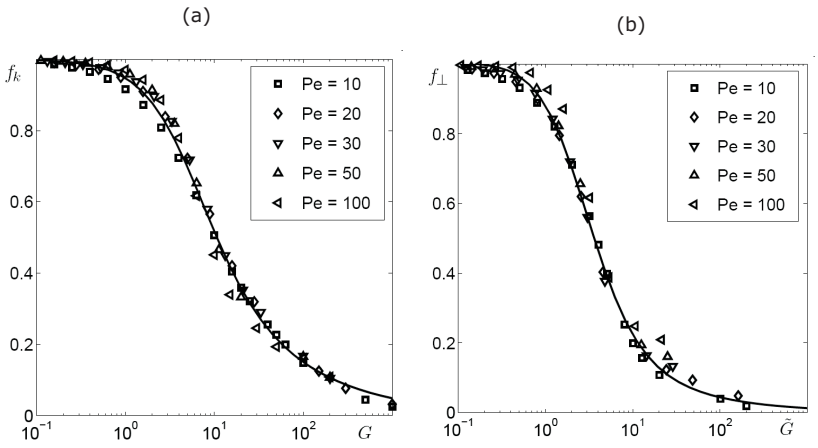

Figure 5.12: Dependence of the correction factors on the gravity number. (a)f_k; (b)$f_\perp$.

5.4.2 Comparison with experimental results

Tracer coefficient

Demidov denotes $D_\perp^0$ as the tracer dispersion coefficient. Recalling that $D_\perp^0$ is in fact a scaled coefficient with D_{mol} as the scaling variable. The tracer coefficient is assumed to be linearly dependent on the Peclet number, i.e., $D_\perp^0(Pe)$. Figure 5.13 compares the dependence of $D_\perp^0$ on Pe as predicted by the homogenization model with tracer data from the PM2 and PM3 experiments. For this comparison the Peclet number is denoted as,

$$Pe = \frac{ql}{D_{mol}} \tag{5.20}$$

where q is the specific discharge and the representative length scale l was assumed to be the average grain size. It can be observed that the homogenization model predicts slightly higher tracer coefficients. However, this behaviour is mostly confined to a range of Peclet values between approximately 10 and 200. In this range the dependence of the tracer coefficient on Pe appears to follow a power-law function. Next, the results of the homogenization model are corrected with a function following,

$$D_\perp^0 = Pe^a \tag{5.21}$$

where the value of the coefficient a was found to be 0.7. In Chapter 4 a similar power-law dependence of the tracer dispersion coefficient on Pe was reported. Note that differences between tracer data from PM2 and PM3 are only minor, suggesting that the dependence on Pe is medium-independent. This also implies that the

absolute value of the length-scale, l, does not play a role and the qualitative results by the homogenization model compare to the observed behaviour in the laboratory experiments.

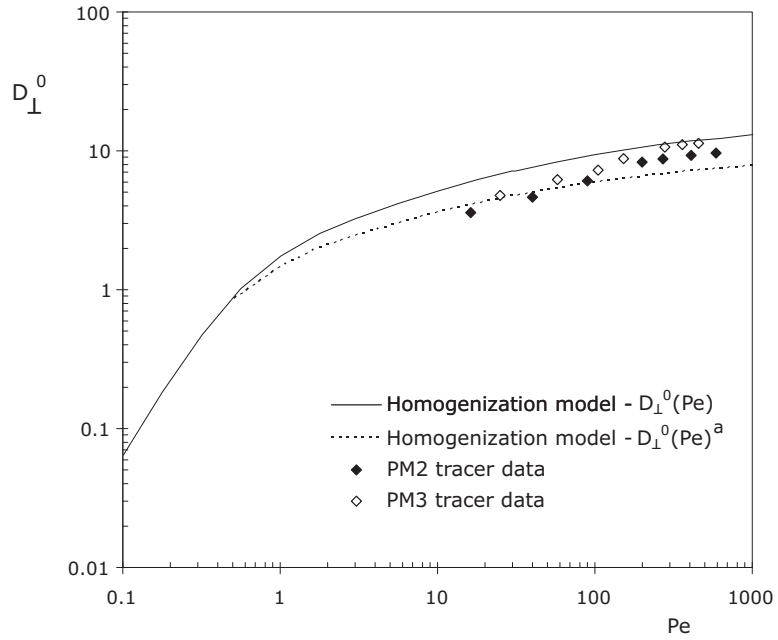

Figure 5.13: Dependence of the tracer dispersion coefficient on Pe and comparison with experimental data.

Density effects

The effects of density variations can be assessed in terms of an apparent decrease. That is, the dispersion coefficient obtained under brine conditions ($\Delta\rho > 0$) is divided by the dispersion coefficient under tracer conditions ($\Delta\rho = 0$). The apparent decrease of the effective dispersion coefficient ($\frac{D_\perp}{D_\perp^0}$) is plotted as a function of the gravity number. The results from the homogenization model are given in Figure 5.14a. Note that the apparent decrease is virtually independent of the Peclet number and reaches a minimum value of about 0.38 for Ng > 100. Next, the apparent decrease obtained from the brine experiments is shown in Figure 5.14b. The experiments reveal an apparent decrease of the dispersion coefficient which is also practically independent of the Pe. The apparent decrease reaches a minimum of approximately 0.3 which is only slightly lower than the predicted by the homogenization model. In addition, this minimum is also reached at Ng

values higher than 100.

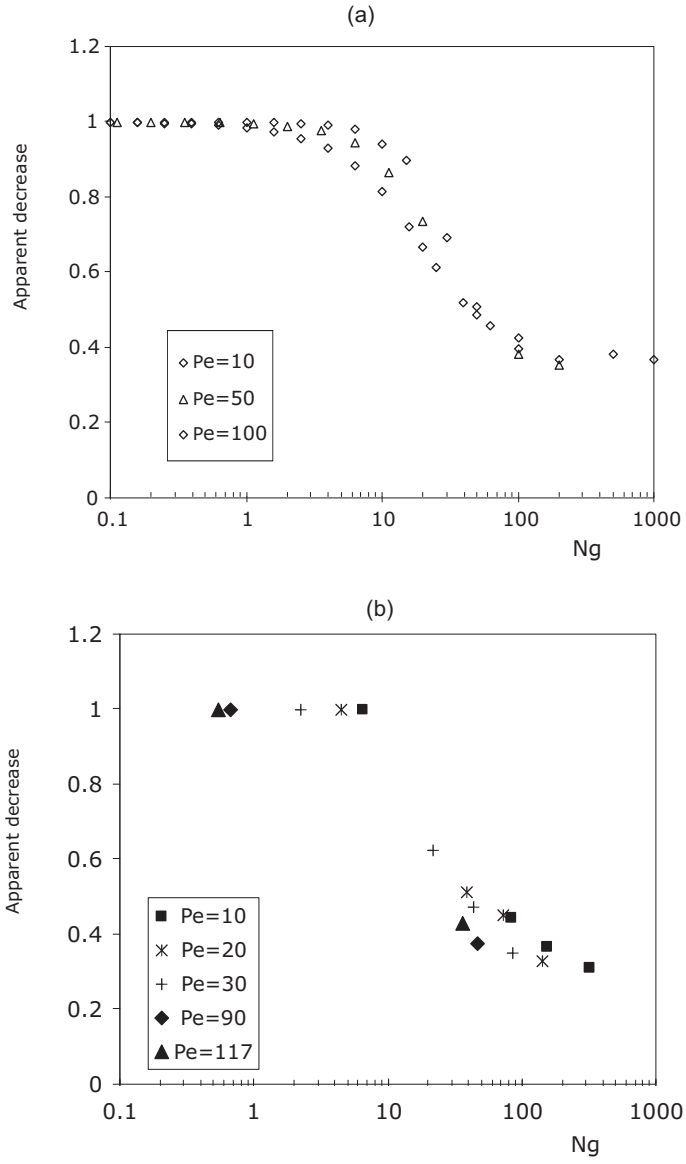

Figure 5.14: Apparent decrease of the dispersion coefficient as predicted by (a) the homogenization model and (b) experimentally observed.

Demidov introduces the correction factor $f_\perp$ to account for the density effects on the dispersion coefficient. This factor is defined in Eq. (5.17). A correction

factor for density effects is extracted from the experimental which is defined as,

$$f_{exp} = \frac{D_\perp - \zeta}{D_\perp^0} \tag{5.22}$$

where the tortuosity factor ζ for the experiments was 0.667 (see Chapter 4). Note that as oppose to Eq. (5.17), f_{exp} does not contain the term $D_\perp^\infty$. This is because the largest Ra number during the experiment is approximately 3200, hence contribution of $D_\perp^\infty$ to correction factor can be neglected. In order to compare the experimental results with the homogenization model, the gravity number is normalized by the tracer dispersion coefficient and denoted as $\tilde{N}g$. Figure 5.15 compares the experimentally-determined correction factor f_{exp} and results by the homogenization model $f_\perp$ as defined by expression (5.19). Although the qualitative behaviour is similar, the homogenization model curve is shifted with reference to the experiments. A possible explanation for this shift may be that the experimental correction factor does not take into account the effects at $Ra \to \infty$, i.e., $D_\perp^\infty$. This can only me ascertained for experimental data at higher Ra numbers.

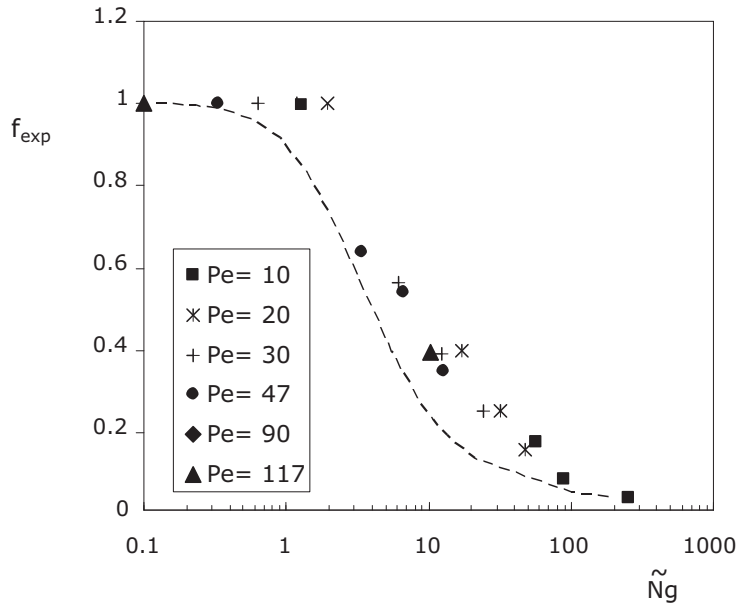

Figure 5.15: Correction factor predicted by the experiments. Dashed line corresponds to the approximation curve given by formula (5.19)

.

Parameter	Variable	Units	*PM3*
Grain size	d_{50}	(m)	$1.86 \cdot 10^{-3}$
Intrinsic permeability	k	(m^2)	$3.1 \cdot 10^{-9}$
Reference viscosity	μ	(Pa/s)	0.001
Reference density	ρ_0	(kg/m^3)	1000
Diffusion coefficient	D_{mol}	(m^2/s)	$1.24 \cdot 10^{-9}$

Table 5.2: Experimental Parameters

5.5 Oberbeck-Boussinesq approximation

As reviewed in Chapter 2, density-dependent flow and transport problems are classically modelled with a set of governing equations which include the continuity equation, the solute mass conservation, Darcy's Law, Fick's Law and equations of state. Additional simplifications such as the Oberbeck-Boussinesq (OB) approximation are commonly adopted in order to simplify these system of governing equations. One of the starting point in the homogenization model is the assumption of the OB approximation at the pore-scale. In a recent publication by Landman & Schotting (2007) the OB-approximation was revisited and formal limits were derived for which the OB is applicable. For isothermal brine transport (condition applicable to this study) the following criterion must be fulfilled in order to ensure that continuity equation holds, i.e., fluid volume changes can be neglected. This limit reads,

$$NPe = \frac{kg\rho_0 x_0}{\mu D_{mol}} \gg 1 \tag{5.23}$$

where x_0 denotes a length scale related to density variations. Note that this limit is independent of the density difference (only the reference density ρ_0) and the flow velocity. This criterion is now tested for the brine experiments of this study. The experimental parameters are summarised in Table 5.2. With these experimental values and substituting in Eq. (5.23) yields,

$$NPe = 2.45 \cdot 10^7 \cdot x_0 \tag{5.24}$$

The choice of characteristic length x_0 is related to the length where density changes occur (density gradient). At the scale of the laboratory experiments a characteristic length can be defined for the width of the mixing zone. This width is the vertical distance where the scaled concentration (or density) changes from 1 to 0. In Chapter 4 this mixing width was shown to be for brine experiments as small as 0.04 m. However, and as Demidov shows, another length scale for density changes also occurs at the pore-scale. In this case the pore size can be considered as the characteristic length. In practice it is difficult to measure the size of the pores. A common approach is to relate the pore size to a fraction of the average grain size d_{50}. In this case the pore size is obtained as (1/10) of

the average grain size. This yields $1.865 \cdot 10^{-4}$ m. Substituting both the lab-scale and the pore-scale characteristic lengths into Eq. (5.24) yields values of $9.81 \cdot 10^5$ and 4573, respectively. This implies that the condition (5.23) is fulfilled at both the experiment- and pore-scales. The volume effects which render the OB-approximation not applicable for certain conditions, are in this case not important. The OB-approximation applies to the experimental conditions.

5.6 Summary and Conclusions

In this Chapter the experimental results outlined in Chapter 4 are compared to numerical and theoretical predictions for density-dependent transverse dispersion. The numerical study presented in Nick *et al.* (2008) confirms experimental observations that the presence of density differences between the fluids affects transverse dispersion. In addition, the numerical experiments also confirm that parameter that controls this behaviour is the gravity number, Ng. The gravity number is a relation between the strength of the density effect (gravity forces) opposed by forced convection. The higher the gravity number the higher the action of stabilizing gravity forces. The gravity forces act on the perturbations in the mixing zone which are caused by local velocity variations. When these perturbations (wiggles) are eliminated the width of the mixing zone becomes smaller resulting in a smaller transverse dispersion coefficient (and thus transverse dispersivity).

The apparent reduction in transverse dispersivity in the numerical simulations shows that for a medium with heterogeneity equivalent to the laboratory experiments (i.e., σ^2=0.1) the decrease is of maximum 10%. In contrast, the laboratory experiments show that it can be up to 80%. Two reasons for this discrepancy may be: i) The computer code d^3f used in the numerical computations is based on the classical (linear) form of Fick's law and valid at the Darcy average scale. Consideration of other alternative forms of the Fick's Law like the nonlinear model by Hassanizadeh & Leijnse (1995) may be able to better represent the observed experimental behaviour. ii) physical processes occurring at a different scale, e.g., the scale of pores have to be taken into account. The homogenization model of Demidov is derived starting from the pore-scale level.

The theoretical model by Hassanizadeh and Leijnse for brine dispersion is based on a modified, nonlinear form of Fick's Law. An additional dispersion parameter β is introduced in order to account for the effects of brine transport (e.g., high-concentration gradients) on dispersion. This model has been previously tested against longitudinal dispersion data but no comparison with experimental data on transverse dispersion has been reported up to now. The comparison for with transverse dispersion experiments reveals that the nonlinear dispersion parameter β is non-unique and has to be related to: i) changes in density differences $\delta\rho$, ii) changes in flow velocity q and it is direction-dependent. The first two dependencies, however, are linked to each other and can be represented as a single dependency of β with Ng. With this dependence, the nonlinear effects can be attributed to the

physical processes of stabilizing gravity forces, although not explicitly accounted for in the nonlinear model.

However, in the homogenization model by Demidov the interaction between density differences and flow velocity is explicitly accounted for already at the pore-scale. This interaction re-structures the flow at the pore-space and causes a set of reversing currents or vortices. These vortices in effect reduce the space available for flow which in turn reduces the medium permeability (typically considered a medium constant) and also hinders transverse dispersion. Only experimental data for the latter is available to test these results. The behaviour of the transverse dispersion coefficient predicted by the homogenization model confirms observations from the laboratory experiments. That is, the apparent decrease is virtually independent of the Peclet number but dependent on the gravity number. Since the Ng does not dependent on a characteristic length scale (as opposed to the Peclet number), the observed behaviour appears to be medium-independent and hence can also be found in other porous media. The mechanisms of suppression of transverse dispersion due to the appearance and evolution of vortices at the pore-scale under the influence of gravity may be regarded as generally applicable.

Bibliography

Bear, J. Dynamics of Fluids in Porous Media. American Elsevier, New York, 1972.

Demidov, D., 2005. Upscaling of density-driven flow and transport, Ph.D. Thesis (in Russian), Kazan State University, Kazan, Russia.

Diersch, H.J., and Kolditz, O., 2002. Variable-density flow and transport in porous media: approaches and challenges. Adv. Water Resour. 25(812), 899944.

Gelhar, L.W., Axness, C.L., 1983. Three-dimensional stochastic analysis of macrodispersion in aquifers. Water Resour. Res. 19(2), 161-180.

Hassanizadeh, S. M., Leijnse, A., de Vries, W. J., and Stapper, R. A. M., Experimental study of brine transport in porous media. RIVM Report 728514005, Bilthoven, The Netherlands, 1990.

Hassanizadeh, S.M., and Leijnse, A., 1995. A non-linear theory of high-concentration-gradient dispersion in porous media. Adv. Water Resour., 18, 203-215.

Hellström, G., Tsang, C. F., and Claesson, J., 1988. Buoyancy flow at a two-fluid interface in a porous medium: analytical studies. Water Res. Research, 24(4), 493-506.

Johannsen, K., 2003. On the validity of the Boussinesq approximation for the Elder problem. Computational Geosciences, 7(3), 169182.

Johannsen, K., Kinzelbach, W., Oswald, S., and Wittum, G., 2002. The saltpool benchmark problem - numerical simulation of saltwater upconing in a porous medium. Adv. Water Resour. Res., 25(3),335-348.

Landman, A.J., 2005. Analysis of physical mechanisms underlying densitydependent transport in porous media, Ph.D. Thesis, Delft University of Technology.

Landman, A.J., and Schotting, R.J., 2007. Heat and brine transport in porous media: the Oberbeck-Boussinesq approximation revisited. Transport in Porous Media, 70, 355-373.

Nick., H.M., Schotting, R.J., Gutierrez-Neri, M., and Johannsen, K., 2008. Modeling transverse dispersion and variable density flow in porous media. Transport in Porous Media.DOI 10.1007/s11242-008-9277-x

Starke, B., 2005. Experimental and numerical investigations of macrodispersion of density-dependent flow and transport in stochastic porous media. PhD Thesis (in German), University of Kassel.

Starke, B., and Koch, M., 2006. Laboratory experiments and monte carlo simuations to validate a stochastic theory of density-dependent macrodispersion. Proceedings of the XVI Conference on Computational Methods in Water Resources, Copenhagen, Denmark.

Schotting, R.J., Moser, H., Hassanizadeh, S.M., 1991. High-concentration-gradient dispersion in porous media: experiments, analysis and approximations. Adv. Water Resour. Res. 22(7), 665-680.

Scheidegger, A.E., 1961. General theory of dispersion in porous media. J. Geophys. Res. 66(10), 3273-3278.

Watson, S.J., Barry, D.A., Schotting, R.J., and Hassanizadeh, S.M., 2002. Validation of classical density-dependent solute transport theory for stable, high-concentration-gradient brine displacements in coarse and medium sands. Adv. Water Resour. Res. 25, 611-635.

Chapter 6

Analytical modelling of fringe and core biodegradation in groundwater plumes [1]

This chapter presents analytical approach to modelling contaminant plumes with degradation occurring both at the fringe and at the core. The approach relies on the use of readily available analytical solutions for solute transport. An approximate solution is derived for the maximum plume length in steady-state conditions. This is verified through the use of a numerical solution.

6.1 Introduction

Monitored natural attenuation (MNA) can be an acceptable remediation method for managing subsurface contamination, particularly, for organic pollutants (Weidemeier *et al.*, 1999; Kao and Wang, 2000). However, there is a continued need to understand natural attenuation processes and, moreover, apply new techniques in predicting field-scale MNA scenarios (Wilson *et al.*, 2004). Mathematical modelling has, therefore, become an increasingly important tool to assist in analysing natural attenuation and understanding environmental systems (Cirpka *et al.*, 1999; Mayer *et al.*, 2001; Prommer *et al.*, 2002). To this mean, a range of analytical and numerical models exists that, when combined with field data, enable the prediction of the fate of contamination plumes in groundwater (Barry *et al.*, 2002).

[1] M. Gutierrez-Neri, P.A.S. Ham, R.J. Schotting, D.N. Lerner, 2009. *Journal of Contaminant Hydrology* 107, 1-9.

These modelling techniques have advantages and disadvantages. Typically, analytical models use simplifying assumptions about an environmental system in order to yield quick-to-implement explicit expressions of fate and transport. For example, in the case where hydraulic parameters are assumed isotropic and homogeneous Ham *et al.* (2004) provide estimates of steady-state plume lengths for a two-dimensional continuous point source where solutes undergo an instantaneous reaction. In comparison, numerical models are better suited to cases when geological conditions are heterogeneous, or the natural attenuation process involves complex chemical/biological interactions (Prommer *et al.*, 2002, 2006), however they generally require a deeper knowledge of the processes being modelled. Consequently, analytical models can provide first-order estimates of plume characteristics (e.g., plume lengths, concentration profiles) and may act as a pre-cursor for more detailed numerical modelling exercise. Such models are therefore of particular relevance in the formulation and assessment of an MNA framework.

The effectiveness of natural attenuation relies heavily on naturally occurring hydrological and biogeochemical processes. In terms of aquifer remediation, the most important process is biodegradation. Biodegradation can be divided into two categories depending on the location at which it occurs within the plume: degradation occurring at the plume fringes, and degradation occurring in the interior (core) of the plume (Lerner *et al.*, 2005). Oxidisable organic contaminants may undergo aerobic respiration, denitrification, and sulphate reduction at the plume fringes (Davis *et al.*, 1999; Van Breukelen *et al.*, 2004). Dispersion causes the contaminant species (electron donor) to mix with background groundwater-containing electron acceptors species (i.e. dissolved oxygen, nitrate, and sulphate) enabling reactions to occur (Davis *et al.*, 1999; Van Breukelen *et al.*, 2004; Tuxen *et al.*, 2006). The fast kinetics of these reactions implies that they are often controlled by mechanisms of hydrodynamic dispersion (Cirpka *et al.*, 1999; Klenk and Grathwohl, 2002; Thornton *et al.*, 2001a; Huang *et al.*, 2003). Conversely, in the plume core degradation is the result of anaerobic processes involving manganese reduction, iron reduction (consumption of sediment-bound mineral oxides), sulphate reduction and fermentation processes (methanogenesis) (Christensen *et al.*, 2000; Essaid *et al.*, 1995; Thornton *et al.*, 2001b). Large content of such electron acceptors compared to, e.g. dissolved oxygen, often causes anaerobic processes to be important mechanisms for overall plume degradation (Lovley *et al.*, 1989). Typically a kinetic representation is used for these slow reactions (Van Breukelen *et al.*, 2004).

With respect to analytical models, a number of them exist that consider degradation processes using first-order kinetics, e.g., Bear (1972); Hunt (1978); Domenico (1987). In those models, degradation processes are represented by a first-order rate constant applied over the whole volume of the plume. Such a modelling approach is referred to as the 'core-style degradation model' in this paper. Other models consider degradation as a process limited by electron acceptor mixing, including, most recently, Ham *et al.* (2004); Cirpka *et al.* (2007); Liedl *et al.* (2005); Chu *et al.* (2005). In those models, degradation is assumed to occur as

an instantaneous reaction between the electron donor and the electron acceptor, which is an appropriate assumption except (*i*) close to the contaminant source, and (*ii*) when flow velocities are very high (Koussis *et al.*, 2003). Here, this is referred to as the 'fringe-style degradation model'.

Given that existing analytical solutions assume that biodegradation follows either a core- or fringe-style degradation model, a different approach to NA modelling is presented in this paper. A general analytical solution is derived that accounts for the combined effects of degradation processes occurring both in the core and at the fringe of the plume. Existing analytical solutions readily available in the literature can be used for various initial and boundary conditions. A well-known analytical solution from Domenico and Robbins (1985) is used to derive an explicit solution for the steady-state plume length which allows to explore the controlling factors on the plume size. Lastly, the applicability of the combined model is demonstrated in a very well documented field case study.

6.2 Conceptual Model

In many cases where NA is occurring, the contaminant (e.g., an organic compound) acts as the electron donor (ED). At time $t = 0$, the three-dimensional domain Ω contains only the electron acceptor species (EA), which has a constant concentration ${C_{EA}}^0$ throughout the domain. ED species with a constant concentration, ${C_{ED}}^0$, enters the flow domain. The flow field in Ω is considered steady and uniform. As the plume develops, fringe degradation occurs as a result of mixing with pristine groundwater containing the dissolved EA species such as oxygen and nitrate (Borden and Bedient, 1986). Sulphate species (if occurring close to the fringe) may also be considered as part of the fringe reactive species (Davis *et al.*, 1999). Experimental and numerical evidence suggests that in many cases degradation at the plume edges progresses rapidly and as a mixing-limited process, e.g., Huang *et al.* (2003). Therefore, in this paper an instantaneous reaction between ED and EA is considered to occur at the plume fringe. In contrast, inside the plume, where dissolved oxygen is usually absent, anaerobic degradation can occur as a result of interactions with metal oxides, e.g., manganese and iron (Christensen *et al.*, 2000), or as a result of sulphate reduction and methane fermentation (Thornton *et al.*, 2001b). A common approach to represent anaerobic degradation is to simplify these biotransformations to first-order reactions (Lovley *et al.*, 1989). This approach is followed here, with the assumption that the EA species are not exhausted. Figure 6.1 is a schematic representation of the problem description.

For contaminants continuously injected into an aquifer, plume growth is initially time-dependent as the ED is transported downgradient of the source zone, i.e. the injection point. However, when the combined effects of NA processes balance the ED influx, a steady-state condition is achieved and the maximum plume length is attained. In terms of groundwater risk assessment this is of relevance, as

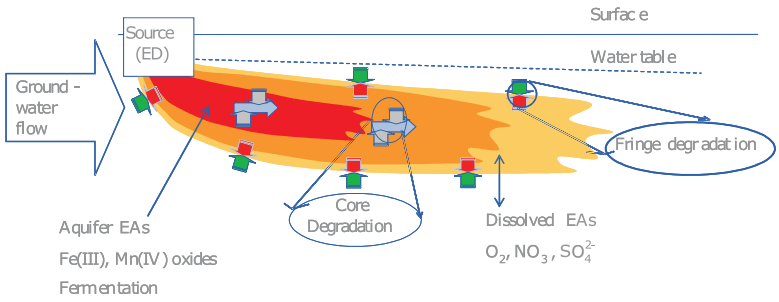

Figure 6.1: Schematic representation of fringe and core processes occurring in a contaminant plume emitted from a continuous source, adapted from Lerner *et al.* (2005).

it is usually necessary to predict the maximum potential reach of a contaminant plume. Therefore, the focus of this work is on continuously emitted sources. However, for completeness, instantaneous injection and exponentially decaying sources are also discussed.

6.3 Analytical Approach

6.3.1 Non-reactive transport

Assuming an isotropic and homogenous porous medium, the three-dimensional advection-dispersion equation (ADE) describing the transport of a non-sorbing, conservative species, is given by (Bear, 1972)

$$\frac{\partial C(k)}{\partial t} = \alpha_x v \frac{\partial^2 C(k)}{\partial x^2} + \alpha_y v \frac{\partial^2 C(k)}{\partial y^2} + \alpha_z v \frac{\partial^2 C(k)}{\partial z^2} - v \frac{\partial C(k)}{\partial x}, \qquad (6.1)$$

where C denotes the concentration of species k, t is the time, v is the average fluid velocity, α_x, α_y and α_z are the longitudinal, transverse horizontal and transverse vertical porous media dispersivities respectively. Two remarks are made on the form of Eq. (6.1): i) the hydrodynamic dispersion coefficients (longitudinal and transverse) assume that molecular diffusion is considerably small and therefore neglected; dispersion is modelled as the product $\alpha_i \cdot v$; and ii) the effects of sorption (or retardation) on transport are also neglected as it will be the steady-state solution that is of interest here. For stationary conditions, it has been demonstrated by e.g., Ham *et al.* (2004), that only the time-scales to reach steady-state is affected.

Closed-form solution techniques can be employed to solve equation (6.1); these solutions are usually written as the product of three one-dimensional solutions

(Hunt, 1978; Domenico and Robbins, 1985),

$$C_{ED}{}^{T}(x,y,z,t) = S \cdot F_1(x,\alpha_x,t) \cdot F_2(\alpha_y,y) \cdot F_3(\alpha_z,z), \tag{6.2}$$

where $C_{ED}{}^{T}$ denotes the total aqueous concentration of species ED in domain Ω, i.e. a conservative species (Ham *et al.*, 2004). S denotes the source term, F_1 is the function in the x-direction that accounts for advection and longitudinal dispersion, F_2 and F_3 are the solution functions in y- and z-directions that account for the transverse dispersion effects.

It should be noted that the form of the source term S and functions F_1, F_2, and F_2 depends on the assumptions made and thus varies from solution to solution. Some analytical solutions assume the aquifer to be finite, semi-infinite or infinite. The source geometry can be a point, a line, or a plane. The source regime is usually continuous but can also be instantaneous, or following a time function.

An example is presented using the analytical solution by Domenico and Robbins (1985) for three-dimensional transport emitted from a continuous planar source. Equation (6.2) now reads,

$$\begin{aligned} S &= \frac{C_{ED}{}^{0}}{8}, \\ F_1 &= \left[\operatorname{erfc}\left(\frac{x-vt}{2\sqrt{\alpha_x vt}}\right)\right], \\ F_2 &= \left[\operatorname{erf}\left(\frac{y+Y/2}{2\sqrt{\alpha_y x}}\right) - \operatorname{erf}\left(\frac{y-Y/2}{2\sqrt{\alpha_y x}}\right)\right], \\ F_3 &= \left[\operatorname{erf}\left(\frac{z+Z/2}{2\sqrt{\alpha_z x}}\right) - \operatorname{erf}\left(\frac{z-Z/2}{2\sqrt{\alpha_z x}}\right)\right], \end{aligned} \tag{6.3}$$

where $C_{ED}{}^{0}$ is the species initial concentration, Y is the source width and Z is the source height. Alternative solution forms can be obtained by replacing $F_i < i = 1,2,3 >$ and S with the appropriate values for different source conditions. For example, if dispersion is neglected in the vertical direction, the resulting two-dimensional expression is obtained by setting $F_3 = 2$, i.e., $\operatorname{erf}(\infty) \rightarrow 1$, and adjusting the source term S, so that

$$\begin{aligned} C_{ED}{}^{T}(x,y,t) &= S \cdot F_1(x,\alpha_x,t) \cdot F_2(\alpha_y,y), \text{ where} \\ S &= \frac{C_{ED}{}^{0}}{4}, \end{aligned} \tag{6.4}$$

and F_1 and F_2 are as previously defined in equation (6.3).

The steady-state condition, i.e. when $t \rightarrow \infty$, is reached when the term F_1 in (6.2) equals 2. At steady-state, the three-dimensional solution reduces to

$$\begin{aligned} C_{ED}{}^{T}(x,y,z,\infty) &= S \cdot F_2(\alpha_y,y) \cdot F_3(\alpha_z,z), \text{ where} \\ S &= \frac{C_{ED}{}^{0}}{4}. \end{aligned} \tag{6.5}$$

Equally, the two-dimensional steady-state solution takes the following general form

$$\begin{aligned} {C_{ED}}^T(x, y, \infty) &= S \cdot F_2(\alpha_y, y), \text{ where} \\ S &= \frac{{C_{ED}}^0}{2}. \end{aligned} \tag{6.6}$$

6.3.2 Reactive transport

In the case of simultaneous transport and biodegradation, the addition of a reaction term to the governing ADE, equation (6.1) now yields,

$$\frac{\partial C(k)}{\partial t} = \alpha_x v \frac{\partial^2 C(k)}{\partial x^2} + \alpha_y v \frac{\partial^2 C(k)}{\partial y^2} + \alpha_z v \frac{\partial^2 C(k)}{\partial z^2} - v \frac{\partial C(k)}{\partial x} - r^{C(k)}, \tag{6.7}$$

where r is the reaction rate.

Core Degradation Model

If biodegradation is assumed to follow a first-order kinetic law (i.e., decay), r can be written as

$$r = \lambda\, C(k), \tag{6.8}$$

where λ is the decay constant of the biodegradable species. Analytical solutions to the ADE, including species decay, may be generalised in the form

$$C_{ED}(x, y, z, t) = {C_{ED}}^T \cdot K(x, \lambda), \tag{6.9}$$

where C_{ED} denotes the concentration of the ED species, and K is a function that accounts for first-order decay. The analytical solution provided by Domenico (1987) defines K as

$$K(\lambda) = \exp\left[\left(\frac{x}{2\alpha_x}\right)\left(1 - \sqrt{1 + \frac{4\lambda\alpha_x}{v}}\right)\right]. \tag{6.10}$$

Other existing analytical solutions that consider species transport and decay include work by Hunt (1978); Bear (1972) and Domenico (1987) to list but a few. In this paper, equation (6.9) is referred to as the 'core degradation model'.

Fringe Degradation Model

Under the assumption that biotransformations occur fast in comparison to transport, Borden and Bedient (1986) introduced an instantaneous reaction model for a bimolecular chemical reaction of the form

$$Y_1 ED + Y_2 EA \rightarrow Y_3 P, \tag{6.11}$$

where Y_1, Y_2 and Y_3 are stoichiometric coefficients. In that paper a superposition method is used to compute the concentration distribution of the EA and ED species. However, recently in a study by Ham *et al.* (2004), an explicit analytical solution was derived for this type of reaction, applied to a continuous point source in a two-dimensional model domain. Here, the analytical derivation outlined in Ham *et al.* (2004) is adopted for the fringe degradation model. Assuming, for simplicity, that the stoichiometric coefficients in the bimolecular reaction (6.11) are all unity, i.e. Y_1=Y_2=Y_3=1, without loss of generality, analytical solutions incorporating the instantaneous reaction model take the form

$$C_{ED}(x,y,z,t) = {C_{ED}}^T \cdot \left(1 + \frac{{C_{EA}}^0}{{C_{ED}}^0}\right) - {C_{EA}}^0. \tag{6.12}$$

Equation (6.12) is referred to as the 'fringe degradation model'.

Combined Degradation Model

A solution to equation (6.7), where the reaction term accounts for both first-order kinetics and the instantaneous reaction, is obtained through the combination of the two independent solutions for core degradation and fringe degradation. It follows that the combined degradation model can be mathematically represented as

$$C_{ED}(x,y,z,t) = {C_{ED}}^T \cdot \quad K(x,\lambda) \cdot \left(1 + \frac{{C_{EA}}^0}{{C_{ED}}^0}\right) - {C_{EA}}^0. \tag{6.13}$$

The procedure proposed in equation (6.13) implies that the degradation of the electron donor is two-fold, first occurring throughout the entire plume following a first-order decay law, and subsequently as an instantaneous reaction at the plume fringe with the species EA in the resident groundwater.

It follows from equation (6.10) that if $\lambda = 0$, equation (6.13) reduces to solution for fringe degradation, i.e., (6.12). If ${C_{EA}}^0$ is small, the solution is reduced to core degradation, i.e., equation (6.9). In addition, if $\lambda = 0$ and ${C_{EA}}^0$ is small, the solution reduces to expression (6.2) for non-reactive transport.

An example is given below to illustrate the implementation of the combined degradation model in available analytical solutions, using the two-dimensional form of the original solution by Domenico (1987), equation (6.13) takes the form

$$C_{ED}(x,y,t) = S \cdot F_1(x,\alpha_x,t) \cdot F_2(\alpha_y,y) \cdot K(x,\lambda) \cdot \left(1 + \frac{{C_{EA}}^0}{{C_{ED}}^0}\right) - {C_{EA}}^0, \tag{6.14}$$

where $S = \frac{{C_{ED}}^0}{4}$ the other terms are as previously given.

Note on Multiple Species

So far, the bimolecular reaction (6.11) has been considered but it is possible to handle multiple EAs and EDs with two simplifying assumptions. These are that

there is no preferential order of reaction for the multiple species and that there are no preferred pairings between EAs and EDs. If additional EAs need to be considered in the fringe reaction, e.g., nitrate and/or sulphate, unit stoichiometry can be retained if all units of mass of EA are converted to units of mmols electrons per litre (mmol e/L). That is, when converted to (mmol e/L), the reactions have unit stoichiometry, since one electron is donated and one electron is accepted (Thornton *et al.*, 2001a). Consequently, the sum of several EAs can be reacted with the electron donor. A similar process can be applied to multiple EDs. Table 6.1 gives an example of the conversion to mmol e/L.

	Units	**EA**	**EA**
Species		Oxygen	Nitrate
Molecular weight	(g/mol)	62	32
Example concentration	(mg/l)	10	8
Concentration in moles	(mmol)	0.161	0.25
Electrons transfer in half reaction		5	4
Concentration	(mmol e/L)	0.806	1
		${C_{EA}}^0 = 1.806$	

Table 6.1: Example of conversion of concentration in mg/l to mmol e/L for dissolved oxygen and nitrate

Alternative Source Regimes

In this section, additional source regimes such as an instantaneous pulse source and a decaying source are considered, as an alternative to the continuous source scenario. An exponentially decaying source term can be denoted as

$$S^{decay} = S \cdot \exp^{-\xi t}, \tag{6.15}$$

where ξ is the source term decay constant. Analytical solutions to exponentially decaying input take the form

$${C_{ED}}^T(x, y, z, t) = (S \cdot \exp^{-\xi t}) \cdot F_1(x, \alpha_x, t) \cdot F_2(\alpha_y, y) \cdot F_3(\alpha_z, z), \tag{6.16}$$

with all the terms as previously defined.

If a pulse injection is considered, ${C_{ED}}^T$ is similarly denoted as in equation (6.2) except that the source term S is a function of the mass of the solute injected

$$S^{pulse} = \frac{M}{V}, \tag{6.17}$$

where M denotes the injected mass of solute over the volume V. Solutions considering instantaneous pulse sources take the form

$${C_{ED}}^T(x, y, z, t) = \frac{M}{V} \cdot F_1(x, \alpha_x, t) \cdot F_2(\alpha_y, y) \cdot F_3(\alpha_z, z), \tag{6.18}$$

Parameter	Value
Y	2 m
v	1 m/day
α_x	1 m
α_y	0.1 m

Table 6.2: Parameter values used in the two-dimensional modelling comparison

These forms of ${C_{ED}}^T$ can be directly substituted into the combined model as shown in equation (6.14), if the environmental conditions to be modelled better suit an alternative source regime. It should be noted that for these source regimes only the transient solutions can be used as steady-state conditions cannot be attained.

6.3.3 Numerical Validation of the Combined Degradation Model

In order to validate equation (6.14), a comparison was undertaken with PHT3D (Prommer *et al.*, 2003), a verified multicomponent transport model for three-dimensional reactive transport in saturated porous media. PHT3D combines MT3DMS (Zheng and Wang, 1999) for the simulation of advective-dispersive multi-species transport with the geochemical model PHREEQC-2 (Parkhurst and Appelo, 1999) to simulate reactive processes, i.e., equilibrium and kinetic reactions.

A two-dimensional model grid was constructed, extending 75m in the x-direction (i.e., the principal flow direction) and 30m in the y-direction. The model domain consisted of 18618 grid cells with minimum and maximum spatial discretisation as follows: $\Delta x_{min} = 0.25$ m, $\Delta x_{max} = 1$ m, $\Delta y_{min} = 0.125$ m, $\Delta y_{max} = 2$ m. The values of the hydrological parameters used in the numerical model are shown in Table 6.2. Steady-state flow was created using a *Neumann* boundary condition at the upstream boundary and a *Dirichlet* boundary condition at the downstream boundary.

In accordance with the initial and boundary conditions for the analytical solution, the concentration of species EA was selected to be ${C_{EA}}^0 = 1\ mmol/l$ throughout the domain. Constant concentration cells across at the upstream boundary of the numerical model domain, with a concentration of ${C_{ED}}^0 = 4\ mmol/l$ over a 2 m wide strip, were used to simulate the continuous source injection of species ED.

The reaction (6.11) was included into the PHREEQC-2 database. This was achieved by including the instantaneous (fringe) reaction as a complexation between EA and ED (log K =20), whilst core degradation was represented by a simple first-order reaction, where $\lambda = 0.01$. The TVD scheme (Leonard, 1988) was used to solve the advective transport problem and the model was run for a simulation period of 80 days ($\Delta t = 0.5$ days), during which steady-state concentration profiles were reached. Figure 6.2 shows block-centered results obtained from

the numerical simulations. Comparison of results for $C_{ED}(x, 0, \infty)$ shows good agreement between the profiles generated by the numerical model and those produced by the analytical model, particularly in the downstream part of the plume which is usually the most important for risk assessment. Numerical profiles show plumes that are only marginally larger than those generated analytically, with small discrepancies confined to the core of the plume.

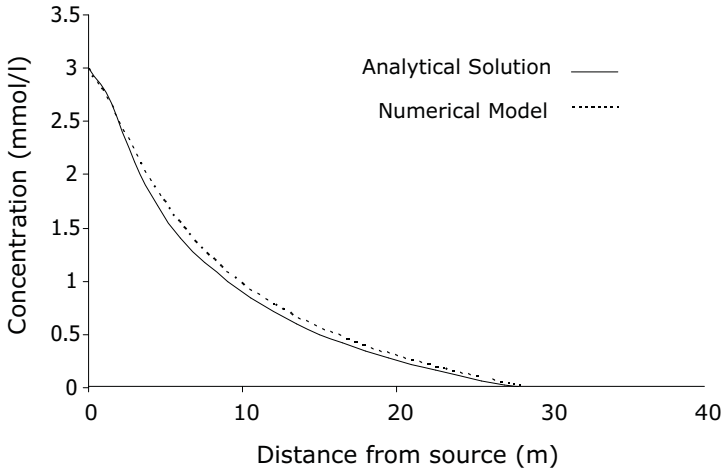

Figure 6.2: Comparison of numerical and analytical profiles for ED species along the plume centreline.

6.3.4 Plume Length

As shown in Ham *et al.* (2004) and Liedl *et al.* (2005), the maximum stationary plume length is given by the distance measured along the centreline of the plume to where all of the electron donor species are completely exhausted, i.e., $C_{ED} = 0$. The same approach is used here. Taking the three-dimensional solution by Domenico and Robbins (1985) for steady-state conditions (see Eqs. (6.3) and (6.5)) and modifying it to account for fringe and core degradation, the stationary plume length L can be obtained from solution to the following expression,

$$\frac{{C_{EA}}^0}{{C_{ED}}^0 + {C_{EA}}^0} = \operatorname{erf}\left(\frac{Y}{4\sqrt{\alpha_y L}}\right) \operatorname{erf}\left(\frac{Z}{4\sqrt{\alpha_z L}}\right) \exp\left[\frac{L}{2\alpha_x}\left(1 - \sqrt{1 + \frac{4\lambda\alpha_x}{v}}\right)\right]. \tag{6.19}$$

It is noted that an iterative numerical method has to be used to solve for the exact value of L. However, as it will be shown below, simplifying assumptions can be introduced to obtain an explicit expression for L. The following sections explore the effects of the some of the variables on the maximum plume length.

Influence of Longitudinal Dispersivity

In equation (6.19) the dimensionless group $(\alpha_x \lambda / v)$ contained within the exponential term is a form of the Damkohler number and is defined as the (bio)degradation rate relative to the advective transport

$$Da = \frac{\lambda \alpha_x}{v}, \tag{6.20}$$

with the longitudinal dispersion length, α_x, as the characteristic length.

The exponential term can be recast as

$$\exp\left[\frac{L}{2\alpha_x}\left(1 - \sqrt{1 + 4Da}\right)\right]. \tag{6.21}$$

Figure 6.3 is a plot of plume length, L, obtained from the exact solution, Equation (6.19), for different values of Da when Y =5 m, Z =2 m, α_z = 0.01 m, and the rest of the parameter values as outlined in Section 6.3.3. It can be seen that for increasing values of Da above the unity, the length of the plume reduces to a small value. This behaviour can be explained as follows: a large value of Da implies either a fast degradation rate or a low fluid velocity. This in turn means that degradation dominates over transport and results in an almost total consumption of the contaminant over a short travel distance. As Da increases further, the size of the plume is already too small but cannot be zero as Da occurs within the exponential function.

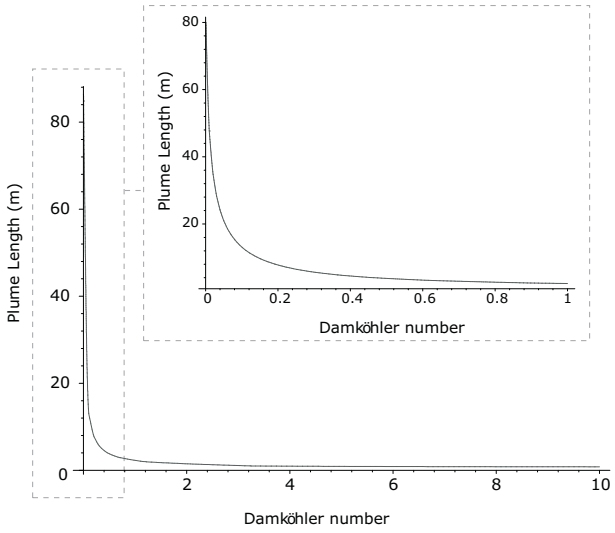

Figure 6.3: Variation of plume length with value of Da.

Therefore, if only values for $Da \ll 1$, are considered to be of importance, the exponential term can be simplified to

$$\exp\left(\frac{-L\,\lambda}{v}\right), \tag{6.22}$$

thus equation (6.19) reduces to

$$\frac{{C_{EA}}^0}{{C_{ED}}^0 + {C_{EA}}^0} = \operatorname{erf}\left(\frac{Y}{4\sqrt{\alpha_y L}}\right)\operatorname{erf}\left(\frac{Z}{4\sqrt{\alpha_Z L}}\right)\exp\left(\frac{-L\,\lambda}{v}\right). \tag{6.23}$$

Note that this approximation implies that plume length L is a function solely of the transverse dispersivities α_y and α_z, i.e., independent of longitudinal dispersivity α_x. This condition was previously observed in several experimental studies (e.g.,Grathwohl *et al.* (2000))and demonstrated mathematically by Ham *et al.* (2004) and Cirpka *et al.* (2007) when fringe degradation was the only degradation process considered. It now appears that also under conditions of both fringe and core degradation, the influence of α_x on the plume size is minor. This is illustrated in Figure 6.4, which shows a plot of the exact solution, i.e., Equation (6.19) for the same parameter values outlined in Section 6.3.3 and α_x values of 0.001 m and 100 m. The difference between computed plumes lengths is only marginal.

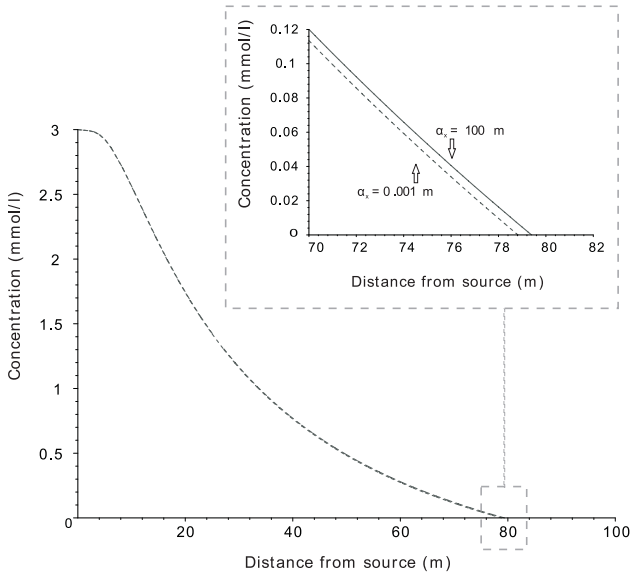

Figure 6.4: Centreline concentration profiles for species ED for values of $\alpha_x = 0.001$ m and 100 m.

An explicit expression for the plume length L can be obtained if the error function and the exponential function are both approximated by their respective

series expansion

$$\mathrm{erf}(\beta) = \frac{1}{\sqrt{\pi}}\left(2\beta - \frac{2}{3}\beta^3 + \frac{1}{5}\beta^5 - \frac{1}{21}\beta^7 ...\right), \tag{6.24}$$

and

$$\exp^{\gamma} = 1 + \frac{\gamma}{1!} + \frac{\gamma^2}{2!} + \frac{\gamma^3}{3!} + ... \tag{6.25}$$

If only the first term and the first two terms of both the series expansion respectively are considered, a first approximation for the plume length L is

$$L \approx \frac{Y\ Z}{4\pi\sqrt{\alpha_y\ \alpha_z}\ {C_{EA}}^0 / \left({C_{ED}}^0 + {C_{EA}}^0\right)\ +\ Y\ Z\ \lambda/v}. \tag{6.26}$$

From Equation (6.26) it can be seen that the steady-state plume length is dependent on (i) size of contaminant source, (ii) ratio of EA to ED, (iii) transversal dispersivities, and (iv) the ratio between the degradation rate constant to velocity λ/v. A comparison of the approximate solution (Equation 6.26) and the exact solution (Equation 6.19) for different values of λ/v is shown in Figure 6.5. Plume lengths predicted by the approximate solution, i.e. Equation (6.26), tend to be shorter than those predicted by the exact solution. However, the difference between the results becomes barely visible as $\lambda/v < 0.1$.

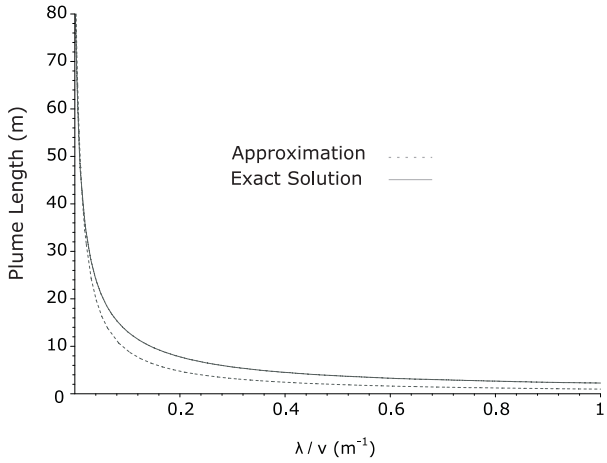

Figure 6.5: Variation of plume length with values of λ/ν.

Equation (6.26) strongly resembles those solutions for fringe degradation reported in Ham *et al.* (2004); Liedl *et al.* (2005); Cirpka *et al.* (2007); Chu *et al.* (2005), if the exponential term within $K(\lambda)$ equals 1, i.e., if core degradation is neglected. However, the solution presented here is more general, and applies to a broader range of NA scenarios.

Relative Importance of Core/Fringe Degradation

In Figure 6.6 plume length predicted by Equation (6.19) is plotted against λ/v for different values of the ratio ${C_{EA}}^0/\left({C_{ED}}^0+{C_{EA}}^0\right)$.

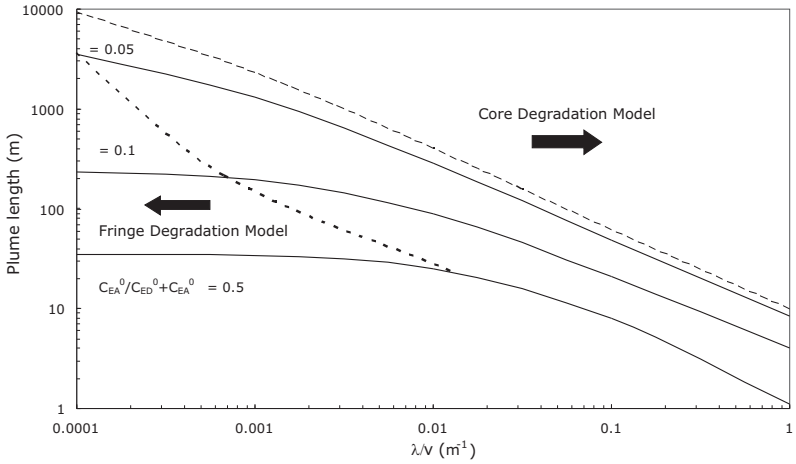

Figure 6.6: Variation of plume length with values of λ/v for different values of ratio ${C_{EA}}^0/\left({C_{ED}}^0+{C_{EA}}^0\right)$. The solid lines denotes the combined model. The upper dashed line denotes the limit where the combined model approximates the result of the core degradation model. Below the lower dashed line the combined degradation model approximates the fringe degradation model.

The relative importance of core degradation in the overall plume degradation can be easily assessed from the value of λ/v. A small λ/v means that the half-life ($t^{1/2}$) of the ED increases, $\lambda = ln(2)/t^{1/2}$ decreases, λ/ν decreases and in turn the exponential term in equation (6.19) approaches the value of 1. In this limit, the solution is similar to that of the fringe degradation model given by Eq. (6.12). That is, a small λ/v value means the mass of ED in the plume core is migrating fast relative to the decay rate making core degradation ineffective. Conversely, for short half-lives λ is relatively large, implying that λ/v increase and core degradation accounts for most of the contaminant depletion. Therefore the mass of ED in the core of the plume decays faster than it is transported making fringe degradation insignificant.

The fringe degradation model is independent of λ/v but dependant on the ratio ${C_{EA}}^0/\left({C_{ED}}^0+{C_{EA}}^0\right)$. If this ratio equals 0.5 and for $\lambda/v < 0.01$, the plume length predicted by the combined degradation model approximates the fringe degradation model (see Fig. 6.6); core degradation becomes insignificant as λ/v decreases. For the same ratio, and for $\lambda/v > 0.001$, the combined degradation model should yield better predictions for plume length than the core degradation model. However, if ${C_{EA}}^0/\left({C_{ED}}^0+{C_{EA}}^0\right)$ decreases, results from the combined

Parameter	Measurement
Y	2.5m
v	0.06 m day^{-1}
α_x	1 m
α_z	0.036 m
λ	0.00065 day^{-1}
${C_{ED}}^0$	10 mmol e/L
${C_{EA}}^0$	0.5 mmol e/L

Table 6.3: Parameter values and plume characteristics, obtained from Essaid *et al.* (1995, 2003)

degradation model are comparable to the core degradation model. Figure 6.6 also illustrates that the combined model is applicable within the region bounded by the dashed lines.

6.4 Application to a Field-Scale Natural Attenuation Study

In this section the combined degradation model is applied to a suitable field-case. Moreover, the combined model is compared to the fringe and core models to demonstrate the difference between the values predicted. The field-case, discussed in detail in Essaid *et al.* (1995) and Essaid *et al.* (2003), relates to the attenuation of a plume of petroleum hydrocarbons. In 1979 a buried oil pipeline located in a pitted and dissected glacial outwash plain near Bemidji, Minnesota, spilled approximately 11,000 barrels of crude oil resulting in the formation of a BTEX plume. The plume developed anaerobic conditions in the interior and was subject to aerobic degradation at the fringes due to mixing with oxygen in the ambient groundwater. The plume has been extensively investigated, and two-dimensional contour plots constructed from data analysis are available. Concentration, first-order degradation rates for the individual BTEX compounds and dissolved oxygen (DO), and transport parameters have been reported. The parameters values used are listed in Table 6.3.

Essaid *et al.* (1995) indicates that it is necessary to consider both fringe and core processes in order to accurately quantify the fate of the hydrocarbon plume. A simple assessment is to check λ/v and ${C_{EA}}^0/\left({C_{ED}}^0+{C_{EA}}^0\right)$ values. In this case, the plume λ/v gives a value of 0.012 and the ratio ${C_{EA}}^0/\left({C_{ED}}^0+{C_{EA}}^0\right)$ is approximately 0.05. Figure 6.6 indicates that with these values the field site may be better represented by the combined degradation model. In order to compare available data, the modelling exercise is based on the two-dimensional combined degradation model given by Equation (6.14), the core degradation model (for

$C_{EA}{}^0$ =0), and the fringe degradation model (for λ =0).

In Figure 6.7, centerline profiles are shown for the three models which allows the determination of the plume length, i.e., at $C_{ED}(L, 0, \infty) = 0$. Previous field estimates and numerical modelling efforts indicate the length of the plume to be approximately 195 m (Essaid *et al.*, 1995, 2003).

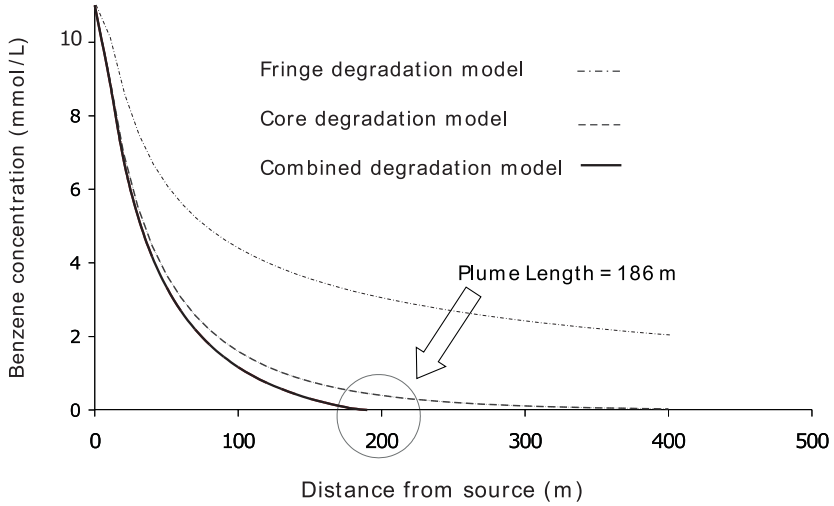

Figure 6.7: BTEX plume centreline concentration as predicted by the three models. The long-dash line denotes the fringe degradation model, the doted line denotes the core degradation model, the solid line denotes the combined model.

In this case, the maximum plume length is given by benzene, which in this particular case was the less attenuated compound. As illustrated in Figure 6.7, in order to better match the reported plume length, consideration of both fringe and core processes is necessary. If only fringe degradation, i.e., aerobic degradation, is considered, the plume length is estimated to be approx 4km (not shown in plot). Conversely, consideration of only core degradation, i.e., anaerobic degradation, is not enough to account for the attenuation reported. However, it should account for most of the plume degradation as shown in Figure 6.7. This behaviour agrees with previous findings reported in Essaid *et al.* (1995) and with results from an inverse modelling analysis on the controlling plume size variables by Essaid *et al.* (2003).

6.5 Discussion

The degradation of a contaminant plume can be characterised by processes occurring in the core and at the fringe. Within the context of NA, core degradation is typically considered to be a slow anaerobic process, whilst fringe degradation

can often be considered a fast (instantaneous) process whereby reactions between EA and ED occur and new reaction products are formed. However, for relatively high degradation rates and/or relatively low EA availability, it is necessary to account for both core and fringe degradation processes in order to better describe the observed plume attenuation.

These processes were implemented into the well-known solution by Domenico and Robbins (1985). This steady-state solution provides a first order approach to evaluate risk at a particular site, in terms of the potential plume length, in cases where both fringe and/or core degradation processes are important. The model provides insight into the main variables controlling the maximum plume size. The minor influence of α_x upon plume length, suggested in this study, is in line with previous findings by Ham *et al.* (2004); Chu *et al.* (2005) and Liedl *et al.* (2005). As a result, it is the values of λ/v (which indicates the competition between decay and transport) and not of the Da number (as defined by Equation 6.20), that provides a quick check on the relative weights of transport to core degradation. This parameter is extremely useful as it may be used to estimate the importance of core degradation in the overall plume attenuation. The relative contribution of fringe degradation (represented as an instantaneous reaction between ED and EA) can be assessed by the ratio ${C_{EA}}^0/\left({C_{ED}}^0+{C_{EA}}^0\right)$.

Some of the assumptions made about reactions will affect the application of the model to some field sites. Real pollution plumes often comprise a complex mixture of pollutants, possibly with different loading histories. Not all electron donors are equally degradable by all electron acceptors and there may be inhibitions operating in the plume. Reduced compounds formed in the core of the plume will migrate to the fringe where they may be reoxidated, consuming electron acceptors. These issues are beyond the scope of this, and other, analytical solutions to solute transport and the model should only be applied within the bounds of these assumptions. Indeed, a detailed evaluation of such processes, and their spatial and temporal variability, is only feasible through numerical modelling studies, e.g., (Prommer *et al.*, 2006), or using high-resolution field sampling techniques as shown by Tuxen *et al.* (2006). However, the strength of the approach lies in the possibility of obtaining explicit mathematical expressions for plume characteristics such as maximum plume length.

6.6 Conclusions

The analytical approach presented in this paper couples fringe and core degradation (referred to as the 'combined degradation model') and overcomes the previous limitation of available analytical solutions considering either fringe degradation or core degradation. In addition, the approach was shown to be readily used with existing analytical solutions of lower or higher dimensionality, different source geometry, and for different source regimes. The model is able to reproduce the plume length of a field case study.

Interpretation of the analytical solution shows that:

1. At the steady state transverse dispersion controls the plume length;
2. the value of λ/v (which indicates the competition between decay and transport) and not of the Da number (as defined by Equation 6.20), provides a quick check on the relative weights of transport to core degradation;
3. the relative contribution of fringe degradation can be assessed by the ratio ${C_{EA}}^0 / \left({C_{ED}}^0 + {C_{EA}}^0\right)$.

Analytical solutions are based on simplifying assumptions which limit their application but enable rapid evaluation. As well as the standard assumptions of a simple flow field, this model has assumptions about reactions. For example, it is assumed that electron acceptors are not depleted in the core of the plume and that multiple EAs and EDs can be lumped. The model is therefore most suitable for use as as a screening tool rather than for detailed and precise calculations of plume behavior.

Bibliography

Barry, D.A., H. Prommer, C.T. Miller, P. Engesgaard, and C. Zheng, 2002. Modelling the fate of oxidizable organic contaminants in groundwater. Adv. in Water Resour. 25, 899-937.

Bear, J., 1972. Dynamics of Fluids in Porous Media. Elsevier Science, New York.

Borden, R.C., and P.B. Bedient, 1986. Transport of dissolved hydrocarbons influenced by oxygen-limited biodegradation: 1. Theoretical development. Water Resour. Res. 22(13), 1973-1982.

Christensen, T.H., P.L. Bjerg, S.A. Banwart, J. Jakobsen, G. Heron, and H. Albrechtsen, 2000a. Characterisation of redox conditions in groundwater contaminant plumes. J. Contam. Hydrol. 45(3-4), 165-241.

Chu, M., P.K. Kitanidis, and P.L. McCarty, 2005. Modeling microbial reactions at the plume fringe subject to transverse mixing in porous media: When can the rates of microbial reaction be assumed to be instantaneous?. Water Resour. Res. 41(6), 1-15.

Cirpka, O.A., E.O. Frind, and R. Helmig, 1999. Numerical simulation of biodegradation controlled by transverse mixing.J. Contam. Hydrol. 40(2), 159-182.

Cirpka, O.A., and A.J. Valocchi, 2007. Two-dimensional concentration distribution for mixing-controlled bioreactive transport in steady state. Adv. in Water Resour 30(6-7), 1668-1679.

Davis, G.B., C. Barber, T.R. Power, J. Thierrin, B.M. Patterson, J.L. Rayner, and Q. Wu, 1999. The variability and intrinsic remediation of a BTEX plume in anaerobic sulphate-rich groundwater. J. Contam. Hydrol. 36(3-4), 265-290.

Domenico, P. A., 1987. An analytical model for multidimensional transport of a decaying contaminant species. J. Hydrology 91(1), 49-58.

Domenico, P. A., and G. Robbins, 1985. A new method of contaminant plume analysis. Ground Water, 23(4), 476-485.

Essaid H. I., B.A. Bekins,E. Godsy, E. Warren, M.J. Baedecker, and I.M. Cozzarelli, 1995. Simulation of aerobic and anaerobic biodegradation processes at a crude oil spill site. Water Resour. Res. 31(12), 3309-3327.

Essaid H. I., I. M. Cozzarelli, R.P. Eganhouse, W.N. Herkelrath, B.A. Bekins, and G.N. Delin, 2003. Inverse modelling of BTEX dissolution and biodegradation at the Bemidji, MN crude-oil spill site. J. Contam. Hydrol. 67(1-2), 269-299.

Grathwohl, P., I.D. Klenk, C. Ederhardt, and U. Maier, 2000. Steady state plumes: mechanisms of transverse mixing in aquifers. In C.D. Johnston: Contaminant Site Remediation: From Source Zones to Ecosystems, Proc. CRSC, Melbourne, Vic., 4-8 Dec., Centre for Groundwater Studies, CSIRO, Perth, Western Australia, pp.459-466.

Ham, P.A.S., R.J. Schotting, H. Prommer, and G.B. Davis, 2004. Effects of hydrodynamic dispersion on plume lengths for instantaneous bimolecular reactions. Adv. in Water Resour 27(8), 803-813.

Huang, W.E., S.E. Oswald, D.N. Lerner, C.C. Smith, and C. Zheng, 2003. Dissolved oxygen imaging in a porous medium to investigate biodegradation in a plume with limited electron acceptor supply. Environ. Sci. Technol. 37(9), 1905-1911.

Hunt, B.W, 1978b. Dispersive sources in uniform groundwater flow. J. Hydrol. Div., Proc. Amer. Soc. Civil Eng. 104, 75-85.

Kao, C.M. and C.C. Wang, 2000. Control of BTEX migration by intrinsic bioremediation at a gasoline spill site. Water Research. 13, 3413-3423.

Klenk, I.D., and P. Grathwohl, 2002. Transverse vertical dispersion in groundwater and the capillary fringe. J. Contam. Hydrol. 58(1-2), 111-128.

Koussis, A. D., S. Pesmajoglou, and D. Syriopoglou, 2003. Modelling biodegradation of hydrocarbons in aquifers: When is the use of the instantaneous reaction approximation justified?. J. Contam. Hydrol. 60(3-4), 287-305.

Lerner, D.N., P. Bjerg, J. Datel, A. Gargini, P. Grathwohl, C. Hollinger, P. Morgan, T. Ptak, R. Schotting, H. Slenders, and S.F. Thornton, 2005. CORONA - Confidence in forecasting of natural attenuation as a risk-based groundwater remediation strategy. Final report of the EU research project EVK1-2001-00087. University of Sheffield, UK. 26 pages. Available from www.shef.ac.uk/corona.

Leonard, B.P., 1989. Universal limiter for transient interpolation modeling of the advective transport equations: The ULTIMATE conservative difference scheme. NASA Technical Memorandum 100916, ICOMP-88-11, Washington, DC.

Liedl, R., A.J. Valocchi, P. Dietrich, and P. Grathwohl, 2005. The finiteness of contaminant plumes. Water Resour. Res. 41(12), W12501. doi:10.1029/2005WR004000.

Lovley, D.R., J.C. Woodward, and F.H. Chapelle, 1989. Oxidation of aromatic compounds coupled to microbial iron reduction. Nature 339(6222), 297-299.

Mayer, K.U., S.G. Benner, E.O. Frind, S.F. Thornton, and D.N. Lerner, 2001. Reactive transport modelling of processes controlling the distribution and natural attenuation of phenolic compounds in a deep sandstone aquifer. J. Contam. Hydrol. 53(3-4), 341-368.

Parkhurst, D.L., and C.A.J. Appelo, 1997. User's guide to PHREEQC (Version 2)-A computer program for speciation, batch-reaction , one-dimensional transport, and inverse geochemical calculations. U.S. Geological Survey Water-Resources Investigations Report 99-4259.

Prommer, H., D.A. Barry, and C. Zheng, 2003. MODFLOW/MT3DMS-based reactive multicomponent transport modelling. Ground Water 41(2), 247-257.

Prommer, H., G.B. Davis, and D.A. Barry, 2002. Modelling of physical and reactive processes during biodegradation of a hydrocarbon plume under transient groundwater flow conditions. J. Contam. Hydrol. 59(1-2), 113-131.

Prommer, H., N. Tuxten and P.L. Bjerg, 2006. Fringe-Controlled Natural Attenuation of Phenoxy Acids in a Landfill Plume: Integration of Fiel-Scale Processes by Reactive Transport Modelling. Environ. Sci. Technol. 40(15), 4732-4738.

Sun, Y., J.N. Petersen, and T.P. Clement, 1999. Analytical Solutions for multiple species reactive transport in multiple dimensions. J. Contam. Hydrol. 35(3-4), 429-440.

Thornton, S.F., D.N. Lerner, and S.A. Banwart, 2001a. Assessing the natural attenuation of organic contaminants in aquifers using plume-scale electron and carbon balances: model development with analysis of uncertainty and parameter sensitivity. J. Contam. Hydrol. 53(1-2), 199-232.

Thornton, S.F., S. Quigley, M. Spence, S.A. Banwart, S. Bottrell, and D.N. Lerner, 2001. Processes controlling the distribution and natural attenuation of phenolic compounds in a deep sandstone aquifer. J. Contam. Hydrol. 53(3-4), 233-267.

Tuxen, N., H.J. Albrechtsen, and P.L. Bjerg, 2006. Identification of a reactive degradation zone at a landfill leachate plume fringe using high resolution sampling and incubation techniques. J. Contam. Hydrol. 85(1-2), 179-194.

Van Breukelen, B., and J. Griffioen, 2004. Biogeochemical processes at the fringe of a landfill leachate pollution plume: potential for dissolved organic carbon, Fe(II), Mn(II), NH4, and CH4 oxidation. J. Contam. Hydrol. 73(1-4), 181-205.

Van Breukelen, B., J. Griffioen, F.M. W. F. M. Rlingc and H. W. van Verseveldc, 2004. Reactive transport modelling of biogeochemical processes and carbon isotope geochemistry inside a landfill leachate plume. J. Contam. Hydrol. 70(3-4), 249-269.

Wiedemeier, T.H., H.S. Rifai, C.J. Newell, and J.T. Wilson, 1999. Natural Attenuation of Fuels and Chlorinated Solvents in the Subsurface. John Wiley and Sons, New York.

Wilson, J.L., and P.J. Miller, 1978. Two-dimensional plume in uniform groundwater flow. J. Hydraulics Div., ASCE, 104(4), 503-512.

Wilson, R.D., S.F. Thornton, and D.M. MacKay, 2004. Challenges in monitoring the natural attenuarion of spatially variable plumes. Biodegradation, 15, 359-369.

Zheng, C., and P.P. Wang, 1999. MT3DMS: A modular three-dimensional multispecies model for simulation of advection, dispersion and chemical reactions of contaminants in groundwater systems; Documentation and User's Guide. Contract Report SERDP-99-1, U.S. Army Engineer Research and Development Center, Vicksburg, MS.

Chapter 7

Effects of biodegradation on the apparent transverse dispersivity

This Chapter explores the effects of biodegradation on the transverse dispersivity. Given simplifying assumptions, an explicit expression is presented that relates the size of the reactive mixing zone to the apparent dispersivity. This relationship is applied to a field problem for which high-resolution sampling data is available.

7.1 Introduction

Risk-based strategies for managing the widespread pollution of groundwater resources by for instance organic contaminant rely on naturally occurring processes. From these natural attenuation (NA) processes, dispersion and biodegradation appear to be the main mechanisms for aquifer remediation (Lerner *et al.*, 2005). Biodegradation reactions can be broadly divided into two categories, those requiring one single substrate (e.g., fermentation processes) and those requiring the presence of electron donor (ED) species and electron acceptor (EA) species. In the former case, biodegradation rates are slow compared to transport and become the controlling mechanism. When the latter is the case, biodegradation rates are usually fast compared to transport and the controlling mechanism is dispersive mixing (Koussis *et al.*, 2003).

These key NA processes take place in the transition zone between the contaminant plume and surrounding clean groundwater, i.e., the plume fringe. In this reactive mixing zone (RMZ), electron donor and electron acceptor species mix and react. The RMZ width is the result of an interplay between hydrodynamic dispersion and biodegradation, i.e., dispersion acting towards the widening of the

RMZ and biodegradation shrinking its size. Indeed, Chu *et al.* (2005) showed that even if the overall plume spreading is controlled by transverse dispersion, the actual size of the RMZ is strongly influenced by degradation rates. That is, depending on the degradation rate, the plume fringe narrows or expands. Hence, for fast degradation rates it is common to find relatively narrow RMZ widths compared to the rest of the plume body. For instance, Thornton *et al.* (2001a) showed that aerobic and nitrate-reduction degradation were the main processes acting in a 2 m fringe accounting for most of the degradation of a 20 m thick plume of phenolic compounds. An additional observation is that for fast redox reactions the concentration gradients at the plume fringe are steep and almost non-overlapping. This means that high quality field data is required in order to capture the steep concentration distribution at the plume fringe. However, if the sampling resolution is too large, the fringe thickness can be poorly captured and the actual size of the plume fringe is overestimated. Therefore, predictions of plume behaviour by numerical (or analytical) models based on plume fringe estimates can result in erroneous calculations (Thornton *et al.*, 2001a). Using the analytical approach shown in Chapter 6 to account for biodegradation reactions, an approximated expression for the transverse dispersivity is given when knowledge of the width of RMZ is available. This dispersivity is in fact an effective value as it represents the interaction between plume spreading and reaction. This approach applies to naturally degrading plumes with fringe degradation-only, with additional contribution of core degradation if present. Plumes with core degradation-only are not considered here. A case study is presented where data from a well-documented contamination site for which highly-resolved vertical profiles are available. The obtained values are compared to those previously reported for the same field-problem.

7.1.1 Problem Statement

Consider the case of a steady plume from a continuously emitted ED source in a homogeneous uniform flow field. At the plume fringe biodegradation takes place as an instantaneous reaction limited only by transverse mixing. Whilst, in the core of the plume, biodegradation follows a first-order reaction. This is schematically shown in Figure 7.1.

7.2 Analytical Approach

The analytical approach is based on the methodology outlined in Chapter 6 repeated here for convenience.

7.2.1 Non-reactive transport

Assuming an isotropic and homogenous porous medium, the three-dimensional advection-dispersion equation (ADE) describing the transport of a non-sorbing,

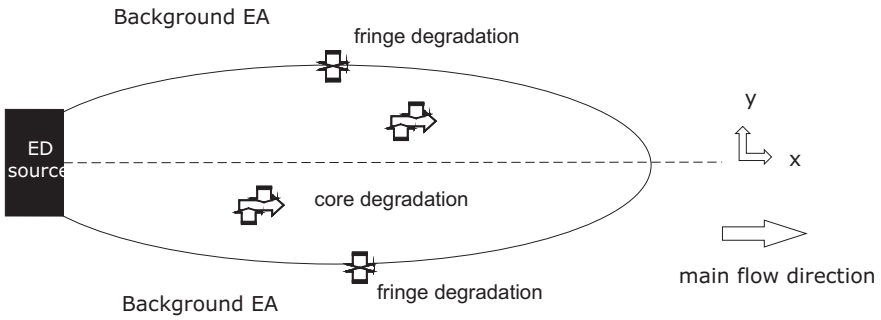

Figure 7.1: Steady state ED plume with fringe and core degradation.

conservative species, is given by (Bear, 1972)

$$\frac{\partial C(k)}{\partial t} + v\frac{\partial C(k)}{\partial x} = D_L\frac{\partial^2 C(k)}{\partial x^2} + D_T\left(\frac{\partial^2 C(k)}{\partial y^2} + \frac{\partial^2 C(k)}{\partial z^2}\right) \tag{7.1}$$

where C denotes the concentration of species k, t is the time, v is the average fluid velocity, where D_L and D_T are the longitudinal and transverse dispersion coefficients respectively. Here, the species k involved are electron donors (ED) and electron acceptors (EA). It is noted that in equation (7.1) the effects of sorption (or retardation) on transport are neglected as it will be the steady-state solution that is of interest here. For stationary conditions, it has been demonstrated by e.g., Ham *et al.* (2004), that only the time-scales to reach steady-state is affected.

Closed-form solutions are employed to analytically solve equation (7.1). These solutions are often written as the product of one-dimensional solutions (Domenico and Robbins, 1985). The three-dimensional form written in terms of ED species reads,

$${C_{ED}}^T(x, y, z, t) = S \cdot F_1(x, D_L, t) \cdot F_2(D_T, y) \cdot F_3(D_T, z), \tag{7.2}$$

where ${C_{ED}}^T$ denotes the total aqueous concentration of species ED in domain Ω, i.e. a conservative species. S denotes the source term, F_1 is the function in the x-direction that accounts for advection and longitudinal dispersion, F_2 and F_3 are the solution functions in y- and z-directions that account for the transverse dispersion effects. Note that the form of the source term S and functions F_1, F_2, and F_2 depends on the assumptions made with respect to dimensionality, source geometry and source regime (see also Chapter 6).

7.2.2 Reactive transport

In the case of simultaneous transport and biodegradation, the addition of a reaction term to the governing ADE (7.1) now yields,

$$\frac{\partial C(k)}{\partial t} + v\frac{\partial C(k)}{\partial x} = D_L\frac{\partial^2 C(k)}{\partial x^2} + D_T\left(\frac{\partial^2 C(k)}{\partial y^2} + \frac{\partial^2 C(k)}{\partial z^2}\right) - r^{C(k)}, \qquad (7.3)$$

where r is the reaction rate.

Core Degradation- First Order Decay Model

Biodegradation that follows a first-order kinetic law (i.e., decay), r can be written as,

$$r = \lambda\, C(k), \qquad (7.4)$$

where λ is the decay constant of the biodegradable species. Analytical solutions to the ADE, including species decay, may be generalised in the form

$$C_{ED}(x, y, z, t) = {C_{ED}}^T \cdot K(x, \lambda), \qquad (7.5)$$

where C_{ED} denotes the concentration of the ED species, and K is a function that accounts for first-order decay. The function K may be defined as

$$K(\lambda) = \exp\left(-\lambda\frac{x}{v}\right) \qquad (7.6)$$

where x/v is the travel time to the x-location.

Fringe degradation - Instantaneous Reaction Model

Under the assumption that biodegradation occurs fast in comparison to transport, an instantaneous reaction model for a bimolecular chemical reaction of the form

$$Y_1 ED + Y_2 EA \rightarrow Y_3 P, \qquad (7.7)$$

where Y_1, Y_2 and Y_3 are stoichiometric coefficients. Assuming, for simplicity, that the stoichiometric coefficients in the bimolecular reaction (7.7) are all unity, i.e. Y_1=Y_2=Y_3=1, analytical solutions incorporating the instantaneous reaction model take the form

$$C_{ED}(x, y, z, t) = {C_{ED}}^T \cdot \left(1 + \frac{{C_{EA}}^0}{{C_{ED}}^0}\right) - {C_{EA}}^0 \qquad (7.8)$$

where ${C_{EA}}^0$ is the initial concentration of EA species.

Combined Degradation

Combining the effects of core degradation (equation 7.5) and fringe degradation (equation 7.8) yields,

$$C_{ED}(x,y,z,t) = {C_{ED}}^{T} \cdot \quad K(x,\lambda) \cdot \left(1 + \frac{{C_{EA}}^{0}}{{C_{ED}}^{0}}\right) - {C_{EA}}^{0}. \tag{7.9}$$

The form of equation (7.9) implies that the degradation of the ED plume is two-fold, first the concentration of ED decays following a first-order kinetic law, and subsequently this decayed ED reacts instantaneously at the plume fringe with the species EA in the background groundwater. From equation (7.9) it follows that if core degradation is negligible (i.e., $\lambda \to 0$), equation (7.9) reduces to solution (7.8) for fringe degradation-only. If $\lambda = 0$ and ${C_{EA}}^{0}$ is small, the solution reduces to that of conservative transport.

7.3 Symmetrical problem

The governing ADE equation for the two-dimensional problem outline in Figure 7.1 for stationary conditions where longitudinal dispersion can be omitted is written as,

$$v\frac{\partial C(k)}{\partial x} = D_T \frac{\partial^2 C(k)}{\partial y^2} \tag{7.10}$$

written as the product of one-dimensional solutions and in terms of ED species, the ADE equation yields,

$${C_{ED}}^{T}(y) = S \cdot F_2(D_T, y), \tag{7.11}$$

The problem schematically outlined in Figure 7.1 can in fact be regarded as symmetrical (w.r.t. the dashed line) which then simplifies the analysis to half of the domain only. Moreover, away from the source, the problem can be treated as one-dimensional flow with transverse dispersion. The analytical solution for this scenario reads,

$$\begin{aligned} {C_{ED}}^{T}(y) &= S \cdot F_2(D_T, y), \\ S &= \frac{{C_{ED}}^{0}}{2}, \\ F_2 &= \operatorname{erfc}\left(\frac{y}{2\sqrt{D_T x/v}}\right) \end{aligned} \tag{7.12}$$

where ${C_{ED}}^{0}$ is the ED species initial concentration. Next, equation (7.12) is modified to include core and fringe degradation following procedure outlined (7.9),

$$C_{ED}(y) = \frac{{C_{ED}}^{0}}{2} \cdot \operatorname{erfc}\left(\frac{y}{2\sqrt{D_T x/v}}\right) \cdot \exp\left(-\lambda\frac{x}{v}\right)\left(1 + \frac{{C_{EA}}^{0}}{{C_{ED}}^{0}}\right) - {C_{EA}}^{0}. \tag{7.13}$$

7.3.1 Mixing zone thickness

If the plume is conservative, i.e., no reaction with the ambient fluid, the concentration profiles developing transverse to the axis of the plume are illustrated for the non-reactive species ED_T and EA_T in Figure 7.2a. Here, the only mechanism is dispersive mixing. If there exists reaction between ED and EA the concentration profiles that develop are given in Figure 7.2b. Here, the interacting mechanisms are dispersive mixing and biodegradation.

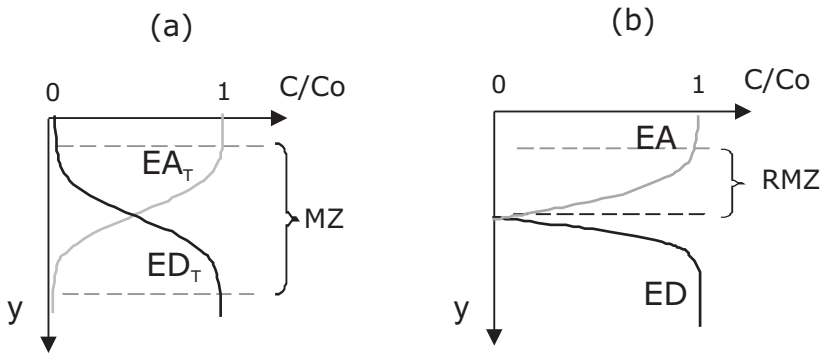

Figure 7.2: Schematics of the mixing zone. (a) vertical profile of a conservative species; (b) the vertical profile of reacting species.

Figure 7.2 shows schematically the depth-orientated concentration profiles for non-reactive and reactive species. The size of the mixing zone for conservative species is denoted by (MZ) and for reactive species is denoted by (RMZ). Note that in both cases, the size of the mixing zone is delineated as the vertical distance where the scaled concentration C/C_0 changes from 1 to 0. For the conservative scenario (i.e., only dispersive mixing), an S-shaped concentration profile is commonly observed and the profiles overlap each other. In practice, typical MZ profiles may not be easily delineated between the scaled concentration limits of 0 and 1. The MZ limits can also be taken as the 0.1 and 0.9 of scaled concentration. However, when reaction occurs the mixing zone the profiles no longer overlap and the mixing zone reduces in size. Note also that the scaled concentration profiles of the non-reactive and reactive species are in fact symmetrical with respect to the x-axis. Because of this symmetry either of the species profiles can be chosen to delineate size of MZ or RMZ. Here, the top profile is used to delineate the mixing zone and it is assumed to correspond to the ED species.

The maximum width of the mixing zone is in both scenarios attained at C/C_0=0, i.e., when y-value is at maximum. Rewriting equation (7.13) when ${C_{ED}/C_{ED}}^0$=0, and rearranging the terms yields,

$$\frac{{C_{EA}}^0}{{C_{ED}}^0 + {C_{EA}}^0} = \frac{1}{2}\,\mathrm{erfc}\left(\frac{y}{2\sqrt{D_T x/v}}\right)\cdot\exp\left(-\lambda\,\frac{x}{v}\right) \tag{7.14}$$

The complementary error function can be recast in terms of the error function (i.e.,$1-\mathrm{erf}$) which in turn can also be given in terms of series expansion,

$$\mathrm{erf}(\beta) = \frac{1}{\sqrt{\pi}}\left(2\beta - \frac{2}{3}\beta^3 + \frac{1}{5}\beta^5 - \frac{1}{21}\beta^7 ...\right), \tag{7.15}$$

Equally, the exponential function can be recast using the series expansions,

$$\exp^{\gamma} = 1 + \frac{\gamma}{1!} + \frac{\gamma^2}{2!} + \frac{\gamma^3}{3!} + ... \tag{7.16}$$

Considering the first term and first two terms of both series expansion respectively, i.e., the first-order approximation, expression (7.14) can be simplified to,

$$\frac{{C_{EA}}^0}{{C_{ED}}^0 + {C_{EA}}^0} = \left(1 - \frac{y}{\sqrt{\pi D_T x/v}}\right)\cdot\left(1 - \frac{\lambda\, x}{v}\right) \tag{7.17}$$

By solving for y in expression (7.17) and denoting $F = \frac{{C_{EA}}^0}{{C_{ED}}^0+{C_{EA}}^0}$, RMZ yields,

$$RMZ_c = \sqrt{\pi D_T x/v}\cdot(1-\chi) \tag{7.18}$$

where the suffix c denotes combined degradation, and $\chi = \frac{2F}{1-\lambda x/v}$. However, if only fringe degradation is taken into account (i.e., λ=0), expression (7.17) now reads,

$$2\cdot F = 1 - \frac{y}{\sqrt{\pi D_T x/v}} \tag{7.19}$$

solving for y yields RMZ influenced only by fringe degradation

$$RMZ_f = \sqrt{\pi D_T x/v}\,(1-2F) \tag{7.20}$$

where the suffix f denotes fringe degradation. It is noted that in both expressions for RMZ (7.18) and (7.20) the term in the square root $\sqrt{\pi D_T x/v}$ is in fact equivalent to the characteristic mass transfer length in a classical one-dimensional diffusion problem. The term in parenthesis can be regarded as a 'correction factor' due to the effects of biodegradation. The correction factor thus ranges between 1 and 0 which indicates that biodegradation reduces the size of the mixing zone. This is an expected behaviour considering that dispersion acts towards widening the mixing zone and biodegradation towards shrinking it.

7.3.2 Apparent transverse dispersivity

An estimation of the transverse dispersivity from the size of RMZ can be obtained if the transverse dispersion coefficient is defined as the product of velocity and dispersivity $\alpha_T \cdot v$ and if molecular diffusion is assumed negligible. Equations (7.18) and (7.20) are now rewritten in terms of transverse dispersivity,

$$RMZ_c = \sqrt{\pi \alpha_T x} \cdot (1 - \chi) \tag{7.21}$$

and

$$RMZ_f = \sqrt{\pi \alpha_T x}\,(1 - 2F) \tag{7.22}$$

where x is the distance from the origin. This indicates that the growth of RMZ is dependent to travel distance. Next, solving for transverse dispersivity in both expressions yields,

$$\alpha_T = \frac{1}{\pi x}\left(\frac{RMZ_c}{1-\chi}\right)^2 \tag{7.23}$$

and

$$\alpha_T = \frac{1}{\pi x}\left(\frac{RMZ_f}{1-2F}\right)^2 \tag{7.24}$$

The obtained explicit expression for transverse dispersivity, although a first-order approximation, show that with knowledge of the size of the reactive mixing zone, and additional parameters such as initial concentration of ED and EA and decay rate constant, a representative transverse dispersivity can be obtained. However, this also indicates that an accurate prediction of the width of RMZ is of paramount importance.

7.4 Determination of field-scale transverse dispersivity

Equation (7.24) is used to extract a transverse dispersivity value from a well-documented field study. The 500 m long phenolics plume has been the subject of extensive research aimed at characterising the naturally-occurring attenuation processes. Fringe degradation is believed to be the only biodegradation mechanisms as the concentration level in the plume core is too high inhibiting any biodegradation activity. Concentration profiles have been obtained using high-resolution vertical sampling techniques. This methods ensures that the sampling resolution at discrete depths is high enough to better capture the true profiles. More details on this phenolics plume, as well as the relevant transport and reactive parameters can be found in (Thornton *et al.*, 2001a,b). Table 7.1 gives the values used to compute the transverse dispersivity. These values were measured at a sampling port located at 350m from the source zone.

Parameter	Value
ED^0	900 mmol e/L
EA^0	6 mmol e/L
RMZ	1 -2 m
x	350 m

Table 7.1: Parameters obtained from the phenolics plume.

The actual size of RMZ is estimated in a range of 1 to 2m. Substitution of the values listed in Table 7.1 into expression (7.24) gives a transverse dispersivity that varies in range between 0.001 - 0.003m. Previous estimates of the field-scale transverse dispersivity were in the order of 0.001 - 0.004m (Huang, 2002).

7.5 Summary and Conclusions

The mathematical approach outlined in Chapter 6 to model analytically transport and biodegradation (in the fringe and core) is employed here. A first order approximation is obtained for the width of the reactive mixing zone (RMZ). The width (or size) of the mixing zone is in fact a measure of the transverse dispersion length or dispersivity. An explicit expression that relates RMZ to the transverse dispersivity is presented. Ensuring a good estimate of the size of RMZ is thus a key issue. High-resolution sampling techniques can be employed to more accurately capture the size of the mixing zone. A transverse dispersivity value obtained from a direct measure of RMZ can prove a better indication of the actual plume-scale dispersivity. A case study was presented where data from a well-documented contamination site is analysed. The estimates of transverse dispersivity (although first-order) agree well with previously reported dispersivity values.

Commonly employed techniques to obtain transport parameters are usually based on the analysis of conservative (non-reactive) species. At the field-scale the concentration profile of a nonreactive solute reflects the combined effects of spreading and mixing. As is if often difficult to account separately for these effects, the resulting transport parameters are usually an overestimation. By using the concentration profiles of reactive species two advantages can be named: i) the reactive profiles show a distinctive pattern of steep gradients where almost no overlapping between species is observed, ii) the profile of a reactive species is the result of the true mixing that occurs between species. Mixing is the mechanism that brings species together for reaction. Hence, the resulting dispersivity is a measure of the true mixing length. This is of practical relevance if predictions of the natural attenuation of a contaminant plume are based on estimates of transverse dispersion parameters.

Bibliography

Bear, J., 1972. Dynamics of Fluids in Porous Media. Elsevier Science, New York.

Chu, M., P.K. Kitanidis, and P.L. McCarty, 2005. Modeling microbial reactions at the plume fringe subject to transverse mixing in porous media: When can the rates of microbial reaction be assumed to be instantaneous?. Water Resour. Res. 41(6), 1-15.

Domenico, P. A., 1987. An analytical model for multidimensional transport of a decaying contaminant species. J. Hydrology 91(1), 49-58.

Domenico, P. A., and G. Robbins, 1985. A new method of contaminant plume analysis. Ground Water, 23(4), 476-485.

Huang, W.E., 2002. The role of transverse mixing of electro acceptors and carbon substrates in natural attenuation. PhD thesis, University of Sheffield, Sheffield.

Ham, P.A.S., R.J. Schotting, H. Prommer, and G.B. Davis, 2004. Effects of hydrodynamic dispersion on plume lengths for instantaneous bimolecular reactions. Adv. in Water Resour 27(8), 803-813.

Koussis, A. D., S. Pesmajoglou, and D. Syriopoglou, 2003. Modelling biodegradation of hydrocarbons in aquifers: When is the use of the instantaneous reaction approximation justified?. J. Contam. Hydrol. 60(3-4), 287-305.

Lerner, D.N., P. Bjerg, J. Datel, A. Gargini, P. Gratwohl, C. Hollinger, P. Morgan, T. Ptak, R. Schotting, H. Slenders, and S.F. Thornton, 2005. CORONA - Confidence in forecasting of natural attenuation as a risk-based groundwater remediation strategy. Final report of the EU research project EVK1-2001-00087. University of Sheffield, UK. 26 pages. Available from www.shef.ac.uk/corona.

Thornton, S.F., D.N. Lerner, and S.A. Banwart, 2001a. Assessing the natural attenuation of organic contaminants in aquifers using plume-scale electron and carbon balances: model development with analysis of uncertainty and parameter sensitivity. J. Contam. Hydrol. 53(1-2), 199-232.

Thornton, S.F., S. Quigley, M. Spence, S.A. Banwart, S. Bottrell, and D.N. Lerner, 2001. Processes controlling the distribution and natural attenuation of phenolic compounds in a deep sandstone aquifer. J. Contam. Hydrol. 53(3-4), 233-267.

Van Breukelen, B., and J. Griffioen, 2004. Biogeochemical processes at the fringe of a landfill leachate pollution plume: potential for dissolved organic carbon, Fe(II), Mn(II), NH4, and CH4 oxidation. J. Contam. Hydrol. 73(1-4), 181-205.

Van Breukelen, B., J. Griffioen, F.M. W. F. M. Rlingc and H. W. van Verseveldc, 2004. Reactive transport modelling of biogeochemical processes and carbon isotope geochemistry inside a landfill leachate plume. J. Contam. Hydrol. 70(3-4), 249-269.

Chapter 8

Summary

In many cases concerning the natural attenuation of organic plumes as well as in density-dependent problems such as seawater intrusion, hydrodynamic transverse dispersion appears to be a controlling mechanism. This thesis deals with some aspects of transverse dispersion in porous media and the interplay of flow and transport processes that affect dispersion. In the context of this thesis, dispersion is analysed from three view-points: 1) *ideal tracer* conditions where the tracer is considered to be a non-reactive species and the concentration is small enough not to change the density or viscosity of the fluid in which the tracer is dissolved and hence its flow behaviour, 2) *brine conditions* where the tracer concentration is high enough to induce density-driven flow and to affect the flow and transport behaviour, and 3) *reactive mixing* where the dispersion of the tracer is affected by reaction. For this particular case, no density and/or viscosity effects on the transport are considered.

Accordingly, this thesis is organised as follows: **Chapter 2** reviews the main governing equations of flow and transport in porous media focussing on the topic of hydrodynamic dispersion discussed from the conceptual and theoretical point of view. **Chapter 3** gives an overview of previous experimental and theoretical findings reported in the literature for the case of vertical brine transport. The latter is included for the purposes of reviewing the main controlling parameters in density-dependent dispersion. Published experimental studies on transverse dispersion investigating density-dependent dispersion are also reviewed and found to be limited in number and scope. However, the main observations are summarised in anticipation of the experimental program presented in the next chapter. Hence, **Chapter 4** presents an experimental study on transverse dispersion processes under tracer and brine conditions. For this purpose, a series of horizontal miscible-displacement experiments were carried out in a two-dimensional flow-through tank. Homogenous porous media were created using two choices of grain sizes. In addition to exploring the effects of density variations on the dispersion coefficient, the effects of fluid velocity were also analysed. Results from these experiments pro-

vide new empirical representations of the behaviour of the transverse dispersion coefficient and the transverse dispersivity with variations in fluid velocity, density differences and porous media characteristics. The fact that transverse dispersivity was found to be dependent on fluid velocity and density difference contradicts the premise that dispersivity is a porous medium constant. **Chapter 5** aims at gaining better understanding of the mechanics of transverse dispersion under the presence of high-concentration gradients, typical of brine transport. First, results from a numerical investigations on transverse dispersion under brine conditions are compared to experimental results. Next, theoretical predictions from two different models, namely Hassanizadeh and Leijnse (1995) and Demidov (2005) are compared to experimental results. Although each theoretical model follows a different mathematical derivation, conclusions can be drawn from each comparison to help building a more complete picture of the underlying mechanisms controlling density-dependent transverse dispersion. In general, it is concluded that the presence of density differences between the fluids affects transverse dispersion. The higher the density difference the higher the degree of suppression of the transverse dispersion coefficient. This apparent decrease is shown to be virtually independent of the Peclet number but dependent of the gravity number. Since the gravity number does not dependent on a characteristic length scale, as opposed to the Peclet number, the observed behaviour can also be found in other media. The mechanism of suppression of transverse dispersion due to the appearance and evolution of local rotational flow (vortices) at the pore-scale under influence of gravity can be inferred as universally applicable.

The second part of this thesis deals with the interaction between transverse mixing and reactions. These two processes are regarded as competing with each other, i.e, dispersion promoting spreading and dilution, and reaction preventing further dispersion by consuming the solute. These two relevant processes occur at the mixing zone of a contaminant plume (plume fringe). The combined effects reflect in the width of the mixing zone which in turn is a direct measure of the effective dispersion coefficient. In **Chapter 6** a mathematical methodology is presented to account for the combined effects of kinetics-controlled and mixing-controlled reactions on transport. The advantage of the procedure is that the resulting governing equations are given in terms of conservative transport for which readily available analytical solutions can be employed. A comparison between a numerical model of the full problem, i.e., transport and reaction, and the analytical model shows very good agreement, validating the proposed method. As direct application, the behaviour of groundwater contaminant plumes under naturally attenuating conditions is studied. This results in an explicit expression for the stationary plume size. The relevance of transverse dispersion as one of the controlling mechanism of the plume extent is confirmed. In **Chapter 7** the same mathematical approach to account for reaction and transport is again employed. However, here the focus is to derive an expression for the size of the reactive mixing zone (RMZ). The size (or width) is in fact a direct measure of the transverse dispersion length or dispersivity. In terms of field-scale problems, this gives a bet-

ter representative value of the local (or plume-scale) dispersivity. Obtaining good estimates of aquifer-scale dispersivity is shown to be possible when combined with high-resolution sampling techniques. Commonly employed techniques to obtain transport parameters are usually based on analysis of conservative transport. In this case an alternative form is proposed using vertical concentration profiles of reactive species. Instant reactive profiles show a distinctive pattern of steep concentration gradients where almost no overlapping between species is seen. This allows a good inference of the actual RMZ, and thus better plume-scale dispersivity estimates. A case study was presented where data from a well-documented contamination site is analysed. The first order estimates of transverse dispersivity agree well with previously reported dispersivity values.

Samenvatting

In veel gevallen waarbij natuurlijke processen een verspreiding van een stofconcentratie veroorzaken, of processen waarbij dichtheidsstroming een rol speelt (bv zeewaterintrusie) lijk de hydrodynamische transversale dispersie een belangrijke rol te spelen. Voor dit proefschrift zijn bepaalde aspecten van de transversale dispersie in poreuze media en het samenspel van stroming en transport dat de dispersie benvloed geanalyseerd. Deze analyse heeft plaats gevonden vanuit drie gezichtspunten: i) *Ideale tracer*. In dit geval is de tracer beschouwd als een niet-reactief deeltje met een concentratie die te klein is om de dichtheid of de viscositeit van de vloeistof waarin de tracer is opgelost te veranderen. De stromings- en transporteigenschappen van de vloeistof veranderen niet. ii) *Brine condities*. In deze situatie is de concentratie van de tracer hoog genoeg om de dichtheid van de vloeistof te veranderen, waardoor dichtheidsstroming optreedt en de stromings- en transporteigenschappen van de vloeistof veranderen. ii) *Menging met reacties*. In het laatste geval is bekeken hoe de dispersie benvloed wordt door reacties van de tracer. Effecten van de dichtheid en/of de viscositeit op het transport zijn buiten beschouwing gelaten.

In Hoofdstuk 2 wordt een beschouwing gegeven van de meest gebruikte stromings- en transportvergelijkingen die het proces van hydrodynamisch dispersie vanuit een conceptueel en theoretisch oogpunt beschrijven. Hoofdstuk 3 geeft een overzicht van reeds uitgevoerde experimenten en theoretische studies op het gebied van dichtheidsstroming. Dit overzicht is gemaakt om te achterhalen welke parameters het meest van invloed zijn op de dichtheidsafhankelijke dispersie. De belangrijkste conclusies en resultaten van de reeds uitgevoerde onderzoeken zijn samengevat en hebben als vergelijking gediend voor de nieuwe experimenten. Deze zijn beschreven in het volgende hoofdstuk. In Hoofdstuk 4 worden de opzet en resultaten van verschillende experimenten beschreven ten einde de effecten van transversale dispersie onder tracer (1) en brine condities (2) te onderzoeken. Uit de experimenten is gebleken dat transversale dispersie afhankelijk is van de stromingssnelheid en het dichtheidsverschil. Deze resultaten zijn tegenstrijdig met de algemene aanname dat de dispersiviteit van een poreus medium een constante is. Hoofdstuk 5 richt zich op het verkrijgen van een beter begrip van de werking van transversale dispersie bij vloeistoffen met een hoge concentratie gradint. In het algemeen kan geconcludeerd worden dat de aanwezigheid van een dichtheidsverschil tussen vloeistoffen

de transversale dispersie benvloed. Hoe groter het dichtheidsverschil, hoe lager de transversale dispersie cofficint. Deze verlaging is nagenoeg onafhankelijk van het Peclet-getal, maar is wel afhankelijk van het gravitatie-getal. Het mechanisme van de onderdrukking van de transversale dispersie als gevolg van de aanwezigheid en ontwikkeling van locale draaikolkachtige stroming op porie schaal onder de invloed van de zwaartekracht, wordt in het algemeen als acceptabel beschouwd.

Het tweede deel van dit proefschrift beschrijft de interactie tussen de transversale menging waarbij reacties optreden (3). Deze twee processen werken elkaar tegen. Als gevolg van dispersie treedt verspreiding en verdunning van een stof op. Reacties van deze stof voorkomen echter een verdere dispersie. Deze twee processen treden op in de zone van een verontreinigspluim waar mening optreedt. Het gecombineerde effect van beide processen benvloed de breedte van mengzone, welke een directe maatstaf is voor de effectieve dispersie cofficint. Hoofdstuk 6 geeft een mathematische methodiek om het gecombineerde effect van kinetisch-gecontroleerde en mening-gecontroleerde op het transport mee te nemen. Als validatie van de voorgestelde methode is een vergelijking uitgevoerd met een numeriek model. De resultaten van beide modellen kwamen goed met elkaar overeen. Als directe toepassing is het gedrag van een verontreinigingspluim met een natuurlijke verspreiding bestudeerd. Dit heeft geresulteerd in expliciete uitdrukking voor de stationaire grootte van de verontreinigingspluim. De relevantie van de transversale dispersie als een van de controlerende processen voor de grootte van een pluim is hiermee bevestigd. In Hoofdstuk 7 is dezelfde mathematisch methodiek nogmaals toegepast. Hier was het doel om een vergelijking af te leiden om de grootte van de reactive mengzone mee te bepalen. De grootte (of breedte) is in feite een directe maat voor de transversale dispersie lengte. Het is aangetoond dat verkrijgen van een goede schatting van een dispersiviteit op aquifer-schaal met hoge resolutie meettechnieken mogelijk is. Een case studie is uitgevoerd waarbij de data van een zeer goed gedocumenteerde verontreinigingslocatie is gebruikt. De eerste orde schattingen van de transversale dispersiviteit kwamen goed overeen met de eerder gerapporteerde waardes van de dispersiviteit.

Acknowledgements

I would have never been able to complete this thesis without the support and help of a number of people. I first thank my promotor Ruud Schotting for his support and guidance in the past years. I still remember our first meeting to discuss the project work: with a beer and bitterballen. Not much has changed ever since. I also thank Majid Hassanizadeh for always having the right encouraging words and critical views when needed. I would like to mention Pieter Kleingeld for helping me with the experimental set-up. You are a true example to all of us. Without your help the experiments would have been an immense task. In this context I'm very grateful to Christian Griebler and Robert Bauer from the Institute of Groundwater Ecology at the Helmholtz Center Munich for showing me their experimental set-up and sharing their experiences. I specially thank Denis Demidov for answering all my questions about his model and for helping me with matlab-related issues. I'm thankful to Peter Grathwohl and Toon Leijnse for being part of my reading committee, and for their inspirational work that contributed to my research. My dear colleagues Marian, Vahid, Amir, Reza, and Jenny not only for their constant support but also for making the research work more enjoyable. I also thank Phil, Hamid, Janneke, Tony and Wijb with whom I had the pleasure to work with and at the same time learn a bit more about my own research. Special mention goes to Margreet Evertman who always help me with all the admin issues, and to Cas Berentsen for all our discussions on dispersion and for always providing with a nice cup of thee!

This thesis is actually the result of time spent also at the Groundwater Protection and Restoration Group of Sheffield University. For this reason I would like to thank the following people: David Lerner for giving me the opportunity to pursue a PhD at the group. Your were the first one who trusted I could do it, despite my lack of experience in the subject. I should also like to mention Ryan, Steve, Maria, Martin and Jenny for their help and support when needed. My ex-colleagues Zuansi, Brenda, Marianne, Mohamed, Helen and Arne for making my time at the group very pleasant. To my friends Rodolfo, Helen, Haruko, Euripides, Enrique, Hector and so many others who made Sheffield the best experience.

During the last years I have been very fortunate to come across with a lot of wonderful people, in- and outside the university life contributing indirectly to this work. I would like to mention a few in particular: Sotiris for his unconditional

support throughout these years, Christian not only for being the best housemate but also for being a good friend, Simona for always listening to my stories, scientific and non-scientific and for being the best running partner. Ueli and Roberta, Beatriz and Frank, Siska, Victor, and Aco for always being there for me, in the good times and in the not so fun times. To my colleagues outside the group Cornelia, Celine, Cöme, Xavier, Joost, Christian, Otto, and Co. for their enthusiasm and ever-presence at the parties in the Riouwstraat. I should also like to thank Guus Willemsen, Coen Dijxhoorn, Han Meijer and Bas Godschalk at IF Technology for making possible I would have time to finalise this thesis, and to Nick Buik for helping me with the Dutch translation. Finally, I thank Marc for his support in the last stages of the thesis and for bringing the balance back into my life. I'm also thankful to his group at ETH Zurich for hosting me when I needed to work on the thesis.

Y por ultimo a mi familia, sin la cual nunca hubiera sobrevivo el doctorado! A mis padres Angelica y Victoriano de quienes heredé el caracter que me ha mantenido aqui. A mi hermano Guillermo, por soportar mi ausencia de los ultimos años. A mi hermano Victor Hugo y su nueva familia, Mayela y Victoriano, por su apoyo y cariño constante. Y a mi hermana Angelica, a quien le dedico esta tesis en especial. Soy muy afortunada de tenerte no solo como hermana sino tambien como amiga. Agradezco infinitamente todo tu apoyo, sin importar la hora del dia o el lugar.

Curriculum Vitae

Mariene Gutierrez Neri was born on May 30, 1978 in Poitiers, France. After some years of residing in France, her family moved back to Torreon, Mexico. There, she completed a degree in Mechanical Engineering at the Instituto Tecnologico de la Laguna where she graduated with honors in December 2001. During her university years she worked at a small engineering firm called *VIMECA, S.A de C.V.*, as a part-time project engineer. In September 2002 she was awarded with a scholarship by the Mexican Research Council for Science and Technology (CONACYT) to pursue postgraduate studies. She moved to the UK to complete a MSc in Energy and Environmental Engineering at the University of Sheffield. The topic of her MSc thesis was related to wastewater treatment technologies. In December 2003 she took on a PhD position at the *Groundwater Protection and Restoration Group* to work in the subject on natural attenuation of contaminant plumes. However, in February 2006 she moved to the Netherlands to the *Environmental Hydrogeology Group* at Utrecht University to work on density-dependent dispersion. This thesis is the result of those years spent at both research groups. She now works at *IF Technology* based in the city of Arnhem.